Electronic Theses and Dissertations   Theses, Dissertations, and Major Papers

2016

Development of a Hydraulic Bulge Test to Determine the Work Hardening Behaviour of Sheet Materials

Mario Vasilescu
University of Windsor

Follow this and additional works at: https://scholar.uwindsor.ca/etd

Development of a Hydraulic Bulge Test to Determine the Work Hardening

Behaviour of Sheet Materials

By

Mario Vasilescu

A Thesis

Submitted to the Faculty of Graduate Studies

through the Department of **Mechanical, Automotive and Materials Engineering**

in Partial Fulfillment of the Requirements for

the Degree of Master of Applied Science

at the University of Windsor

Windsor, Ontario, Canada

2016

Development of a Hydraulic Bulge Test to Determine the Work Hardening

Behaviour of Sheet Materials

by

Mario Vasilescu

APPROVED BY:

_____

Dr. W. Altenhof

Engineering Materials

_____

Dr. D. Pusca

Mechanical Engineering

_____

Dr. D. Green, Advisor

Mechanical Engineering

November 9th,2016

DECLARATION OF ORIGINALITY

I hereby certify that I am the sole author of this thesis and that no part of this thesis has been published or submitted for publication.

I certify that, to the best of my knowledge, my thesis does not infringe upon anyone's copyright nor violate any proprietary rights and that any ideas, techniques, quotations, or any other material from the work of other people included in my thesis, published or otherwise, are fully acknowledged in accordance with the standard referencing practices. Furthermore, to the extent that I have included copyrighted material that surpasses the bounds of fair dealing within the meaning of the Canada Copyright Act, I certify that I have obtained a written permission from the copyright owner(s) to include such material(s) in my thesis and have included copies of such copyright clearances to my appendix.

I declare that this is a true copy of my thesis, including any final revisions, as approved by my thesis committee and the Graduate Studies office, and that this thesis has not been submitted for a higher degree to any other University or Institution.

ABSTRACT

The objective of this research is to develop an experimental facility that is able to characterize the work hardening behaviour of metal sheets up to large deformations greater than 50 percent effective strain.

A hydraulic bulge test die was designed with a 120-mm diameter piston to push the forming fluid against the sheet specimen, a 135-mm diameter opening and a 3-mm radius on the fillet of the die. This die was built and installed in a double-action hydraulic press and is capable of reaching a forming pressure of 60 MPa.

DP600 steel sheet specimens were also flat rolled to effective strains of 0.2, 0.4, 0.6, 0.8 and 1.0 and tensile tests were conducted on the as-rolled specimens following ASTM E8 standards. A power law curve was fitted to the data, and yielded $\bar{\sigma}=1026.851\bar{\varepsilon}^{\,0.1951}$ in the rolling direction and $\bar{\sigma}=1022.456\bar{\varepsilon}^{\,0.1758}$ in the transverse direction. Hydraulic bulge tests were successfully run and the experimental data was fitted to $\bar{\sigma}=1104.6\bar{\varepsilon}^{\,0.2029}$.

Finite element (FE) models of the hydraulic bulge test and uniaxial tensile test were constructed. FE models were validated using an appropriate validation metric, and the predicted uniaxial tension flow curve showed a validation score of 0.97 and the flow curve predicted for the hydraulic bulge test achieved a score of 0.98, compared to the experimental curves.

Power law, Ludwik and Voce functions were fitted to the experimental data and hardening parameters were determined for both the tensile test with successive flat rolling and the hydraulic bulge test flow curves. Comparison metrics were established at 0.94, 0.87 and 0.94, respectively.

Comparisons were made between the tensile test flow curve and the hydraulic bulge test flow curve which showed that the hydraulic bulge test is better suited for the characterization of work hardening behaviour up to large strains.

ACKNOWLEDGEMENTS

TABLE OF CONTENTS

LIST OF FIGURES

x

LIST OF TABLES

NOMENCLATURE

ε^{eng} - Engineering strain

ε^{log} - Logarithmic strain

ε^{lag} - Lagrange strain

ε^{true} - True strain

ε_1 - Principal strain 1

ε_2 - Principal strain 2

ε_3 - Principal strain 3

$\bar{\varepsilon}$ - Effective strain

σ_{True} - True stress

σ_{eng} - Engineering stress

$\bar{\sigma}$ - Effective stress

R_D - Radius of the dome

t_d - Thickness of sheet at the apex of the dome

P   - Pressure

t_o - Original thickness of sheet

r   - Radius

σ_1 - Principal stress 1

σ_2 - Principal stress 2

σ_3 - Principal stress 3

d_c - Diameter of cavity

h_d - Dome height

R_c - Radius of the fillet on bulge test cavity

n   - Strain hardening exponent

K   - Strain hardening parameter

R   - Plastic strain ratio

ε_w - True width strain

w_f - Final width

w_o - Original width

t_f - Final thickness

$\bar{\sigma}_{iso}$ - Isotropic stress

$\bar{\sigma}_{ani}$ - Anisotropic stress

τ_s - Shear stress

F   - Force

L   - Length

L_o - Original Length

γ - Shear strain

u - Displacement of sheared specimen

w   - Width of shearing zone

A   - Area

V   - Volume

E   - Elastic Modulus

V - Validation Metric

E - Error metric

Chapter 1   Introduction

1.1   Background

Sheet metals have been used in a wide variety of industrial applications including the aerospace and automotive sectors [1], but are also used in packaging, casings and other industrial applications [2]. An effective way of saving money in the production of manufactured goods is by reducing the amount of material used in each application: not only does this reduce manufacturing costs, but it also results in savings for the consumer. A new government mandate was passed in 2012 that will require all automotive fleets on the road to have an average of 54.5 miles per gallon by the year of 2025 [3]. One way to approach this fuel economy is to drastically reduce vehicle weight. This is being done by adopting advanced materials, such as Advanced High Strength Steel (AHSS) sheets, since their greater strength allows thickness and mass reduction [4] without compromising stiffness and crash-resistance. Another significant advantage is their increased formability at higher strengths, which allows for greater design flexibility, part complexity, and may lead to part consolidation and reduction of manufacturing costs since fewer parts require less welding and weld flanges [4].

Figure 1-1 illustrates [5] the different steels and their range of total elongation (%) versus tensile strength (MPa). Low strength steels have greater total elongation, which makes them ideal candidates for various high-deformation metal forming applications. However, both their yield and tensile strength are quite low.

Ultra-high strength steels, which are on the right hand side of Figure 1-1, exhibit high tensile strength but low total elongation. A suitable combination of strength and elongation needs to be found in order to effectively contribute to weight reduction. Various efforts have been put forth in order to identify suitable constitutive models for AHSS.
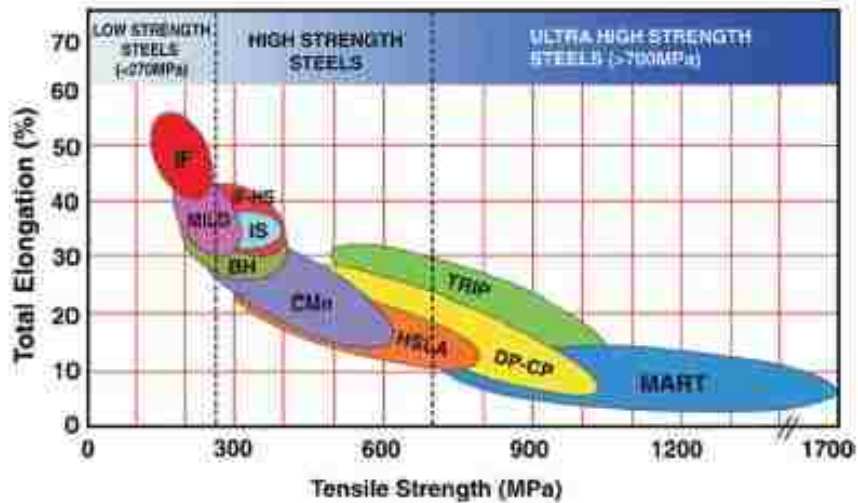
Figure 1-1. Total elongation (%) vs. tensile strength (MPa)

In order to carry out finite element analysis (FEA) simulations and reliably predict the outcome of sheet metal forming operations, critical mechanical properties must be known. A flow stress curve is typically determined from a uniaxial tension test, which provides the work hardening behaviour of the sheet material but this may not be as good as other test data [6]. Values of strain attained in a uniaxial tension test are lower than those in a metal forming process due to the onset of strain localization. Metal forming processes usually result in biaxial states of stress, which are different from uniaxial tension. This requires tensile data to be extrapolated beyond the range of available data in order to be useful for FEA simulations of forming processes up to large deformations. Figure 1-2 illustrates how the extrapolation of tensile data can lead to different results depending on the hardening function that is used to describe the flow curve. The results of numerical simulations are heavily relied upon for building production tools for industrial manufacturing processes such as hydroforming, blanking, stamping, deep drawing, and several others [7]. By carrying out characterization tests that generate biaxial loading conditions, a more accurate representation of the specimen behaviour should be expected [6]. As the experimental flow stress curve is extended to a greater strain range, numerical simulations of forming processes which use the flow curve as input will become more accurate. This in turn should lead to

2

reduced manufacturing costs associated with more accurate design of the tooling and forming process.
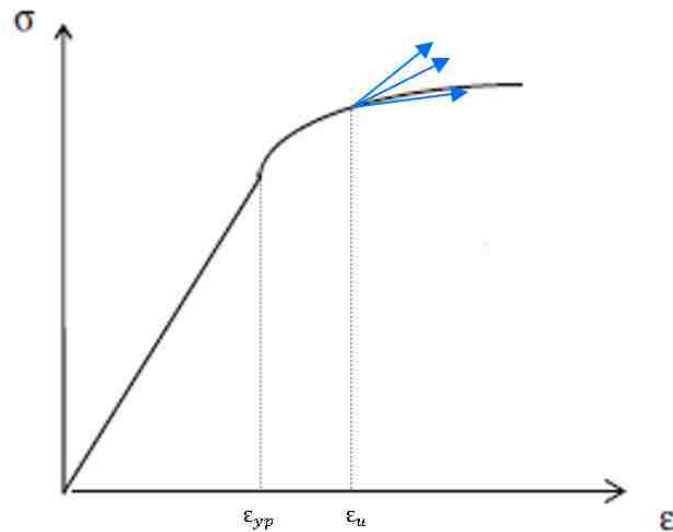
Figure 1-2. Variation in FEA extrapolation [8]

The hydraulic bulge test is commonly used [9] to characterize the flow behaviour of sheet materials under a balanced biaxial state of stress. In this test, a circular sheet is securely clamped around its periphery and pressurized from one side with a hydraulic fluid; as the pressure on the sheet increases, the blank will increasingly stretch and bulge out through the opening in a die. The bulge test can be continued until the onset of fracture. The bulge test can therefore be used to determine the flow curve and work hardening behaviour of any sheet material in balanced biaxial tension.

Another way to determine the work hardening behaviour of sheet materials up to large deformations is to carry out a combination of flat rolling followed by tensile tests. By flat rolling a sheet specimen, the sheet material is pre-strained prior a tensile test, which allows the material to reach a high level of effective strain prior to the onset of strain localization in uniaxial tension. By progressively increasing the thickness reduction in the rolling process, greater values of pre-strain can be applied, thus allowing the total effective strain to be significantly increased prior to failure in uniaxial tension. This

3

allows a flow stress curve to be produced up to much larger deformations (over 100% strain) compared to a uniaxial tension test carried out on the as-received sheet material. However, this method is very time consuming as it requires a minimum of 3-5 tensile tests to be completed after each level of thickness reduction in rolling. Therefore, the bulge test is no doubt a more efficient characterization test.

1.2   Objectives

The challenges with manufacturing automotive parts made from AHSS increase as new higher strength sheet materials are produced; mechanical characterization tests up to large deformations are required for input into FEA codes, and therefore the need for an experimental facility to deform sheet metal specimens in biaxial tension has practically become a necessity in order to support advanced research in sheet metal forming. The objectives of this work are to:

- Characterize the work hardening behaviour of DP600 sheets up to high strains using successive cold rolling and uniaxial tensile tests,
- Design and build a hydraulic bulge test facility that can be installed and operated in the hydraulic, double-action Eagle press in the Mechanical Testing Laboratory, which would in turn require:
    - The integration of suitable equipment for use with the bulge test, such as a piston and seal and a pressure transducer.

    - Determination of the range of materials and sheet thickness that can be burst with the desired pressure requirements of DP600, while also considering future high strength materials.

    - Implementation of a robust clamping mechanism in order to prevent any leaks or the sheet specimen from drawing in.

- Installation of an adjustable camera mount above the press that is in a suitable range to record the full deformation of the specimen during the bulge test. Selecting an appropriate lens, working distance, minimum height and working angle.

- Producing flow stress curves from the experimental bulge test data, using digital image correlation (DIC) to measure strains and the hardware and software necessary to record raw data.

- Development of FEA models of the hydraulic bulge test and tensile test using LS-DYNA in order to predict the outcome of experimental testing and guide the design of the bulge test facility
- Determination of the experimental measure error of flow curves as well as establishing a validation metric [10]

Chapter 2 provides an in depth review on current testing and analysis methods that are used to obtain a flow stress curve from a hydraulic bulge test. The literature review also includes various other mechanical tests that are used to determine the flow behaviour of sheets, including the shear test and cruciform test. A summary of each work hardening test is outlined listing the advantages and disadvantages.

Chapter 3 presents the bulge test design and how the piston size was determined, the available configurations for the clamping ring of the hydraulic bulge test are also outlined. Catia models of the various components associated with the hydraulic bulge test are provided.

Chapter 4 outlines detailed experimental procedures for the tensile test with successive flat rolling as well as for the hydraulic bulge test.

Experimental results are presented in chapter 5 for both the as-received tensile tests, the tensile tests after successive flat rolling and the hydraulic bulge tests.

Chapter 6 describes the implicit finite element models for the tensile test as well as the hydraulic bulge test. The numerical model of the hydraulic bulge test was used to determine how much pressure would be required to burst a referenced high strength material and to help establish the maximum pressure capacity of the hydraulic bulge test. Mesh sensitivity studies were completed and analyzed for both models and validation metrics were established.

Chapter 7 provides a discussion of the flow curves obtained from the successive flat rolling and tensile test, as well as from the hydraulic bulge test. Recommendations are also proposed for future improvements.

Chapter 2   Literature Review

2.1   Work hardening

Work hardening, or strain hardening, is the ability of a metal to increase in strength with plastic deformation. When a metallic specimen is plastically deformed dislocations are generated; as the dislocation density increases, dislocations interact with one another which restricts their mobility. As plastic deformation continues, additional force is required for dislocations to become mobile, thus leading to an increase in the flow stress of the material [11]. Dislocation density is quantified as the total dislocation length per unit volume of material and is proportional to the strength of a material. For example, a metal may have a dislocation density of 10^3 mm^{-2} in the as-received condition, while its dislocation density may increase to 10^9-10^{10} mm^{-2} [12] after cold rolling.

Many forming operations take advantage of the ductility of metals to form and shape products in a deformation process. However, the more a metal is work hardened by plastic deformation, the less ductility remains after forming.

Figure 2-1 [12] illustrates the trend of work hardening. The blue dot represents the yield stress, which can be seen to increase with the percent cold work. The red dot represents the ultimate tensile stress which follows the same trend. The green dot represents the strain at fracture; as percent cold work increases the fracture strain value decreases.
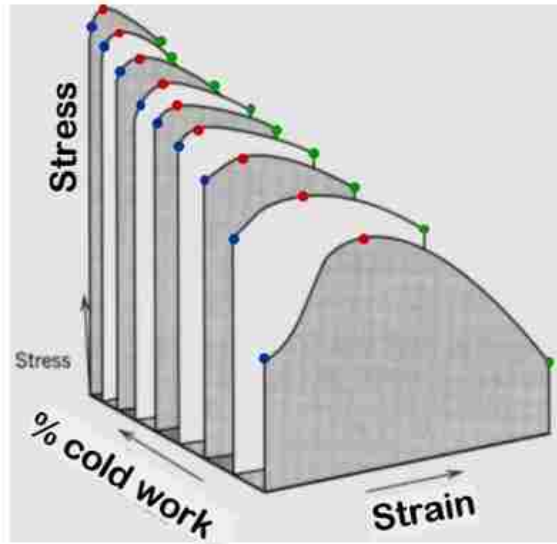
Figure 2-1. Stress as a function of percent prior cold work and strain [12]

2.2   Strain definitions

Before discussing the large deformation behaviour of sheet materials, it is necessary to first review various definitions of strain. The Seth-Hill family of strain is defined as follows [13] [14]:

$$\varepsilon = \frac{1}{\varkappa}(\lambda^{\varkappa} - 1) \tag{1}$$

where λ is defined as $\frac{L}{L_o}$ and $\varkappa$ is a constant that depends on the type of strain. The following types of strain include:

1. Engineering Strain ($\varkappa$=1): $\quad \varepsilon^{eng} = \lambda - 1 = \frac{L - L_o}{L_o} \tag{2}$

2. Logarithmic strain ($\varkappa$=0): $\quad \varepsilon^{log} = \ln(\lambda) = \ln(\frac{L}{L_o}) \tag{3}$

3. Lagrange strain ($\varkappa$=2): $\quad \varepsilon^{lag} = \frac{1}{2}(\lambda^2 - 1) \tag{4}$

If the strain is defined in one of the above manners it can be easily converted into any other form, as needed. Generally, strains are defined in either engineering or

8

logarithmic strain. DIC software calculates Lagrangian strains which must then be converted into more a common type.

If the strain type is not specified, then it is only accurate to one significant digit even though the results may be reported with more than one significant digit. As an example, if an experimental strain was reported with λ= 1.01000, then the three types of strain would be ε^{eng}=0.01000, ε^{log}=0.00995, ε^{lag}= 0.01005. The maximum difference between these strain values is 1.5 %, but this difference increases with the magnitude of the strain.

2.3   Bulge test background

A two-dimensional schematic of a typical bulge test set up is illustrated in Figure 2-2 [15]. A thin sheet specimen is placed firmly on the lower die which has a cavity containing an incompressible fluid; oil is generally preferred over water since it does not corrode the dies as water would. The sheet specimen is then clamped between the upper and lower dies. A lock-bead in the die prevents the sheet specimen from drawing into the die cavity. Generally, drawbeads are used to control material flow into a die cavity to minimize wrinkling and prevent fracture [16]. However, in a bulge test the sheet material should be fully stretched and therefore a lock-bead is used rather than a drawbead. As the lower punch rises, it pushes the piston at a predetermined speed, and causes a gradual increase of the pressure on the sheet specimen. The pressurized fluid causes the sheet specimen to deform and bulge. As the pressure continues to build, thinning occurs at the pole of the bulging specimen as it stretches, and eventually the specimen will burst; the whole forming process is completed with only a fluid in contact with the specimen.
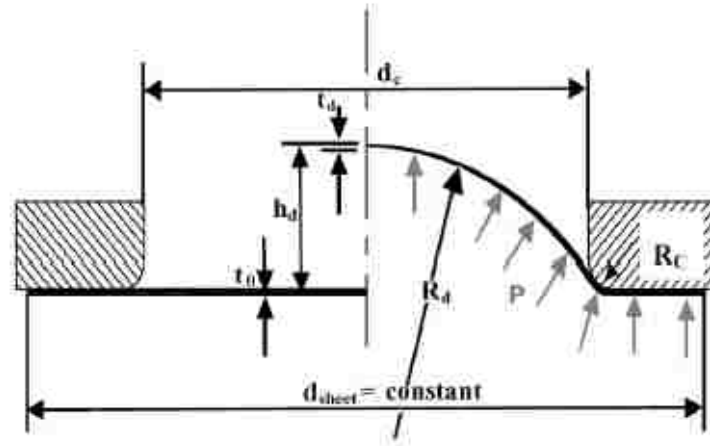
Figure 2-2. Schematic of a typical bulge test showing the important test parameters

Some disadvantages of the bulge test include the large height difference between the as-received specimen and the final bulged specimen. This may result in the sheet moving outside the calibrated field of view of the digital cameras when DIC is used for strain measurement, as the gauge area is quite large compared to that of other tests. Adequate sealing of the specimen in the bulge test apparatus in order to ensure that there are no oil leaks or pressure drops requires specialized equipment such as a piston seal and a suitable technique for sealing the sheet between the upper and lower dies.

There are several different bulge test apparatus configurations, depending on the diameter of the die cavity and the clamping tonnage capability. The bulge test design of Ceok Koh [17] relied on DIC software to track the position of the bulge and a plunger to displace the viscous medium. Gerhard Gutscher [18] designed a bulge test using a position transducer to track the displacement of the apex of the sheet specimen and a punch to displace the viscous medium. Generally, a press with a higher tonnage allows sheet materials with a wider range of tensile strengths to be tested, as well as sheet specimens with greater thickness. Figure 2-3 and Figure 2-4 show the various designs of bulge test facilities, and Figure 2-5 [19] shows an example of a bulged specimen.
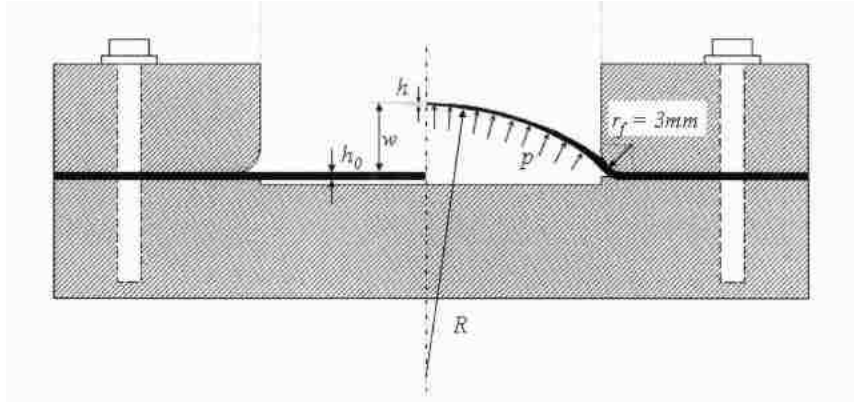
Figure 2-3. Ceok Koh's design of a bulge test [17]
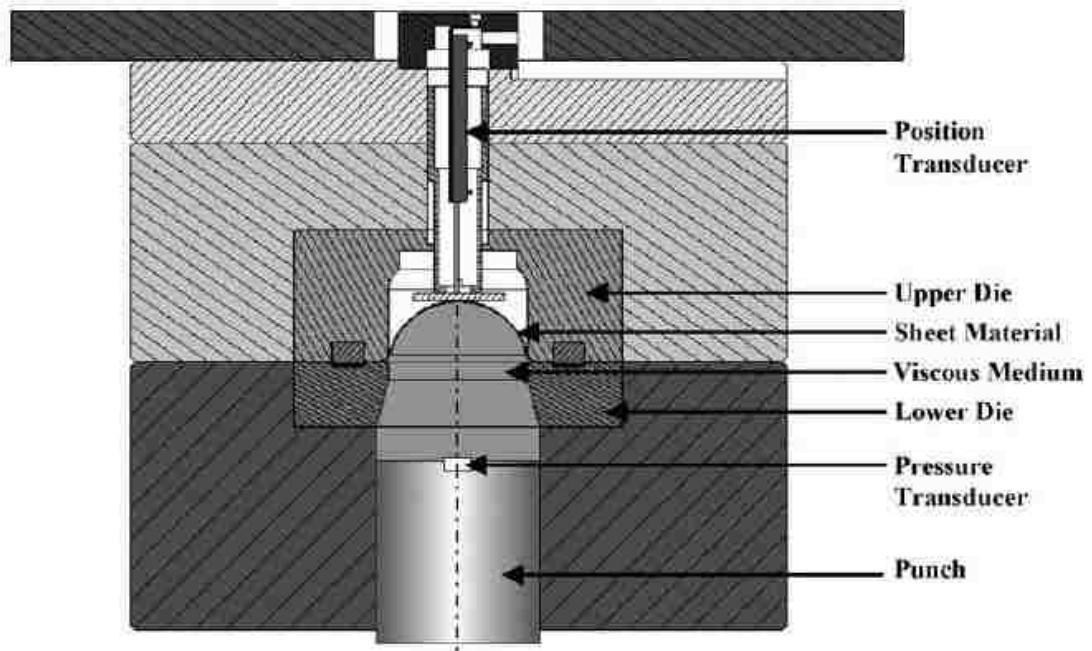
Figure 2-4. Gerhard Gutscher's design of a bulge test [18]

Figure 2-5. Example of a bulged specimen

11

2.4   Bulge test loading methods

There are two common ways of loading a hydraulic bulge test: the most common way, which will be investigated in this paper, is to load the specimen uniformly. This eliminates possible stress waves that may result from impulsive loading. These stress waves can lead to premature bursting with respect to the actual burst pressure of the specimen. Figure 2-6 shows the difference between static loading and impulsive loading [20] [21]. The end results are similar but the intermediate steps vary from one another.
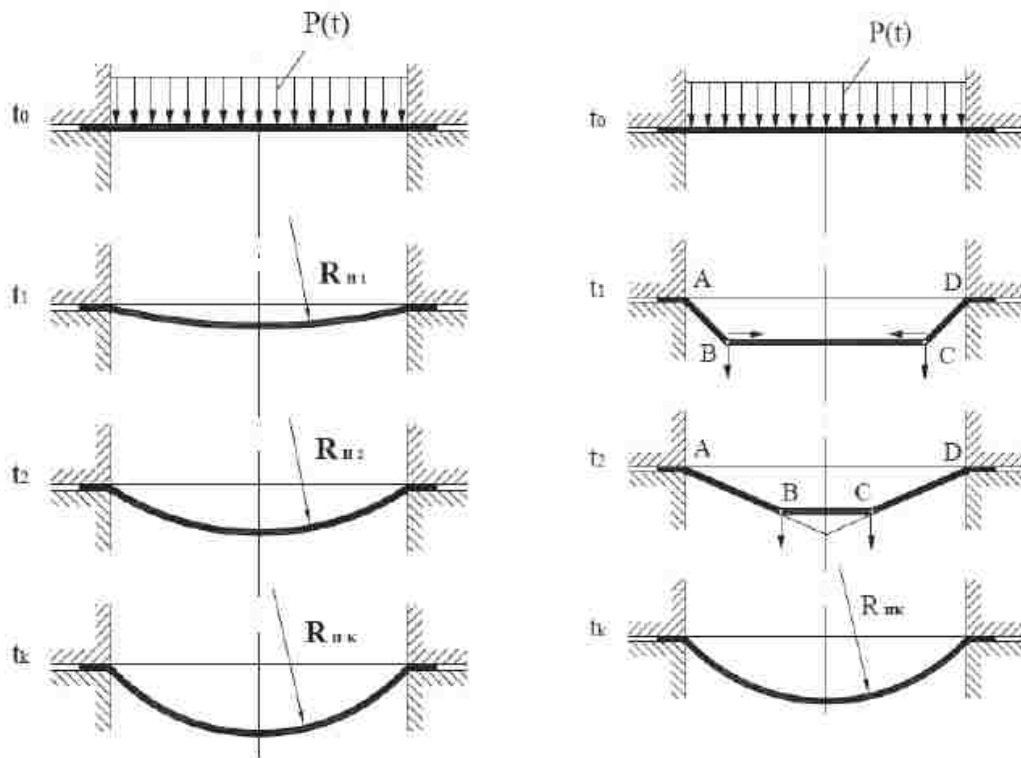
Figure 2-6. Static loading (left) vs. impulsive loading (right)[20]

It is important to apply a quasi-static loading during a bulge test in order to produce accurate flow stress curves. A slower rate of increase with respect to the piston height will allow the pressure to remain uniformly distributed across the sheet specimen. If the piston moves in a jerky fashion, stress waves will be produced and will lead to unreliable

results [20]. Another parameter that may affect the generation of stress waves is the diameter of the fluid cavity. The smaller the cavity is, the lower the pressure increment can be applied since the volume change per millimeter of stroke is small. This will result in a higher maximum pressure that can be achieved but will also result in a lower maximum volume capacity and thus an increased stroke length; an appropriate fluid volume must be chosen for the desired specimens to be tested. At a minimum, the volume of fluid displaced by the piston must be equal to the volume required to bulge the sheet specimen to a height equivalent to half its diameter. For example, a specimen with a 200 mm diameter would require a maximum volume of a half sphere having a radius of 100 mm.

2.5   Introduction to flow stress curve

Determining the flow stress curve from a tensile test is a simple and direct procedure: the raw force-displacement data are exported from the tensile testing machine, and converted to an effective stress versus effective strain curve. Determining the flow stress curve from bulge test data is not as straightforward. The pressure and dome height may be measured throughout the test using a pressure transducer and a potentiometer, respectively. The sheet thickness and radius of curvature at the top of the dome are difficult to measure continuously, and are therefore usually calculated. Once they are determined, however, the flow stress curve can be plotted using Eq. (5) and Eq. (6) below. Equation (5) will be discussed in further detail later in the chapter [15] [22].

$$\bar{\sigma} = \left[\frac{R_D}{t_d} + 1\right]\frac{P}{2} \tag{5}$$

$$\bar{\varepsilon} = -ln\frac{t_d}{t_o} \tag{6}$$

where $\bar{\sigma}$ is the effective stress, R_D is the instantaneous radius at the apex of the dome, t_d is the thickness at the apex of the dome, $\bar{\varepsilon}$ is the effective strain, p is the hydraulic pressure, and t_o is the initial thickness of the sheet.

An experimental setup was designed by Gologranc [23] that allowed all four of these variables to be simultaneously measured. This allowed for a direct measure of the flow stress curve without any need for post-processing of strain data measured with an optical measuring system or mathematical calculations. However, this testing facility was quite complex to build and operate, and difficult to obtain data from.

2.6   Analytical background and methodology

In order to determine a flow stress curve through the use of a bulge test, two methods can be used, a mathematical approach and a DIC approach. Several methods have been conducted in order to determine a flow stress curve, with the use of computation models, experimental results, and DIC software [24] [25] [26]. A common mathematical approach to determining the flow stress curve using the bulge test is to apply the membrane theory [27]. Since the membrane theory neglects bending stresses, it can only be used for thin sheet specimens which is generally applicable to most bulge tests. For a thin walled assumption to be valid there generally must be a wall thickness no greater than one-tenth of its radius [28]. When a sheet specimen is subjected to an internal gauge pressure *p* it will deform into the shape of a dome with radius *r* and wall thickness *t*. In its deformed state, the bulging specimen can be considered as a spherical thin walled pressure vessel, as illustrated in Figure 2-7. Since the spherical specimen is under static equilibrium, it must obey Newton's third law of motion. The stress must thus balance the internal pressure, which leads to the following equation:

$$\sigma * t * 2 * \pi * r = p * \pi * r^2 \qquad\qquad (7)$$
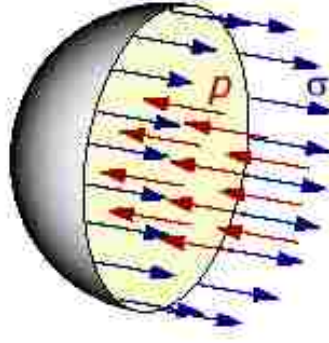
Equation (7) describes the static equilibrium in the pressurized specimen. The mathematical model must relate the known parameters to the unknown parameters, which in this case are the parameters that cannot be measured directly through the use of measuring instruments.

$$\frac{p}{t} = \frac{\sigma_1}{R_1} + \frac{\sigma_2}{R_2} \qquad (8)$$

σ_1 and σ_2 are the principal stresses in the plane of the sheet and R_1 and R_2 are the corresponding radii of the curved surface, t is the sheet thickness at the apex of the dome. In the case of an axisymmetric bulge test, the principal stresses are equal to one another and $\sigma = \sigma_1 = \sigma_2$ and $R = R_1 = R_2$.

Eq. (8) can therefore be simplified to the following:

$$\sigma = \frac{pR_D}{2t_d} \qquad (9)$$

Since the pressure is applied to the inside surface of the sheet, thus no normal forces act on the outer surface. This leads to the average through-thickness stress in the sheet, $\sigma = \frac{1}{2}(-p + 0) = \frac{1}{2}(-p)$. The effective stress can then be calculated using Tresca's yield criterion which states:

$$\bar{\sigma} = \sigma_{max} - \sigma_{min}$$

This leads to Equation (5) as defined earlier:

$$\bar{\sigma} = \left[\frac{R_D}{t_d} + 1\right]\frac{P}{2} \tag{5}$$

It can be seen through Equations (7) to (9) that two of the variables are difficult to measure directly during the experiment, they are:

1. Instantaneous radius of curvature, R_D
2. Instantaneous wall thickness at the apex of the dome, t_d

It is generally assumed that the top of the dome is spherical, which allows for a simplified calculation of the radius at the top of the dome, according to Equation (10) [15]:

$$R_D = \frac{d_c{}^2 + h_d{}^2}{8h_d} \tag{10}$$

where d_c is the diameter of the cavity and h_d is the height of the dome. Equation (10). assumes that there is no fillet in the cavity, but in most bulge test facilities this is not the case. Equation (11) takes into account the fillet of the cavity [15].

$$R_D = \frac{((d_c/2) + R_c)^2 + h_d{}^2 - 2R_ch_d}{2h_d} \tag{11}$$

where R_c is the fillet in the cavity. These equations were demonstrated by Pankin [30] who measured the radius at the top of the dome of the final bulged specimen using radius gauges. These results were compared to the calculated values of the radius at the apex of the dome using the dome height measurement, assuming that the dome is a part of a sphere and considering the fillet in the cavity. It was found that the calculations agreed with the experimental values for values up to $h_d/d_c = 0.28$. In Gologranc's [23] paper the experimental values also agreed for values up to $h_d/d_c = 0.28$.

In order to calculate the thickness at the apex of the dome, Hill [31] assumed that the locus of each point on the sheet is a circle during the physical test. Thus Hill proposed the following relationship:

$$t_D = t_o \left(\frac{1}{1+\left(\frac{2h_d}{d_c}\right)^2} \right)^2 \qquad (12)$$

This equation was used for several years until Chakrabarty and Alexander [32] proposed a slight modification which takes into account the strain hardening of the sheet as it deforms:

$$t_D = t_o \left(\frac{1}{1+\left(\frac{2h_d}{d_c}\right)^2} \right)^{2-n} \qquad (13)$$

where n is the strain hardening exponent in the power law function. Figure 2-8 shows the effects that the strain hardening index has on the sheet thickness at the apex of the dome, as predicted by Eq. (13).
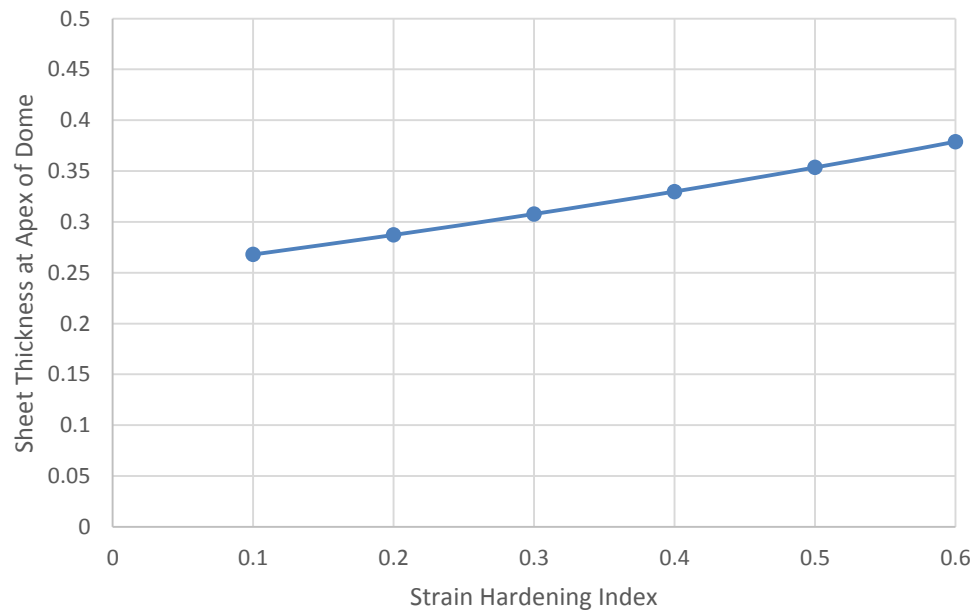
Figure 2-8. Sheet thickness predicted at the apex of the dome vs. the strain hardening index using Eq. (13) [22]

The initial conditions were set to a predetermined value, in this case an original thickness of 1 mm, a die cavity of diameter 100 mm and a dome height of 50 mm. The vertical axis shows what the theoretical thickness at the apex of the dome would

17

correspond to. When the strain hardening index is equal to two there is theoretically no change in thickness.

As Figure 2-8 illustrates, the strain hardening index is a factor that significantly affects the specimen thickness and must be considered in order to achieve accurate results when using Hill's equation.

To determine the flow stress curve, the radius and the thickness were calculated as a function of the dome height and the strain hardening exponent (*n* value). The following iterative process can be used to determine the flow curve. Figure 2-9 illustrates the process.
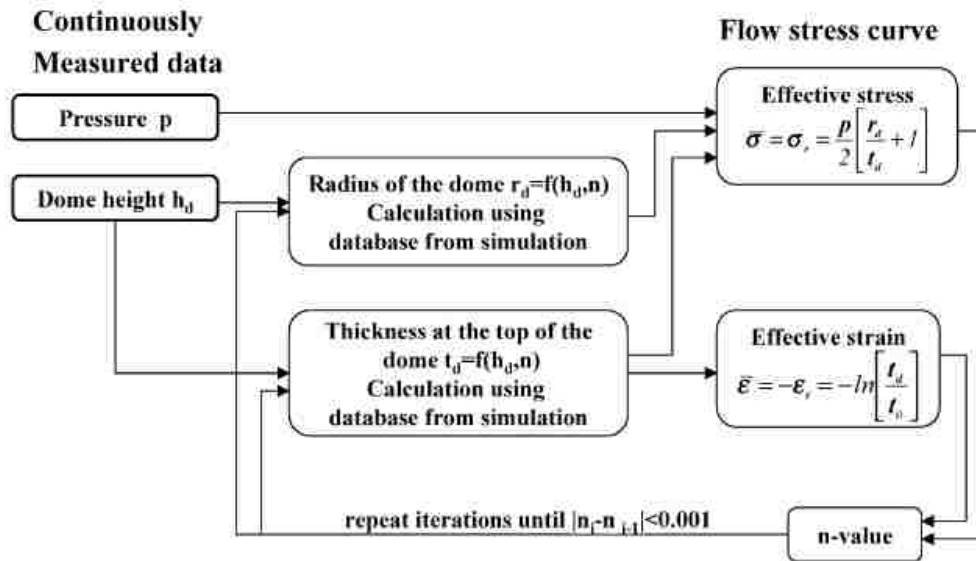
Figure 2-9. Iterative process to determine strain hardening index and the flow curve

A database must be made with a series of FE simulations that involve different material properties, in this case different *n* values. The database illustrates how the thickness and radius of curvature at the apex of the dome change with the dome height as the strain hardening index varies.

From the flow diagram, it is seen that pressure and dome height are easily measured throughout the test. In order to calculate the radius of the dome, an n value must be

assumed. The same is done for the thickness at the top of the dome. Both of these results are taken from the created database.

It was determined that with a constant strain hardening index the strength parameter in the power law function (K-value) varies linearly with stresses. This means that the K value has no influence on the deformation of the specimen when undergoing a bulge test [15]. The K value and the initial n value can be determined from a tensile test.

The effective stress and effective strain can be calculated with the assumed database values, knowing the K value and using the following Hollomon power law equation a new strain hardening index value can be calculated as shown in Eq. (14):

$$\sigma = K\bar{\varepsilon}^n \tag{14}$$

This process is done until the difference between successive n values is equal to or less than 0.001 [22].

More recently (2002), Kruglov et al. [33] proposed a method to determine the instantaneous thickness at the apex of the dome which does not require an iterative calculation. This equation takes into account the bulge radius as well. This was investigated and shown to provide the most accurate results in respect to the thickness at the dome [34]. Equation (15) was proposed by Kruglov et al. [33]

$$t_D = t_o \left(\frac{d_c/R_D}{\sin^{-1}(\frac{r_c}{R_D})} \right)^2 \tag{15}$$

2.7   Considering anisotropy

The above procedure assumes that the sheet material work hardens according to the Hollomon power law equation. It also assumes that the sheet material is isotropic, and therefore the Tresca yield criterion was used to calculate the effective stress. The flow stress curve that is predicted with these assumptions may not be accurate if the sheet

material is anisotropic. Anisotropic sheet materials have mechanical properties that vary from one direction to another and this needs to be accounted for when calculating the flow stress curves [22].

The plastic strain ratio (Lankford coefficient) is defined as:

$$R = \frac{\varepsilon_w}{\varepsilon_t} \tag{16}$$

where ε_w is the true width strain in a uniaxial tensile specimen as defined below:

$$\varepsilon_w = \ln(\frac{w_f}{w_o}) \tag{17}$$

where w_f and w_o are the final and original width of the tensile specimen, respectively, and ε_t is the true thickness strain in the tensile specimen, as defined in Eq. (18):

$$\varepsilon_t = \ln(\frac{t_f}{t_o}) \tag{18}$$

where t_f and t_o are the final and original thickness of the tensile specimen, respectively.

The plastic strain ratio R can be calculated for each of three orientations with respect to the sheet rolling direction, 0°, 45° and 90°, and these values are referred to as R_0 , R_{45}, and R_{90}, respectively. The ASTM standard E517 [35] provides a detailed procedure for determining R values, in which the elastic component of the total strain must be removed in order to calculate the plastic strain ratio.

The following equation shows some modifications that allow the sheet anisotropy to be taken into account [36]:

$$\bar{\sigma}_{ani} = \sqrt{\frac{R_{90}+R_0}{R_{90}\ (R_0+1)}}\ \bar{\sigma}_{iso} \tag{19}$$

If the sheet specimen has a normal anisotropy ($R_0 = R_{90}$) then Equation (19) reduces to:

$$\bar{\sigma}_{ani} = \sqrt{\frac{2}{R+1}}\ \bar{\sigma}_{iso} \tag{20}$$

where $\bar{R}$ is average plastic strain ratio, defined by Eq. (21)

$$\bar{R} = \frac{R_0 + 2R_{45} + R_{90}}{4} \tag{21}$$

2.8　Shear test

The shear test is another simple and effective way to determine the work hardening behaviour up to large strains. The shear test can be readily implemented into a universal tensile testing machine by using appropriate mounting fixtures. One of the main objectives involved with the design of a shear test is to limit the deformation to the intended gauge only, while also producing uniform strains. Miyauchi [37] designed an experimental setup for the determination of planar shear for sheet metals, in which the specimen has symmetrical slits, thus producing two areas of simple shear. Miyauchi's proposed specimen design was tested by several other institutes and was validated as an accurate and effective way of measuring shear strains [38] [39] [40].

Zillman et al. [41] investigated the length of the shear zone as it affects the measured work hardening. A new specimen was proposed that included shorter shear zones which lead to more accurate results. Figure 2-10 shows the different specimens designed by Zillman et al. [41]. Figure 2-11 schematically illustrates the deformation that occurs during a shear test. The indicated areas are clamped and the middle section is displaced vertically. There are several other experimental setups for shear test specimens that have been developed, some include designs by Brosius et al. [42], Yin et al. [43] and Shouler [44].
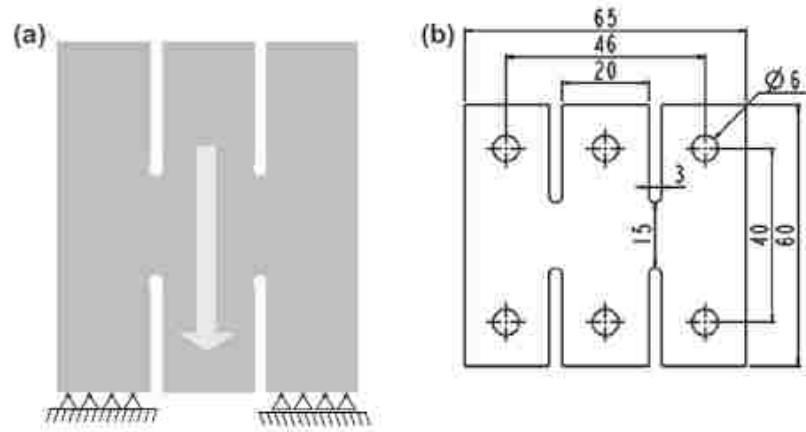
Figure 2-10. Shear test specimens designed by (a) Miyauchi [37] and (b) Zillman et al.[41]
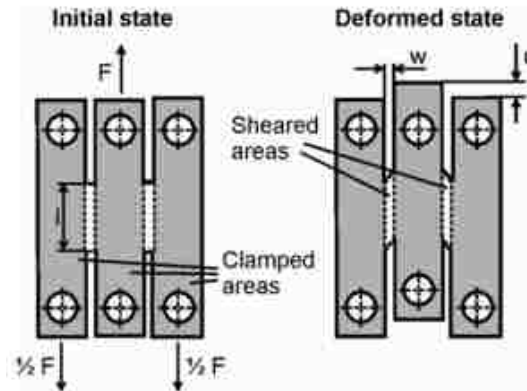
Figure 2-11. Shear test specimen before and after deformation [41]

The shear stress, τ_s , can be calculated from the following formula:

$$\tau_s = \frac{F}{2*l*t}$$
(22)

where F is the applied force, *l* is the length of the sheared area, and *t* is the thickness of the specimen.

The shear strain, γ, can be calculated from the following formula:

$$\gamma = \frac{u}{2*w}$$
(23)

where *u* is the displacement of the sheared specimen and *w* is the width of the shearing zone.

The ASTM B831 shear test standard was developed and designed for thin, wrought sheet metals (see figure 2-12). This simple shear test is designed to measure the ultimate shear strength of thin sheets while being adapted into a tensile testing machine. However, several issues occur with this design: firstly, stress concentrations occur at the notches of the specimen. Secondly, under monotonic loading the specimen also exhibits severe distortion. In order to overcome such issues, a modified specimen was created by Kang et al. [45], which includes a thickness reduction in the gauge section, that helped eliminate the rotation of the shear zone. Another shear specimen was designed by Merklein et al. [46] and includes a slight modification to the ASTM B831 specimen by adding a fixture to avoid any undesired distortion of the specimen. Figure 2-13 illustrates the modified specimen with the added fixture.
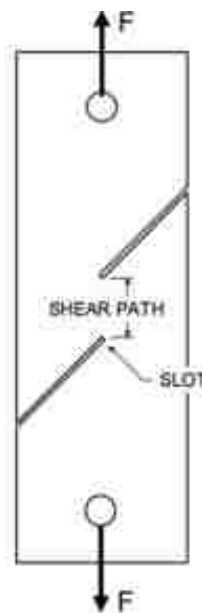
Figure 2-12. ASTM B831 shear specimen
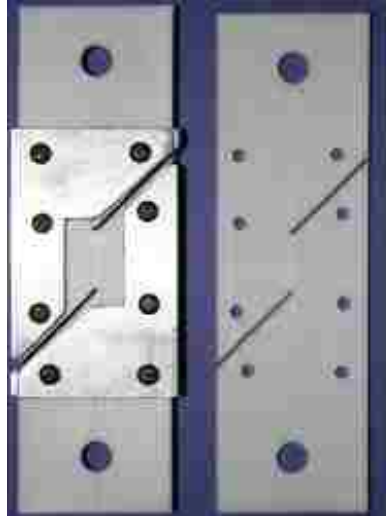
Figure 2-13. Modified ASTM B831 shear specimen with holder [46]

Peirs et al. [47] introduced a shear specimen illustrated in Figure 2-14 that was designed with two eccentric notches. The test was designed for use over a range of strain rates, as well as up to high strains. The geometry of the eccentric notches in the middle of the specimen was optimized in order to produce uniform strain readings throughout the test. As with all of the above tests, DIC was used to measure the strains directly on the surface of the specimen during the test. This allowed for direct readings and easy observation of strain patterns. This specimen was experimentally tested and results were promising, both in terms of uniformity of strains as well as limiting the deformation to the intended gauge area only.
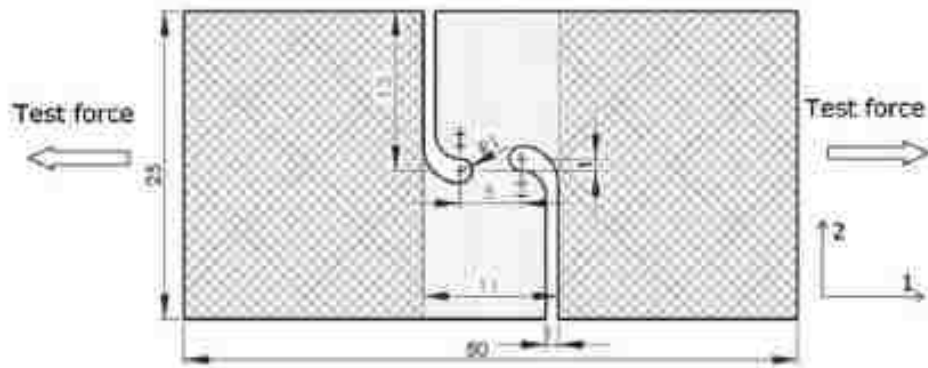
Figure 2-14. Eccentric notch shear specimen [47]

Figure 2-15 shows the typical differences that are seen between the flow curves obtained from a standard tensile test and from a shear test. It can be noted that the yield point in a shear test is much lower compared to that in a tensile test. The yield point is also not as well defined as in the tensile test, and the work hardening behaviour is also different.
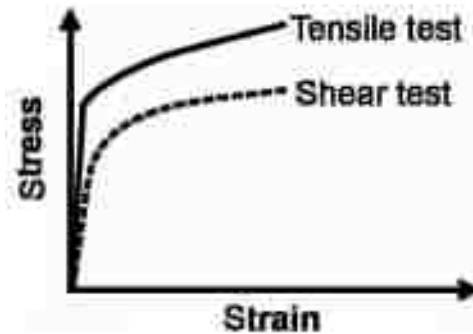
Figure 2-15. Comparison of tensile test and shear test flow stress curves

2.9   Cruciform test

The cruciform test is another method of obtaining biaxial states of stress and has some distinct advantages. This test method can measure the elastic – plastic behaviour of sheet materials for an arbitrary principal stress ratio (σ_2/σ_1) [48]. The entire test is completed in one plane, which is a key advantage compared to the out-of-plane deformations that occur in hydrostatic bulge testing. The four arms of the cruciform specimen are given a displacement, which in turn generates tensile forces in two perpendicular directions.

For successful biaxial testing the strain distribution must be symmetric throughout the test. In order to achieve this, bending must not be induced into the test specimen. A generic cruciform specimen is shown in Figure 2-17 [49]. Tests have been done that show the difference between four actuators (case a) and two actuators (case b). In case a, the cruciform specimen maintains co-linearity which avoids any bending moments. Each arm of the specimen is pulled at a force that is equal to that in the opposing arm, in this case P to P' and F to F'. Another requirement is that the direction of the collinear forces F and F' must be exactly perpendicular to that of forces P and P' [49].

Case b in Fig. 2-16 illustrates the type of cruciform specimens that rely on only two actuators and have the other two arms of the specimen clamped/fixed. As can be seen, the centre of the specimen is subject to lateral bending, which is undesirable. This also leads to non-uniform strain distributions throughout the specimen. In reality, it is very difficult to avoid any bending in the arms of the specimen when it is loaded with only two actuators. Using four actuators allows the specimen to be constantly and evenly loaded in two perpendicular directions throughout the test.
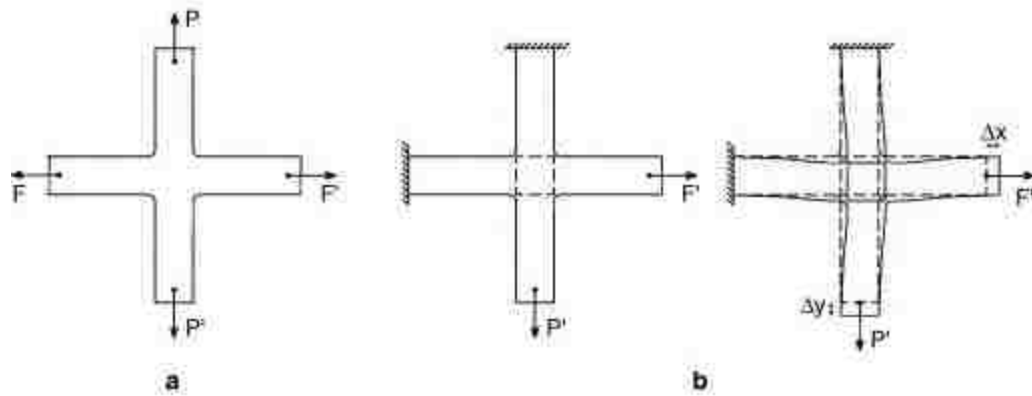
Figure 2-16. Cruciform specimen with four actuators (case a) and two actuators (case b)

The cruciform test was first studied by Kuczynski et al. [50] and Kelly [51]. This was done in the 1960's to late 1970's. The specimens designed were able to achieve a near homogeneous strain distribution but were not able to reach necking or fracture, each for different reasons. Müller and Pöhland [52] were able to design a specimen that was used to determine the yield-locus. Hoferlin et al. [53] also achieved the same thing by using small clamps to prevent bending moments.

Hanabusa et al. [54] stated that the majority of cruciform specimens fall into two categories, the first being specimens that have a reduced thickness area, and the second being specimens that have a uniform thickness. Over the years, several different types of specimens have been proposed. Pascoe introduced a specimen that included spherical recesses on both sides of the central region. [55] Shiratori introduced a specimen that consisted of one cross-shaped sheet sample and eight plates in order to reinforce the four arms [56]. Both of these specimens have a gauge area with a reduced thickness. The fabrication of these types of specimens is quite challenging and requires extra machining. Another issue that results from reduced thickness is the change in material properties due to the manufacturing, such as work hardening.

Kuwabara et al. [57] introduced a cruciform specimen with a uniform thickness that also had a number of slots in each arm. The parallel slots were implemented to ensure that the stress distribution in the gauge area is kept as uniform as possible throughout the

test. Figure 2-17 shows the proposed specimen without any dimensions. Several other authors have also done research on this type of cruciform specimen which shows promising results [53] [57] [58].
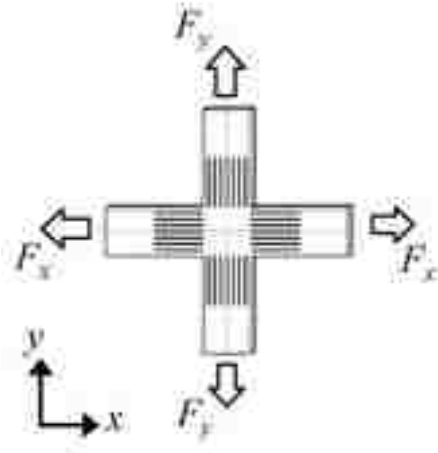
Figure 2-17. Cruciform specimen designed by Kuwabara et al. [57]

Yu et al. [59] introduced a unique specimen that also achieved successful results. The intent behind the design of this specimen was to obtain the most uniform stress distribution as possible in the central region. In order to achieve this the center of the specimen was thinned down, with an additional thickness reduction in the shape of a cross, and inside of that a dished circular area. This specimen geometry was optimized using FEA. The various shades of gray show the thinned areas.
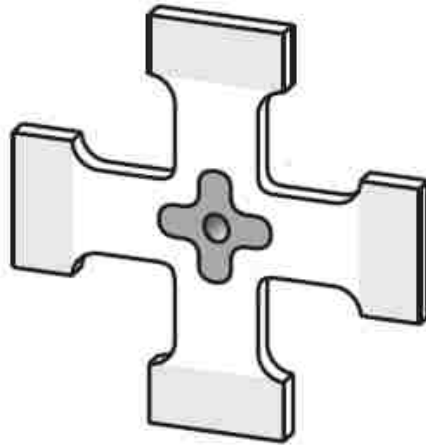
Figure 2-18. Cruciform specimen proposed by Yu et al. [59]

Green et al. [60] used a cruciform specimen with a thinned gauge area and with slots in the arms that allowed the gauge area to exhibit reasonably uniform strain distributions, for a range of stress ratios, up to relatively large deformations ($\varepsilon \approx 0.2$).

The greatest challenge with cruciform specimens is to calculate the stresses in the gauge area, since this cannot be done from direct measurement of the forces applied to the arms. Stresses in the gauge of a cruciform specimen can be calculated using an iterative procedure in which the force-displacement curves in the arms predicted by FEA are compared with the experimental curves. A correction is then applied to the assumed input flow curve of the material and simulations of the test are carried out again until the error between the predicted and experimental force-displacement curves is less than a specified amount.

2.10 Summary of work hardening tests

Tensile testing after successive rolling can achieve strains over 100% compared to results without rolling which leads to uniform elongations of only 15-30 % strain. The pre-strain of the specimen can be calculated and it is known beforehand, allowing for accurate strain increments to be obtained when plotting a flow stress curve. However, this process is labour-intensive and a tensile test is still limited to uniaxial loading.

The shear test can provide data upwards of 40% strain and has the advantage of being able to be implemented into a uniaxial tensile testing apparatus. However, gripping of a shear test specimen is generally an issue and is hard to control. Moreover, producing uniform shear strains in the gauge is also a challenge and the shear test is still limited to a single loading direction.

An advantage of the cruciform test is that it is a biaxial test with no out-of-plane deformations. When manufacturing a cruciform specimen there may be a change in material properties due to the outer layer of the specimen being removed. A complex cruciform specimen can cost over $1000; comparing this to a tensile test specimen at a few dollars leads to a big cost discrepancy. Another disadvantage is the possibility of the specimen being subject to in-plane bending throughout the gauge during the test.

The bulge test is a biaxial test that can produce strains beyond 60% and it does not have as many issues as the other tests mentioned above. A bulge test is not a labour-intensive process, clamping of the specimen is easier to control, and the cost of a specimen is cheaper than a tensile test specimen. However, producing a flow stress curve is more involved compared to the tensile, shear, and cruciform tests.

Chapter 3   Bulge Test Design

The bulge test die was designed such that it could be operated in a 240-ton double-action hydraulic press located in the Mechanical Testing laboratory at the University of Windsor. The features and maximum capacity of this press helped to determine the dimensions and limitations of the bulge test tool. This chapter will present both the design criteria and the final design of the bulge test die, as it was constructed.

3.1   Determination of piston size

A piston and seal will be mounted to the inner punch rod and will be used to displace an incompressible fluid, in this case oil, inside a compression chamber which will cause a circular sheet specimen, clamped around its periphery, to bulge out. The maximum pressure that can be generated in the compression chamber will determine the maximum tensile strength and thickness of sheet materials that can be bulged to failure. Likewise, the maximum pressure will be limited by the design of the piston and the maximum punch force capacity of this press, which is 1000 kN.

Step 1: determination of piston diameter.

A volume versus pressure capacity table was created to determine an appropriate piston diameter that met the desired goals in terms of maximum pressure. The following procedure was implemented in order to determine the required design parameters. The pressure was determined using Eqn. (24):

$$P = \frac{F}{A} \tag{24}$$

where F is the maximum clamping force (1000 kN) and A is the surface area of the blank that is pressurized by the forming fluid. The surface area is calculated from the diameter of the blank that is yet to be determined. Table 1 shows the maximum pressure that can be achieved for corresponding values of piston diameter.

Diameter (mm)	Maximum Pressure (MPa)	Maximum Pressure (psi)
100	127	18466
105	115	16749
110	105	15261
115	96	13963
120	88	12824
125	81	11818
130	75	10927
135	69	10132
140	64	9421
145	60	8783
150	56	8207
155	53	7686
160	49	7213
165	46	6783
170	44	6389
175	41	6029
180	39	5699
185	37	5395
190	35	5115
195	33	4856
200	31	4616

Table 1. Piston diameter versus maximum pressure

This data is also shown in the form of a graph in Figure 3-1.
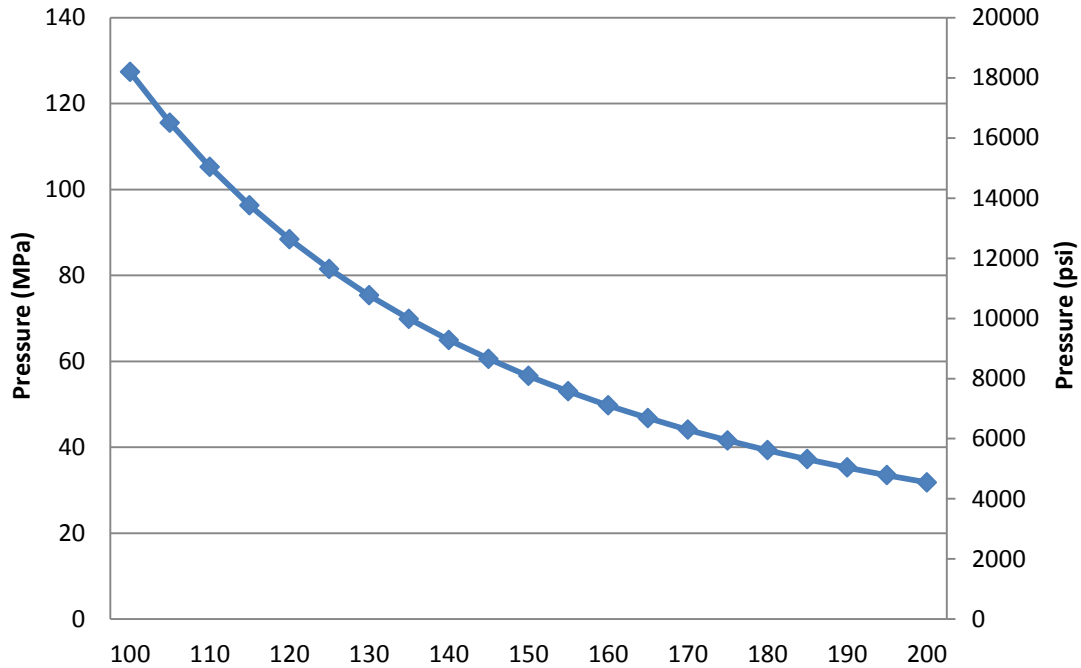
Figure 3-1. Maximum achievable pressure for a given piston diameter

A blank diameter of 135 mm was selected because it allowed sufficient room on the outer edge to clamp the specimen into place. This was also a blanking die configuration available at the University of Windsor, thus allowing for blanks to be made in house.

Step 2: determination of the volume of the pressure chamber

When a 135 mm diameter blank is fully bulged into a hemispherical shape, the radius of the bulged specimens would be 67.5 mm. Even the most ductile sheet materials will not likely bulge further than a perfect hemisphere without rupturing. Assuming this is the limiting case, the maximum volume of fluid that needs to be displaced in order to fully bulge a formable specimen is determined by Eqn. (25)

$$V = \frac{4\pi r^3}{6} \tag{25}$$

where r is the radius of a sphere. If the radius of a fully bulged specimen is 67.5 mm, then the maximum volume of fluid required to fully bulge the specimen would be half of the corresponding sphere, i.e. 1,288,253 mm^3.

Since the maximum punch stroke of the press is 508 mm, the maximum piston stroke must be somewhat less than this in order to displace a volume of fluid within the compression chamber that will fully bulge a sheet specimen. Table 2 presents the volume change per millimeter of piston displacement as well as the piston stroke required to achieve maximum volume capacity, for selected piston diameters.

Piston Diameter (mm)	Volume Change Per 1 mm Piston displacement (mm^3)	Maximum Piston Stroke to Achieve Desired Volume (mm)	% of Maximum Press Piston Stroke
100	7853	266	52.49%
105	8659	241	47.61%
110	9503	220	43.38%
115	10386	201	39.69%
120	11309	185	36.45%
125	12271	170	33.60%
130	13273	157	31.06%
135	14313	146	28.80%
140	15393	136	26.78%
145	16513	126	24.97%
150	17671	118	23.33%
155	18869	111	21.85%
160	20106	104	20.51%
165	21382	97	19.28%
170	22698	92	18.16%
175	24052	87	17.14%
180	25446	82	16.20%
185	26880	77	15.34%
190	28352	73	14.54%
195	29864	70	13.80%
200	31415	66	13.12%

Table 2. Piston diameter, volume change per mm of piston displacement and percentage of maximum stroke

As shown in Figure 3-2 the smallest piston diameter would lead to 53 % of the maximum stroke being used while the largest diameter would lead to 13.12 % of maximum stroke

being used. The entire range of piston diameters is thus acceptable with respect to displacing the required maximum volume of fluid. As mentioned in Chapter 2, a smaller volume change per millimeter of piston displacement is beneficial as it allows better control of the sheet bulging process.

As the maximum piston stroke is increased in the design, so also does the size of the pressure chamber as well as the overall size of the die. In order to minimize the cost of the die, the volume of steel needed to build the die must also be minimized. Therefore, an appropriate combination of piston diameter and piston stroke was determined in order to achieve the complete bulging of sheet specimens and good process control while limiting the cost of the die.
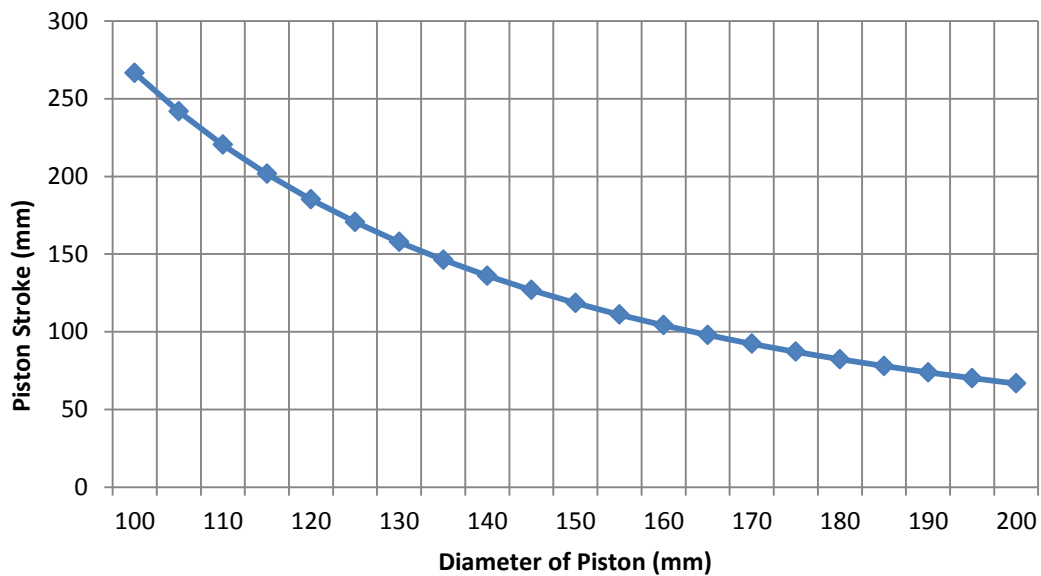
Figure 3-2. Required piston stroke to achieve desired volume

Step 3: determination of piston diameter.

Designing a piston that is capable of sealing pressures illustrated in Figure 3-1 was challenging when considering 100 to 200 mm diameters. After research, the greatest standard piston size that could be purchased was found to seal up to a pressure of 69.9 MPa with a diameter of 120 mm. A pressure greater than this would lead to the seal

failing. Thus a piston diameter of 120 mm was chosen, this provided a good combination of maximum achievable pressure as well as volume change per mm of piston movement. This also allowed the tooling of the press to be small enough to fit into the opening of the hydraulic press; a higher stroke would have required a bigger tool in terms of height. With a piston diameter of 120 mm, the current working space between the upper and lower dies when the press is fully opened is 6 inches; any smaller of a piston would have resulted in a working space of only 4-5 inches, which is not practical.

Two solutions were produced in order to ensure that the pressure does not exceed 69.9 MPa.

Solution 1: The maximum punch force was reduced to 780 kN in order to ensure that with a piston diameter of 120 mm the maximum pressure achievable did not exceed 69.9 MPa.

Solution 2: The pressure transducer was set-up with a cut-off point, as soon as the pressure reached a certain value that was programmed, the press would turn off and thus the pressure would be immediately stopped. A safety factor of 1.1 was also incorporated.

By implementing two safety precautions, one in the maximum press force, and one in the software of the press, the piston pressure will not exceed 69.9 MPa.

Step 4: An FEA model was created in order to ensure that a pressure of 69.9 MPa could burst a 1.5 mm thick DP600 steel. Details of the FEA model can be found in chapter 6

A referenced sheet material, 8650 wrought steel, was used in one simulation. The mechanical properties of this sheet material were taken from Varmint Al's Engineering page [61]. 8650 wrought steel has a yield stress of 1000 MPa and an ultimate tensile stress of 1300 MPa, whereas DP600 has a yield stress of 400 MPa and an ultimate tensile stress of 650 MPa [62]. The sheet thickness that was used in the simulation was also increased to 1.7 mm compared to the thickness of the DP600 steel sheets that will be used which is 1.5 mm.

In the FE simulation, the 8650 wrought steel specimen was bulged to the maximum bulge height, in this case one half of the 135 mm diameter, a bulge height of 67.5 mm, and this required a predicted pressure 52 MPa. This demonstrates that 69 MPa is indeed sufficient to bulge DP600 to the desired bulge height considering that 8650 wrought steel has a higher yield and tensile strength while also being thicker.

A maximum pressure of 69 MPa also provides the capability to carry out bulge tests up to the onset of failure using AHSS sheet specimens with greater tensile strength and/or greater sheet thickness than even this 8650 wrought steel reference material that was used in this numerical simulation.

3.2 Clamping the sheet specimen

When conducting a hydraulic bulge test, it is necessary to stretch-form the specimen so that it is subjected to fully balanced biaxial tension. This requires that the specimen be securely clamped around its periphery in order to avoid any material drawing in. However, the closing force of the blankholder may not be sufficient when testing higher strength sheet materials. If the blankholder force is insufficient, there is a risk that the sheet material will flow into the forming zone. The maximum blankholder force capacity of the press is also 1000 kN. In cases where this blankholder force is not sufficient to securely clamp the specimen, the bulge test die was designed with an additional clamping mechanism.

The hydraulic bulge test die was designed with a support ring that can be used to bolt the sheet specimen into place using 12 M12 bolts which have a minimum tensile strength of 400 MPa [63]. This bolted support ring allows for an additional distributed load to be applied around the periphery of the specimen and also ensures that the specimen will not draw in during a bulge test.

The hydraulic bulge test can be conducted in one of two configurations: configuration 1 consists of conducting a test without the use of the 12 M12 bolts, and configuration 2 makes use of the 12 M12 bolts to add extra clamping force. For lower strength sheet

materials, configuration 1 offers the convenience of saving the time and cost involved in drilling holes in each circular blank prior to testing. However, high strength sheet materials usually require the additional clamping force provided by the bolted support ring.

A third clamping solution was also considered for higher strength sheet materials in which the blank would be held in place using a lockbead. The upper die is removable, and thus it would be possible to design an upper and a lower ring with a mating lockbead. The mating upper and lower rings would be designed with clearances suitable for a narrow range of sheet thicknesses and might also allow for the height of the lockbead to be adjustable, depending on the severity of the bends required to lock the sheet material [64].

The final design of the bulge test die has the following key dimensions shown in Table 3:

Piston Diameter	120 mm
Diameter of the cavity in the upper die	135 mm
Number of M12 bolts	12
Radius of the fillet	3 mm
Maximum Piston Stroke	170 mm
Maximum Force	10,000 kN

Table 3. Bulge test critical parameters

A detailed component list of the bulge test die can be found in Appendix 1

3.3   Main die block

The main die block, shown in Figure 3-3, has a length of 400 mm, a width of 395 mm and an overall height of 265 mm. There are 12 concentric threaded holes around the opening in the block. The piston has diameter of 120 mm. The bottom of the main block has a 100 mm diameter encasement that functions as a downward stopper for the piston, to prevent the piston with its seal from being pulled out from the bottom of the die block as this would damage the seal. The red arrows indicate that the top of the die is designed with a 25-mm-step for protection: in the event that an oil leak occurs during

a test, the oil under pressure will first hit the protective step rather than endangering the press operator.
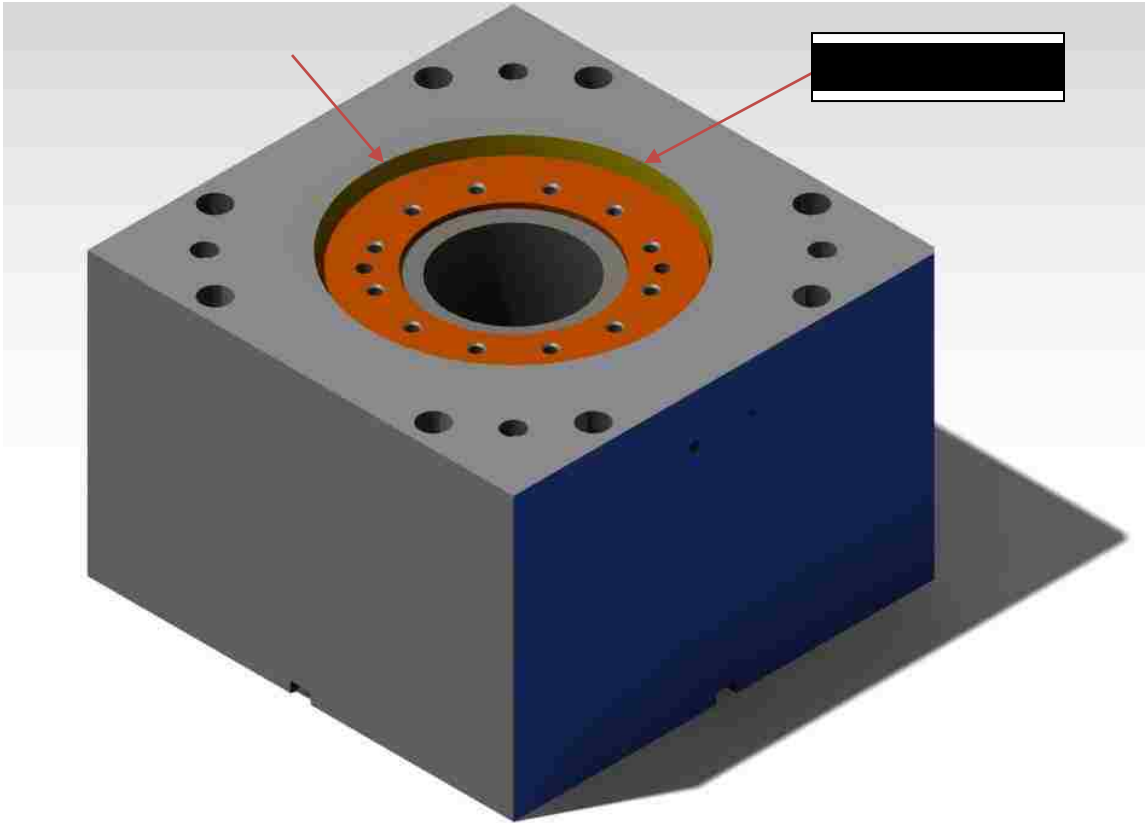
Figure 3-3. Main die block (Catia model)

3.4 Clamping ring

The clamping ring was designed with the purpose of securely clamping and sealing the specimen around its periphery, while allowing it to bulge up inside the ring. The two black arrows show the position of the clamping ring in Figure 3-4. The clamping ring incorporates two locating holes so that the locating pins will ensure that the clamping ring is always located in a consistent position.
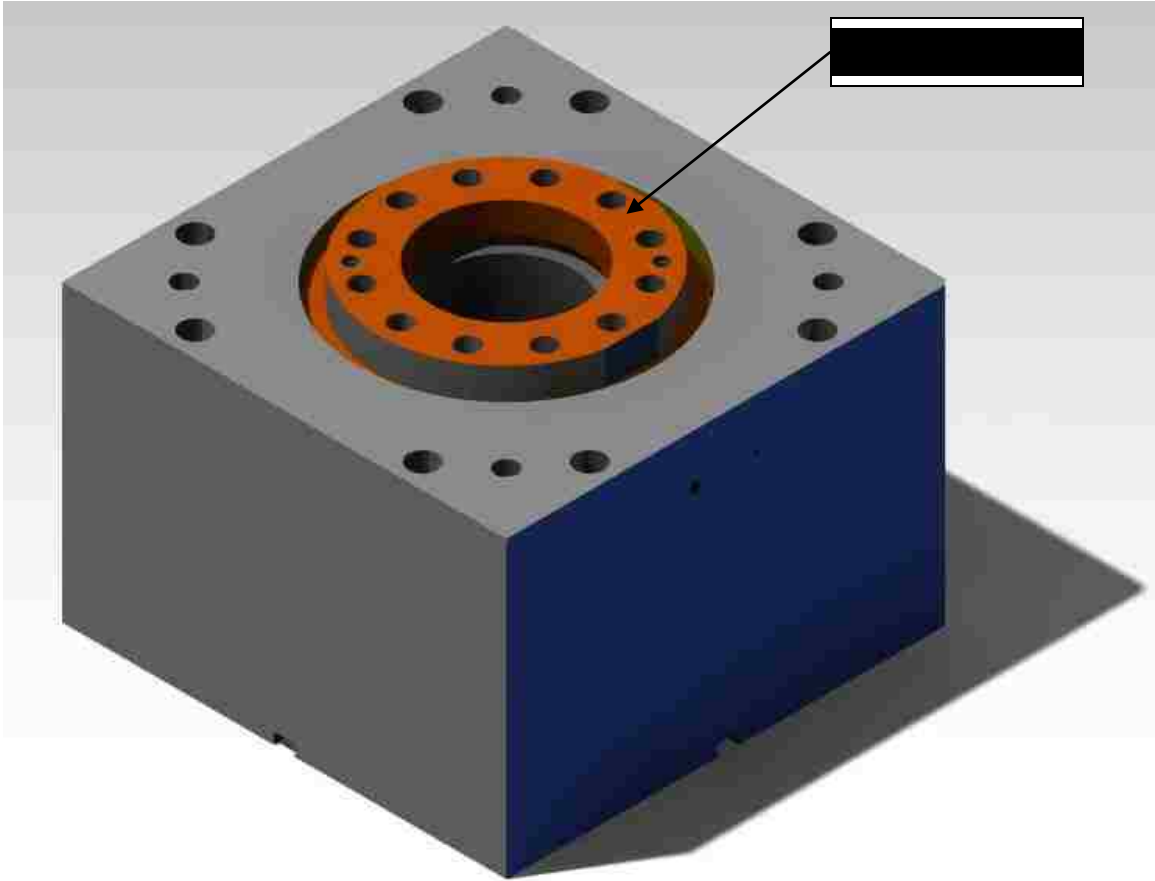
Figure 3-4. Clamping ring with 12 bolt holes and 2 locating holes (Catia model)

The inside diameter of the clamping ring is 135 mm, which allows the sheet material to bulge out within this opening. A 3 mm radius, as can be seen in Figure 3-5, on the inside fillet of the clamping ring ensures that the specimen does not shear when the sheet specimen bulges and wraps around this inside radius.
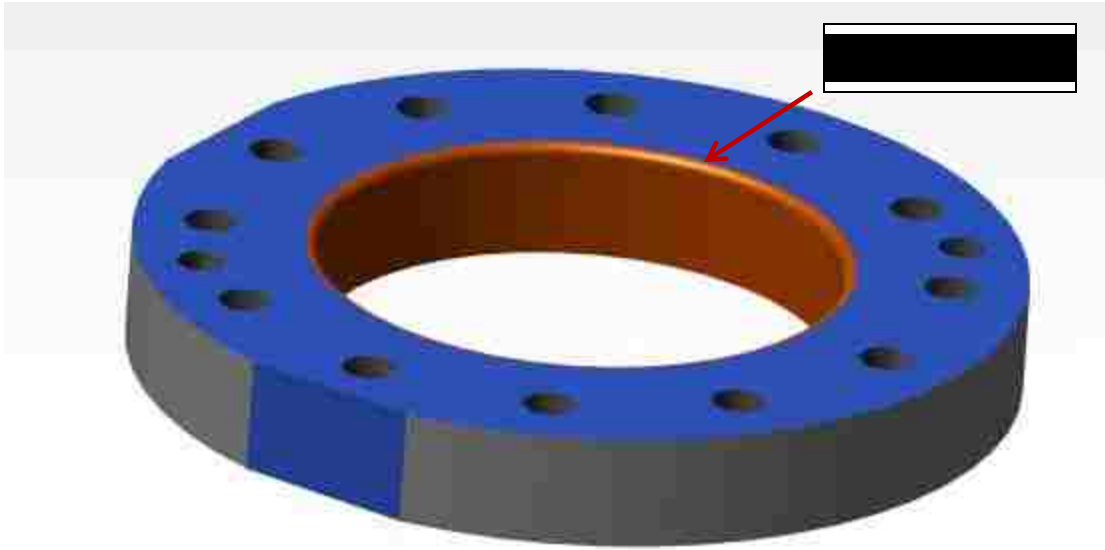
Figure 3-5. Clamping ring with 12 bolt holes and 2 locator holes (Catia model)

3.5   Upper die block

The upper die block was designed to close down onto the clamping ring to hold the sheet specimen in place and seal the pressure chamber during a bulge test. This was implemented by designing a 50° chamfer from top to bottom. The eight threaded holes are used to install the upper block onto the top of the Eagle press, and the four slots are used to locate the upper block in place.

This design of the upper die block also includes a central opening that allows the digital cameras mounted on top of the press to focus on the specimen through the large chamfered opening in the crown of the press, while providing sufficient light to properly illuminate the test specimen. This allows the digital cameras to record higher quality images due to a lower aperture being used. Figure 3-6 illustrates the upper die block.
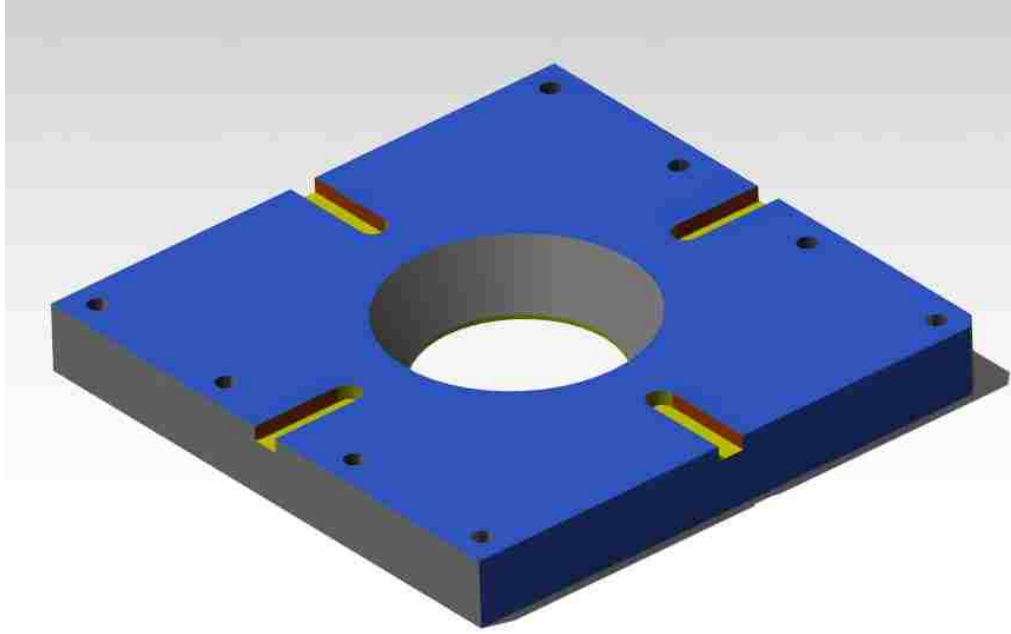
Figure 3-6. Upper die block with central chamfered opening (Catia model)

3.6   Piston and honed tube

A custom piston head was designed so as to be able to accommodate a specialized seal that can operate up to a maximum specified pressure of 69.9 MPa. This piston head was machined and customized in order to meet the requirements of the seal manufacturer and ensure that the maximum operating pressure could indeed be attained.

A custom honed tube was purchased that is specifically designed for uses in hydraulic fluid applications. The honing process involves using abrasive polishing stones and abrasive paper to remove small amounts of material and produce an inside surface with very precise dimensions and tolerances, and a surface roughness no greater than 0.4 µm. A Team Tube-Metric Honed tubing was used with an inner diameter of 120 mm, an outer diameter of 6 inches and a length of 245 mm. The honed tube is made of a specially treated 1026 steel

3.7   Seals, O-rings and fittings

An AS568-225 O-Ring was selected with an inner diameter of 47.22 mm and a cross-section of 3.53 mm, and was mounted on the top surface of the piston head, as indicated by the black arrow in Figure 3-7. Figure 3-8 shows the technical drawing of the seal.
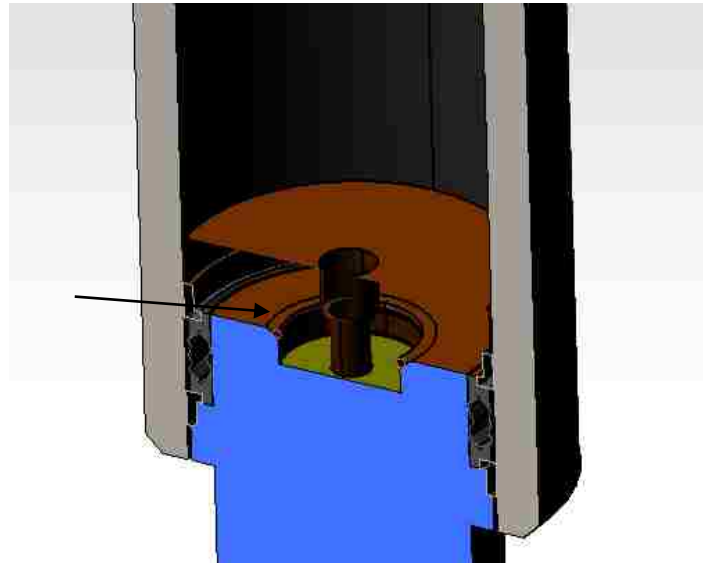
Figure 3-7. AS568-225 O-Ring
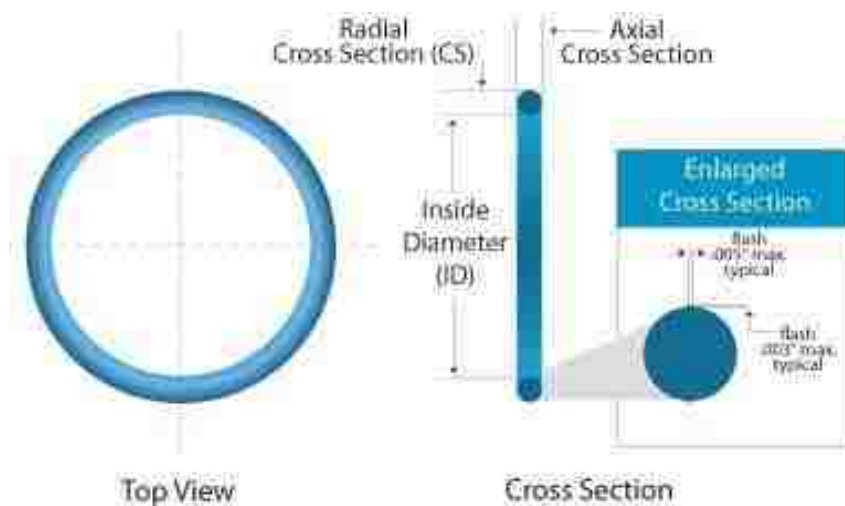
Figure 3-8. Drawing of the AS568 O-rings used in the bulge test die

A specialized Selemaster DSM piston seal was purchased that was selected based on the 120 mm piston diameter size. Selemaster piston seals are manufactured with a highly compression resistant nitrile. This allows it to reach very high pressures. Figure 3-9 shows the schematic for the Selemaster DSM piston seal.
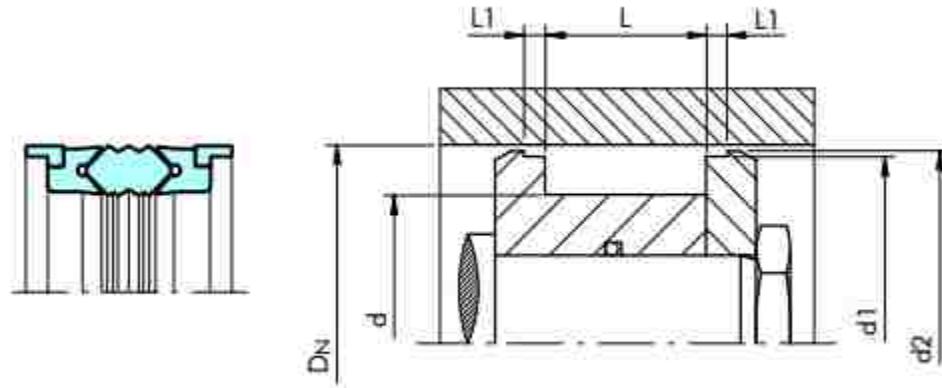
Figure 3-9. Selemaster DSM piston seal schematic

Dn	120 mm
d	100 mm
L	35 + 0.2 mm
L1	9.52 + 0.1 mm
d1	112.80 +/- 0.05 mm
d2	117.5 +/- 0.07 mm

Table 4. Selemaster DSM piston seal parameters

Fittings are used as leak-free connections for power and instrumentation in the bulge test design. In order to properly connect the pressure transducer and the dump valve proper fittings were needed. A Parker high-pressure 69.9 MPa pipe fitting steel ½ '' inch NPT (National Pipe Taper) nipple, Figure 3-10, as well as a Parker high-pressure 10k pipe fitting steel ½ '' NPT 90 degree elbow, Figure 3-11, were used for the pressure transducer and dump valve, respectively. NPT are used for connections where pressure tight joints are made on the threads utilizing a thread sealant. All fittings were made in stainless steel.
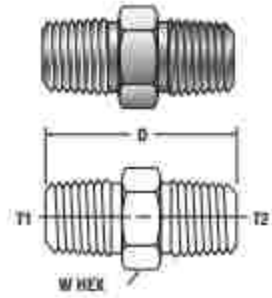
Figure 3-10. Pipe fitting 1/2'' NPT nipple

T1	½ ''
T2	½ ''
W Hex	7/8''
D ins.	1.89 ''

Table 5. NPT nipple parameters

Figure 3-11. Pipe fitting 1/2'' NPT elbow

Thread Size	½''
A	1.31"
B	1.32"
C A/F	1.00"

Table 6. NPT elbow parameters

3.8 Pressure transducer

In order to continuously measure and record the actual pressure inside the pressure chamber of the bulge test die, it was designed to be equipped with a built-in pressure transducer. A Barksdale 423 series general industrial (amplified) pressure transducer was selected because of its compatibility with the control system and data acquisition system of the hydraulic press. An excitation voltage of 24 VDC was used with an output of 4-20 mA and a secondary output possible with 0-10 volts. A range of 0-69 MPa is available with a frequency response of 2 kHz and a resolution of 0.006895 MPa. Figure 3-12 shows a photograph of the pressure transducer that was used. The electrical connection was made with a 3 conductor, 24 American wire gauge (AWG), PVC jacked, shielded cable that is 1.0 m long with integral strain relief and case grounding.

Figure 3-12. Photograph of the Barksdale pressure transducer

Chapter 4　　Experimental Procedures

4.1　Tensile test procedures

Rectangular blanks were flat rolled to effective strains of 0.2, 0.4, 0.6, 0.8 and 1.0 and then were prepared for tensile tests following ASTM E8 standards. Electro-etching was used to measure the width strains of the specimen and DIC measurements were used in conjunction with a mechanical and video extensometer to calculate the principal strains. A Matlab code was created to produce the flow stress curve.

4.1.1　Specimen preparation

A guillotine shear was used to cut tensile specimens to a width of 30 mm and an overall length of 500 mm. Figure 4-1 shows the dimensions required by the ASTM E8 [65] standard for thin sheet metals. The overall length is to be 200 mm, while the overall height should be 20 mm. By shearing the sheet to a length of 500 mm, two tensile specimens can be machined to the final shape using wire-EDM. An overall height of 30 mm allows for a sufficient working tolerance to properly machine the tensile specimens.
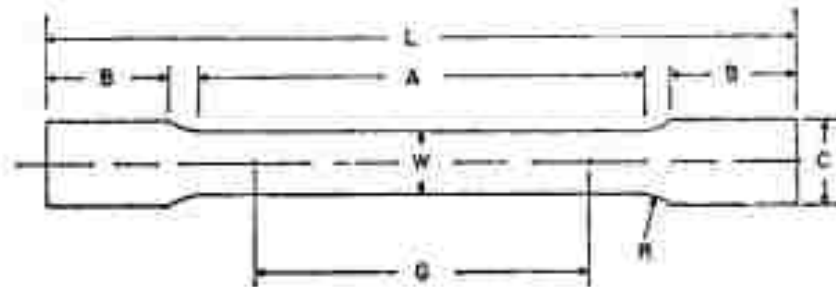
Figure 4-1. Tensile test specimen dimensions[65]

Parameters	Dimension (mm)
L	180
B	41.671
A	60
W	12.5
C	20
G	60
R	30
t	1.5

Table 7. Tensile test specimen parameters and dimensions

4.1.2   Electro-etching

Digital image correlation (DIC) can be used to measure the strain distribution across the gauge area of a tensile test specimen. A random speckle pattern can be applied onto the tensile test specimen and both an initial and a final picture of the specimen can be taken, once the successive rolling is completed. This allows for the DIC to record an original, un-deformed configuration to which all images of deformed configurations can be compared. A virtual width strain can be implemented on the two images and thus a virtual gauge can be applied. The virtual strain gauge would then be used to calculate the width strain that resulted from the rolling.

Etching a grid onto the surface of the specimens is a more common and practical way of determining strains and this method that was used to calculate width strains. Strips of DP600 steel were electro-etched prior to pre-straining by flat rolling. A thorough cleaning of the specimen was first carried out and clean gloves were used to handle the specimen since fingers contain natural oils that would negatively affect the etching process and result in a poorer quality etching finish.

Etching uses an acid or mordant to slightly cut into the uncoated metal. For use on DP600 steel a chemical solvent was made with a mixture of 22 grams of sodium nitrate per liter of water. If the etching is too deep, the material may be damaged and could

lead to less accurate results in the subsequent tensile tests. If the etching is not sufficiently deep, the grid may be removed during the rolling process.

There are several different stencil patterns that can be used for etching a sheet metal blank, and the most common are squares and circles. Squares are easier for calculating the deformation and thus the width strain in this case. An electro-etched specimen is shown in Figure 4-2.
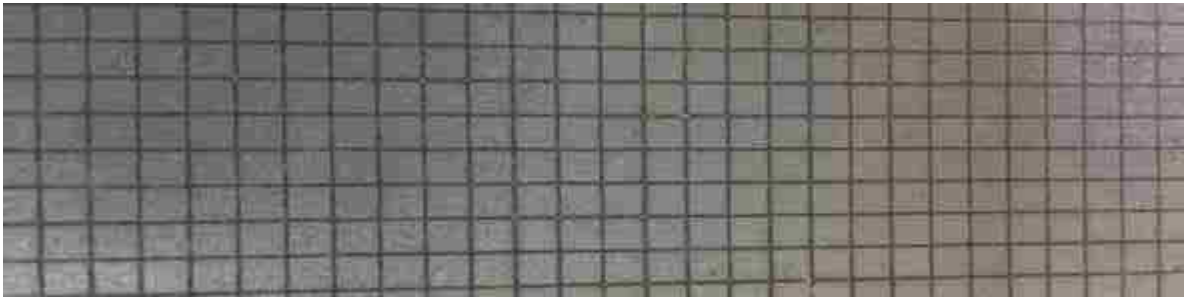
Figure 4-2. Photograph of the electro-etched grid on a tensile specimen

4.1.3 Rolling tests

In order to obtain accurate thickness measurements, three different measurements were taken along the length of the specimen and were then averaged and these values were used for further calculations. A minimum of three tensile tests were conducted after each level of effective pre-strain. Table 8 summarizes the various specimens that were rolled and the average of three thickness measurements that were obtained in both the rolling and transverse directions.

Specimen Designation	Average Thickness Rolling Direction (mm)	Average Thickness Transverse Direction (mm)
SR1-1	1.483	1.484
SR1-2	1.493	1.481
SR2-1	1.494	1.483
SR2-2	1.492	1.484
SR3-1	1.494	1.484
SR3-2	1.490	1.487
SR4-1	1.491	1.486
SR4-2	1.491	1.486
SR5-1	1.491	1.484
SR5-2	1.484	1.482
SR6-1	1.486	1.488
SR6-2	1.491	1.485

Table 8. Specimen name and thickness in rolling and transverse direction

In order to calculate effective strains with proper increments between one another, a theoretical analysis of the rolling was done. By manipulating the following equations:

$$\bar{\varepsilon} = \sqrt{\frac{2}{3}\left(\varepsilon_1{}^2 + \varepsilon_2{}^2 + \varepsilon_3{}^2\right)} \qquad (26)$$

$$\varepsilon_1 = \ln\frac{T_{new}}{T_o} \qquad (27)$$

and assuming constancy of volume

$$\varepsilon_1 + \varepsilon_2 + \varepsilon_3 = 0 \qquad (28)$$

where ε_1, ε_2 and ε_3 are the plastic strains and $\bar{\varepsilon}$ is the total effective strain. Rolling is generally considered to be a plane-strain deformation, i.e. the width strain is assumed to be $\varepsilon_2 = 0$. This leads to the following:

$$\varepsilon_1 = -\varepsilon_3 \tag{29}$$

Rolling was carried out in successive stages, and the desired effective strain increments at each stage were chosen to be 0.0, 0.2, 0.4, 0.6, 0.8, and 1.0 each being associated with specimen SR1, SR2, SR3, SR4, SR5 and SR6, respectively. This allowed for an even distribution of effective strain in successive specimens. With these values being substituted into Eqn. (27), the only unknown left is T_{new}. Table 9 shows the calculated theoretical and the experimental values obtained for the rolling direction.

Specimen Designation	Theoretical Thickness Rolling Direction (mm)	Total Theoretical Effective Strain - Rolling Direction	Measured Thickness Rolling Direction (mm)	Total Experimental Effective Strain - Rolling Direction
SR1-1	1.483	0.0	1.483	0.0
SR1-2	1.493	0.0	1.493	0.0
SR2-1	1.256	0.2	1.262	0.193
SR2-2	1.255	0.2	1.259	0.196
SR3-1	1.057	0.4	1.067	0.386
SR3-2	1.054	0.4	1.067	0.386
SR4-1	0.887	0.6	0.892	0.593
SR4-2	0.887	0.6	0.894	0.591
SR5-1	0.746	0.8	0.764	0.772
SR5-2	0.742	0.8	0.736	0.815
SR6-1	0.625	1.0	0.631	0.993
SR6-2	0.627	1.0	0.625	1.004

Table 9. Rolling theoretical thickness and effective strain in comparison to achieved thickness and effective strain

Table 10 below shows the calculated theoretical and the experimental values obtained for the transverse direction.

Specimen Designation	Theoretical Thickness Transverse Direction (mm)	Total Theoretical Effective Strain - Transverse Direction	Measured Thickness Transverse Direction (mm)	Total Experimental Effective Strain - Transverse Direction
SR1-1	1.484	0.0	1.484	0.0
SR1-2	1.481	0.0	1.481	0.0
SR2-1	1.246	0.2	1.253	0.194
SR2-2	1.247	0.2	1.261	0.187
SR3-1	1.048	0.4	1.064	0.383
SR3-2	1.051	0.4	1.068	0.3801
SR4-1	0.883	0.6	0.891	0.590
SR4-2	0.883	0.6	0.891	0.590
SR5-1	0.742	0.8	0.756	0.778
SR5-2	0.741	0.8	0.751	0.817
SR6-1	0.626	1.0	0.634	0.981
SR6-2	0.625	1.0	0.637	0.976

Table 10. Transverse theoretical thickness and effective strain in comparison to achieved thickness and effective strain

From Table 9 and Table 10 it can be noted that the overall effective strain was closely reached for both the rolling direction and the transverse direction.

A Stanat 10 HP rolling mill was used, and the spacing between the rollers was manually adjusted using a turning wheel. Due to the manual adjustment of the roll gap, the targeted thickness strains were approximately achieved since the rolls experience an elastic deformation each time a specimen is rolled and the final thickness of a rolled specimen is not the same as the roll gap.

In order to ensure that the width strains are indeed approximately zero, the distance across seven etched squares was measured in the width of the strip before and after rolling. The overall width of these seven grids was 17.62 mm before rolling and the maximum distance measured across the same grids after rolling was 17.82 mm, which represents a width strain of 1.12% or 0.0112. This was located on SR6-2 in the rolling

direction. Whether or not this width strain is accounted for in the calculation of the effective strain did not change the value of the effective strain significantly. Therefore, the width strain induced by rolling was considered negligible since it did not contribute to the total effective strain in successive rolled DP600 specimens.

4.1.4   Preparation of tensile specimens

The specimens were machined by wire-cut electrical discharge machining (EDM) according to ASTM E-8 standards. Each rolled strip was used to produce two tensile specimens, yielding a minimum of four tensile specimens for each rolling increment.

In order to obtain accurate DIC results a speckle pattern must be applied onto all specimens. A successful speckle pattern was achieved by applying three layers of white spray paint onto the specimen and allowing it to fully dry. Taking a black spray paint nozzle and slowly applying pressure to the nozzle allowed for bigger black dots to be sprayed onto the specimen. This allowed for the DIC software to produce the most accurate results in comparison with the mechanical and video extensometers. Figure 4-3 was taken directly from the MATLAB code that will be used to calculate the tensile test flow stress curve as shown in the appendix. More details of this code are provided in chapter 5. Figure 4-3 shows the comparison between the mechanical extensometer (blue), video extensometer (orange) and DIC (yellow). The three strain measurements coincide perfectly throughout the test.
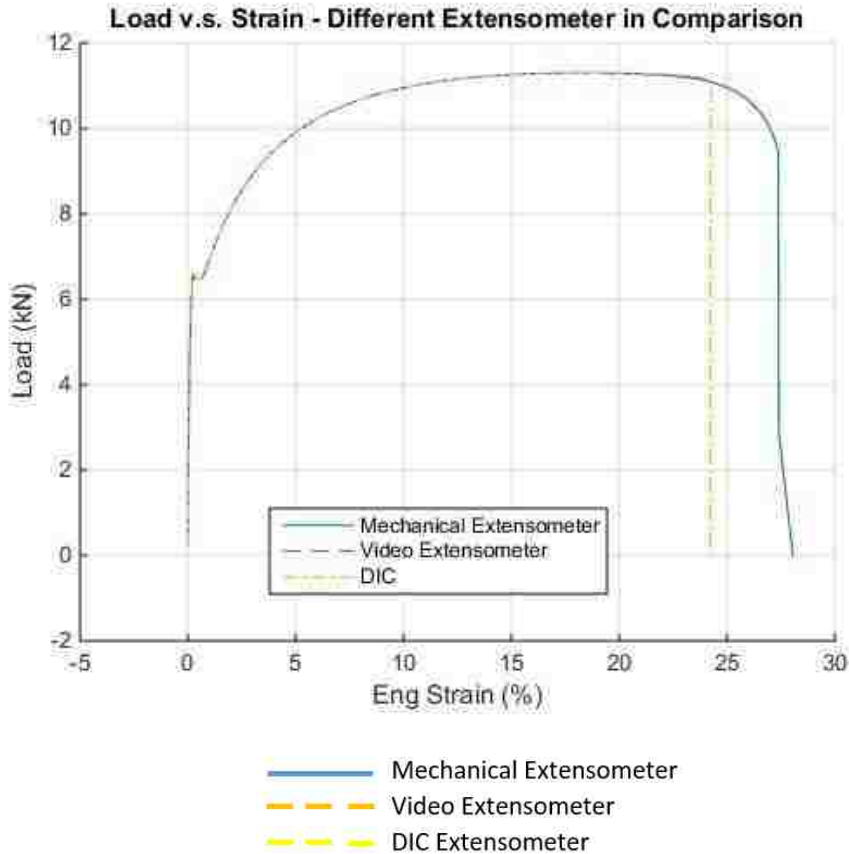
Figure 4-3. Load – strain curve of a DP600 tensile specimen obtained using different strain extensometers

In order to implement the video strain readings from the camera, a blue permanent marker was used to mark circles onto the specimen. The blue circles were spaced 25 mm from each side of the specimen center, and also in the center of the specimen vertically, thus reproducing a 50 mm gauge length in the centre. This allowed an operator to manually select the targets on the video extensometer software beforehand. By marking these dots at the same gauge length as the mechanical extensometer the strain results fully matched with one another. Two dots were also placed 10 mm vertically apart at the centre of the specimen in order to obtain the minor strain. Lastly, three more dots were placed, one in the centre of the specimen, and the final two spaced equidistant of 12.5 mm from the centre, producing a 25 mm gauge length. This allowed for another calculation of the principal strain. Figure 4-4 shows the placement of the dots as well as the speckle pattern implemented.

4.1.5   Tensile tests

All tensile tests were conducted on a 50 kN MTS universal testing machine. The MTS machine uses integrated software, called MTS TestSuite that allows a user to program the same set up for all tensile tests. The set up was specified such that tensile tests were conducted with a crosshead speed of 5mm/min. The software was also programmed to use a video extensometer and a mechanical extensometer with a 25 mm gauge during each tensile test. Once both extensometer profiles were programmed, the specimen was mounted into the lower grip. The mechanical clip gauge was mounted on one edge of the specimen to ensure that it did not block the line of sight for the video camera. Some specimens were rolled to such a reduced thickness that placing the mechanical extensometer on the edge was difficult, and in some cases the extensometer snapped off.

The camera was set up behind the MTS machine and a 1:1.4 25 mm lens with a diameter of 30.5 mm was mounted onto the video camera. Focusing the camera in and out allowed for the field of view to be adjusted accordingly, once initially set up the camera does not need to move again. LED lighting was placed close to the camera in order to be able to narrow the aperture. By having a narrow aperture highly collimated

rays are admitted, which results in a sharp image. If the software shows red dots on the specimen, this indicates that there is too much light being let into the lens, thus over-saturating the camera. The video software allows for targets to be chosen, which should correspond to the previously marked crosses on the specimen. The MTS machine requires the mechanical extensometer and load cell to be verified, which is done manually every time the power button is turned on. Readings were set to zero and the specimen was clamped into the bottom and top jaws. When a tensile test was conducted, the video extensometer recorded images of the gauge area that would later be analyzed by the DIC software. All data, both the MTS raw data and the video files, were saved and exported to a USB drive.

4.1.6   DIC analysis

A DIC system from Correlated Solutions Inc. was used to measure the strain distribution across the specimens as well as the history of the deformation. First, individual images were extracted from the recorded video at a rate of 17 frames per second. Once the images were extracted, they were imported into the VIC-2D software. A seed point location was then selected in an area of the image that is subject to the least movement. A subset size of 30 was chosen, the subset size controls the area of the image that is used to track the displacement between images. A step size of 2 was used, the step size controls the spacing of the points that are analyzed. For example, a step size of 5 means that every 5th pixel in both the horizontal and vertical direction, while a step size of 1 means that every pixel is analyzed in both directions. As the step size is decreased, the calculation time increases significantly, as well as the accuracy of the results. The fastest computation time being a step of five while the most intensive computation time being for a step of one. Once the analysis is complete a virtual extensometer is placed onto the area of interest, in this case the major and minor strain directions. The output of the strain analysis is then exported into a .csv file.

4.1.7 Output

All the DIC results were post-processed using a MATLAB code. The MATLAB code requires customized inputs that are specific to each specimen tested, such as specimen width, thickness, and pre-strain from the initial rolling. All data formats must be in a .txt file with ANSI format in order for MATLAB to be able to read the code. The MATLAB program will then output the desired graphs, and if strain results are appropriate no smoothing is needed. But if the calculated strain results are not monotonically increasing, the strain data may need to be smoothed. In cases where the outputs were not monotonically increasing due to fluctuations in the data, the MATLAB command smooth was used, which eliminates noise from a data set. A final file is then outputted showing the work hardening behaviour of that specimen. Once all tests were completed, all data files were assembled together to output the final flow stress curve. The final output displays an effective stress (MPa) vs. total effective strain. ASTM standards were followed for standard testing methods for tensile strain-hardening exponents [66]. Caution needs to be taken as the mechanical extensometer will have a pre-strain added to it from the clamping of the jaws onto the specimen. This can be treated in two ways, manually adjusting the mechanical data so it starts at zero, or by starting the video analysis before the jaws are tightened.

4.2 Bulge test procedures

4.2.1 Specimen preparation

Sheet specimens were first sheared to a square shape having a size of approximately 250 mm x 250 mm using the guillotine shear. Square specimens were further reduced to circular blanks having a diameter of 230 mm using a blanking die. This size allowed for sufficient space outside the 135 mm diameter bulge zone to securely clamp the specimen. When using 12 concentric M12 bolts to clamp the specimen, the 230-mm diameter blanks would require further drilling of 12 holes around the periphery of the blank. A custom drilling gauge (see Figures 4-5 to 4-7) was created in which several specimens were placed between two steel plates with a hole for each of the 12

fastening bolts and 2 additional holes for the 2 locating dowels. A drill-press was used to drill these holes through several specimens at once.
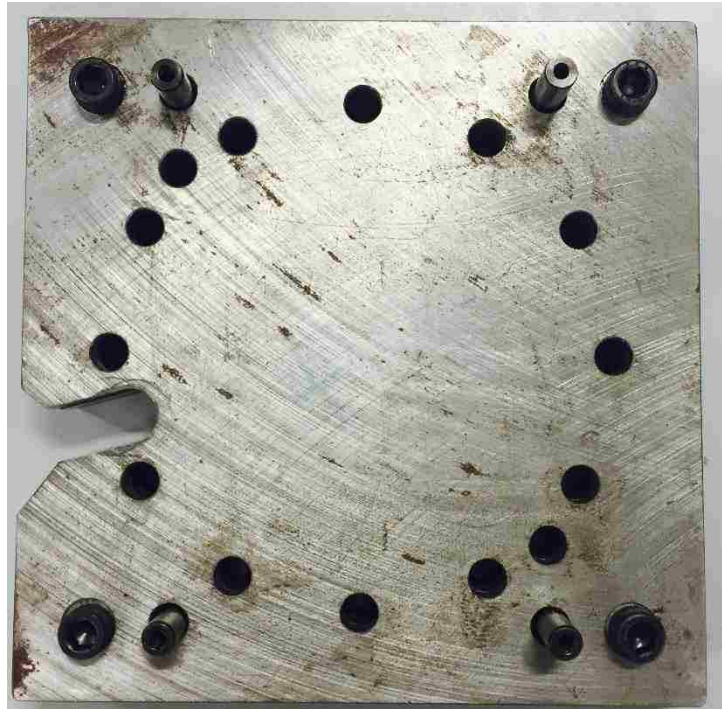
Figure 4-5. Bottom plate of the drilling gauge
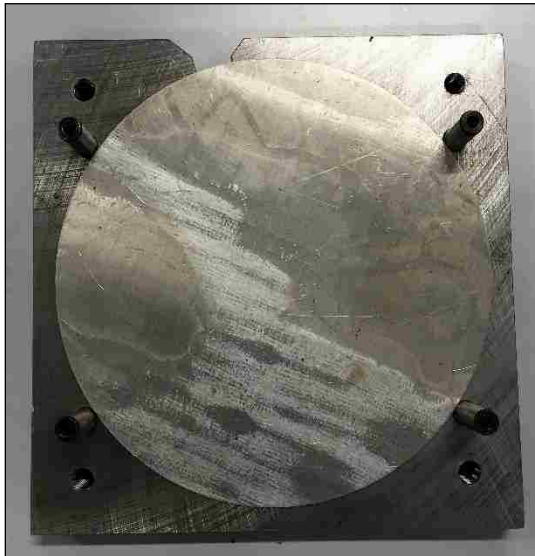
Figure 4-6. Specimen located on the bottom plate   *Figure 4-7. Top plate fixed onto the specimen*

A random speckle pattern of fine dots was then applied to each circular blank by first spraying three layers of white paint, and then by slowly applying pressure to the nozzle in order to apply a random pattern of small black dots. An example of a blank prepared with a speckle pattern is shown in Figure 4-8.
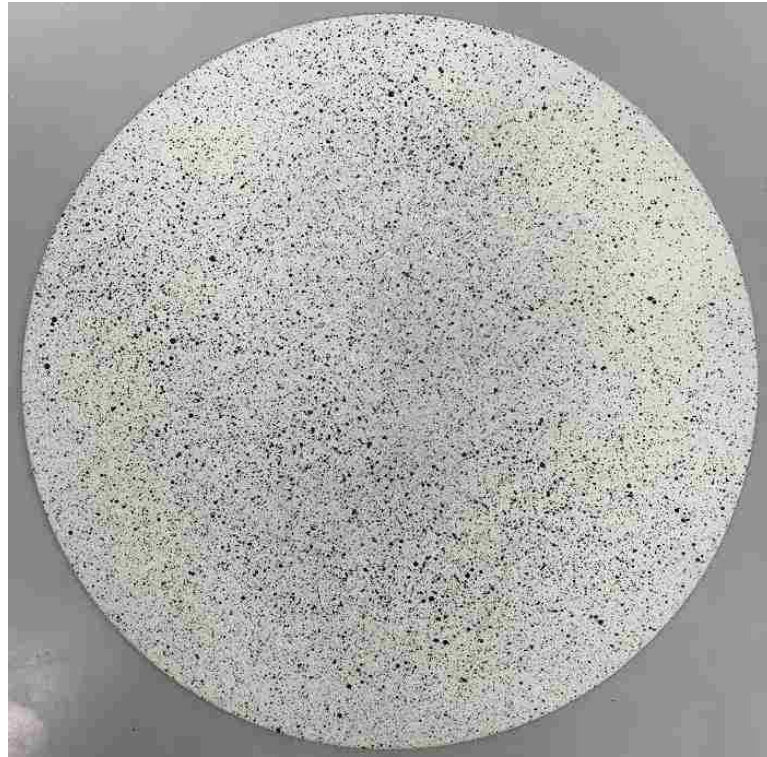
Figure 4-8. Bulge test blank specimen after a random speckle pattern was applied

4.2.2 Press setup

Generally, the operation of a double-action hydraulic press requires that the inner punch and the outer press slide be at the same level before moving together to close the die. Once the die is closed, the punch is made to move through its forming cycle, independently of the outer slide. And once the forming cycle is complete, the punch returns to its "die-closed" position and then both the punch and outer slide retract together to open the die. In order to ensure that the bulge test piston is correctly located at the "bottom dead centre" position relative to the bulge test die prior to a test, the operator must specify an offset of the inner punch relative to the outer press slide. An insufficient offset value could cause the piston to pull out of the bottom of the

die, which would catastrophically damage the piston seal. An excessive offset value would cause the piston to start above the "bottom dead centre" position, which at best would cause an oil spill in the press and leave insufficient oil in the die to fully bulge the test specimen, and at worst, could cause the piston to exit the top of the die, which would risk damaging the piston seal when the piston was drawn back into the oil chamber.

With the die open and the piston in the bottom dead center position, the oil chamber of the bulge test die was filled with food-grade oil to the brim. The oil must be poured into the chamber until a slight overflow occurs in order to ensure that the chamber is indeed completely filled. The sheet metal specimen was then carefully placed on top of the oil-filled chamber. It is important to avoid entrapping air bubbles in the chamber during a test because air is compressible, and this could alter the results of the test [67]. Moreover, the high pressure generated during a test could cause an elastic shock wave when the specimen burst.

The clamping ring was then mounted onto the blank specimen by using the locating pins on the bulge test tool and on the clamping ring. The operator can select one of two different clamping rings: one which can bolt down onto the blank and one which simply rests on the blank. In case the first clamping ring is used, the clamping ring is screwed down onto the specimen using 12 M12 bolts.

4.2.3   Press control

A custom profile was created in the press control system for bulge tests that ensures that a bulge test will be executed correctly and completely in the automatic control mode. The press cycle for a bulge test has three stages that are divided into smaller steps.

Stage one: consists of points 1-4 of the press cycle which control all the actions prior to the forming cycle, in this case the closing of the bulge test tool to its fully clamped condition. Points 2 and 3 are optional points used to slow down the press into the

forming portion of the cycle. The bulge test die must be closed very slowly in order to ensure that the offset between the outer press slide and the inner punch is maintained. If there is any offset, oil may spill and this may lead to air bubbles being introduced.

Stage two: consist of points 5-9 which control the forming cycle. Points 6 through 9 are optional points that can be introduced into the bulge test to control the displacement speed of the inner punch. A bulge test should be carried out, as much as possible, at a constant strain rate. In order to achieve this the displacement speed of the inner punch must be decreased as the test progresses. If the punch speed is not slowed down as the test progresses, a higher strain rate will be seen towards the end of the test, which is undesirable.

Stage three: consists of points 10-14 which control the opening of the bulge test die and its return to its starting position. Points 11-13 are not mandatory.

4.2.4 Protecting the cameras

A bulge test has the potential to burst a specimen thus causing the pressurized oil to shoot up toward the cameras. Oil cannot shoot out through the side due to the protective casing designed in the die. But in the event that a sheet specimen does burst, the digital cameras located above the opening in the top of the press must be protected. Therefore, a sheet of Lexan glass was placed over the opening in the press to act as a protective cover. In order to test the durability of Lexan glass and to ensure that the glass can take the projectile involving the specimen and oil, several tests were conducted right to burst without the cameras installed. DP600 and TRIP780 steel were rapidly bulged and ruptured thus causing the oil to shoot upward, nevertheless the Lexan glass was able to take the impact without any damage to the glass. 8 repeat tests were conducted.

The procedures detailed above allow for the determination of the flow stress curves. The results of both the tensile test and the hydraulic bulge test will be presented in chapter 5.

Chapter 5 Experimental Results

All experimental tests were conducted on DP600 having the mechanical properties as shown in Table 11. Table 11, 12, and 13 are referenced from the Metal Forming Process Research project [68].

Yield Strength at .2 %	380 MPa
Ultimate Tensile Strength	619 MPa
Total Elongation	25.1 %
Thickness	1.496 mm
Coating Type	Galvanized

Table 11. DP600 mechanical properties

The chemical composition of DP600 is displayed in Table 12.

C	0.107
Mn	1.497
P	0.011
S	0.001
Si	0.175
Al	0.038
Cu	0.05
Ni	0.015
Cr	0.181
Sn	0.004
Mo	0.214
V	0.0044
Nb	0.0017
Ti	0.025
B	2E-04
Ca	0.003
N	0.006
W	0.003
Sb	0.0013

Table 12. Chemical composition of DP600

The phase volume fractions are presented in Table 13.

Phase	Ferrite	Martensite	Bainite
Volume Fraction (%)	92	4.7	3.3

Table 13.Phase volume fractions of DP600 steel

5.1 Tensile test results

All experimental data obtained from tensile tests were processed through a custom MATLAB code (attached in the appendix) in order to determine true stress and true strain data.

Section one of the MATLAB code indicates all the variables associated with the specimen and the variables that need to be defined by the user; these include specimen properties, the points that determine the linear portion of the experimental data that will be used to calculate the elastic modulus and also the pre-strain that is induced by flat rolling prior to the tensile test. Finally, the name of the output file must also be defined in the "name" variable, and the code will export the calculated effective stress vs. effective strain data as a text file.

Section two loads the test data from the MTS, video, and DIC machines. Each variable is indicated in the code. In order to add the pre-strain from placing the specimen into the MTS test, the first strain value was added from the MTS machine data to the video and DIC data. The first data point from the MTS machine is the pre-strain from the clamping of the specimen.

Section three synchronizes the DIC strain data to the video extensometer and MTS strain data. This is done by interpolating the DIC strain data and the number of readings, to the number of frames in the video time. The video extensometer reads 17 frames per second, thus the strain from the DIC data is interpolated in respect to the 17 frames per second multiplied by the length of the video. The true stress is also calculated from the strain measured by the mechanical extensometer. Equation (30) is used to obtain true stress.

$$\sigma_{True} = \sigma_{eng}(1 + \varepsilon^{eng}) \tag{30}$$

In order to obtain strain values from the DIC system, a virtual extensometer is placed on the first un-deformed image. As the digital images of the specimen gauge show increasing evidence of deformation, the virtual extensometer becomes elongated and the engineering strain is calculated from the following equation.

$$\varepsilon^{eng} = \frac{L - L_o}{L_o} \tag{31}$$

where L is the final length of the virtual extensometer and L_o is the initial, un-deformed length of the virtual extensometer. The engineering strain is then converted to true strain in the MATLAB code using the following equation:

$$\varepsilon^{true} = \ln(1 + \varepsilon^{eng}) \tag{32}$$

In order to determine the elastic modulus and yield stress from the experimental data, two points must be defined by the user. The first point Ep1 is located at the start of the linear portion of the true stress vs. true strain curve, and Ep2 near the end of the linear portion. The elastic modulus is defined as the ratio of the stress to the strain in the linear elastic region:

$$E = \frac{\sigma}{\varepsilon} \tag{33}$$

An interpolation is made to determine the values of stress and strain at the user-defined points, and the elastic modulus is then calculated. The yield stress at 0.2% offset and the corresponding yield strain were determined using a MATLAB code obtained online from Douglas Schwarz [69]

In order to correctly determine the flow curve, defined as the true stress vs. true plastic strain curve, the total strain data must be further processed to remove the elastic strain, so that the curve starts at the yield stress and ends at the point that corresponds with the maximum engineering stress. In order to achieve this a MATLAB command called "trunc" was used to truncate the data at user defined points [beginning, end]. The first user-defined point being the yield stress and the second user-defined point being the

maximum engineering stress. The elastic strains are then subtracted from the total strain values using the following equation in the elastic region.

$$\varepsilon^{elastic} = \frac{\sigma}{E} \tag{34}$$

The last section of the MATLAB code calculates the von Mises effective stress and strain. The von Mises effective stress, $\bar{\sigma}$, is defined as follows:

$$\bar{\sigma} = \frac{\sqrt{2}}{2}\sqrt{(\sigma_1 - \sigma_2)^2 + (\sigma_2 - \sigma_3)^2 + (\sigma_3 - \sigma_1)^2} \tag{35}$$

where σ_1, σ_2, and σ_3 are the principal stresses. In this case of uniaxial tension, σ_2 and σ_3 are zero thus the equation reduces to:

$$\bar{\sigma} = \frac{\sqrt{2}}{2}\sqrt{(\sigma_1)^2 + (0)^2 + (-\sigma_1)^2}$$

$$\bar{\sigma} = \frac{\sqrt{2}}{2}\sqrt{(2\sigma_1)^2}$$

Leading to

$$\bar{\sigma} = \sigma_1$$

The von Mises effective strain is defined as:

$$\bar{\varepsilon} = \sqrt{\frac{2}{3}(\varepsilon_1{}^2 + \varepsilon_2{}^2 + \varepsilon_3{}^2)} \tag{36}$$

In the case of a uniaxial tensile test, ε_1 was measured using the mechanical extensometer whereas ε_2 and ε_3 were taken from the DIC analysis. ε_2 and ε_3 are approximately zero and results were not affected by incorporating ε_2 and ε_3. Plotting $\bar{\sigma}$ vs. $\bar{\varepsilon}$ leads to the desired flow curves for both the rolling and transverse directions, as shown in Figure 5-1 and Figure 5-2.
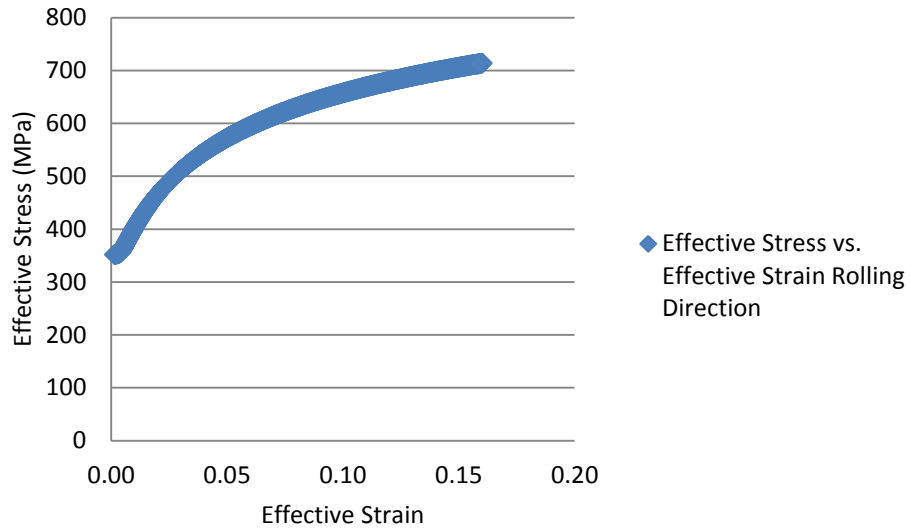
Figure 5-1. Effective stress vs. effective strain behaviour of DP600 steel in uniaxial tension in the rolling direction
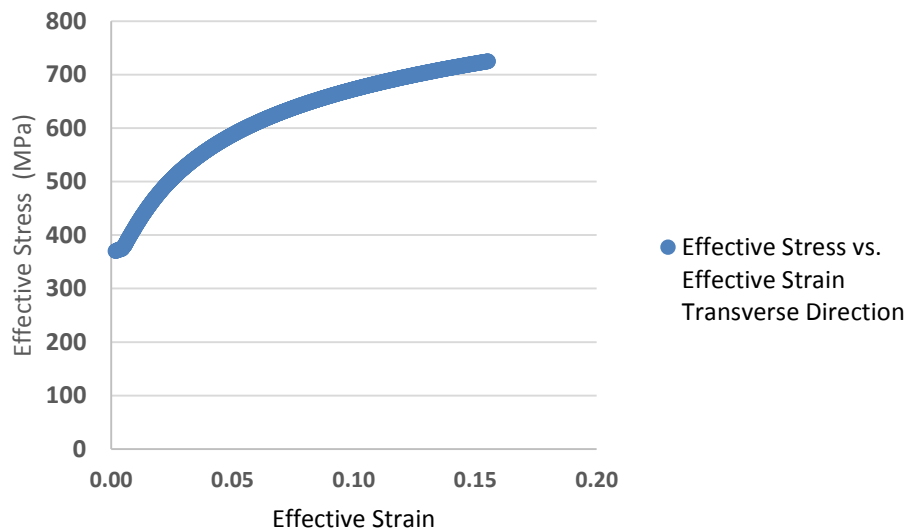
Figure 5-2. Effective stress vs. effective strain behaviour of DP600 steel in uniaxial tension in the transverse direction

5.1.1 Fitting of tensile test data with successive rolling

The same analysis that was used to determine the tensile flow curve of the as-received sheet material was also used to determine the flow curve for specimens that were tested in uniaxial tension after successive flat rolling. These tensile tests were conducted with specimens that were flat rolled to 0.2, 0.4, 0.6, 0.8, and 1.0 effective strain along

the rolling direction of the sheet. The entire flow curve of the as-received sheet was then plotted on a stress-strain diagram, but only one data point from each flow curve obtained from specimens prestrained to 0.2, 0.4, 0.6, 0.8, and 1.0 effective strain was plotted on the same diagram: for each level of prestrain, the single data point plotted corresponded with the maximum engineering stress. Due to this, there are many more data points between 0 and 0.2 effective strain compared to the number of points in the range from 0.2 to 1.0 effective strain. The flow curves obtained by combining the data from each level of rolling prestrain are shown in Figures 5-3 and 5-4 for the rolling and transverse directions of the sheet.

$$\bar{\sigma} = 1035.7\bar{\varepsilon}^{\,0.1999}$$
$$R^2 = 0.9907$$
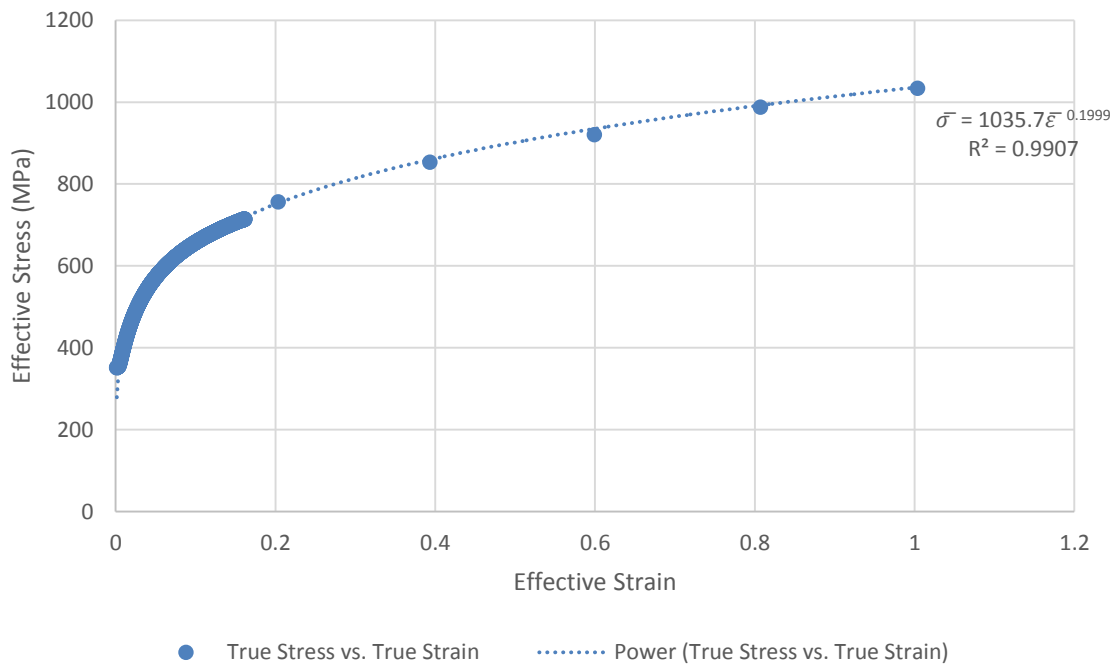
Figure 5-3. Effective stress vs. effective strain curve in the rolling direction of DP600 after successive rolling passes

$$\bar{\sigma} = 1051.3\bar{\varepsilon}^{\,0.1961}$$
$$R^2 = 0.991$$
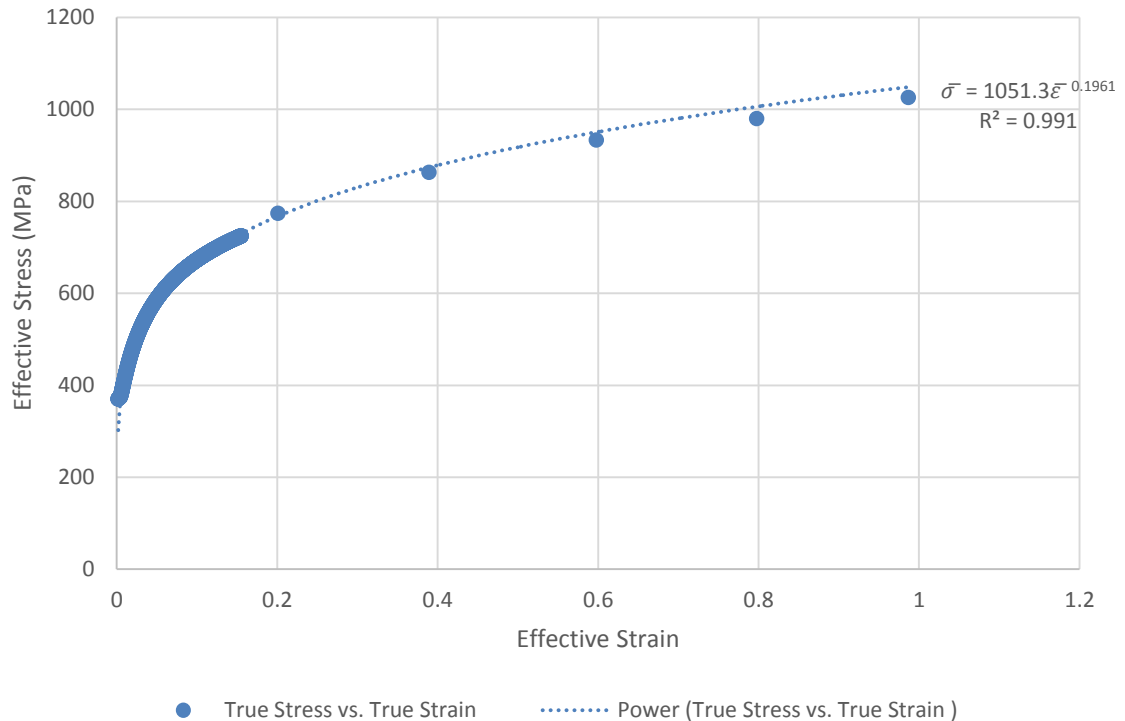
Figure 5-4.Effective stress vs. effective strain curve in the transverse direction of DP600 after successive rolling passes

If one was to fit a power law function to this unique set of data, the fitting would be heavily influenced by the beginning portion of the curve, which contains the majority of the data. Thus a MATLAB code was created to reduce the number of points at the beginning of the test in order to fit a power law curve that is more evenly distributed among all points.

The MATLAB code was designed to retain every "Xth" data point in a sequential fashion from the data for the first tensile test (0.0 induced effective prestrain), while keeping the data from prestrained specimens untouched. For example, in the rolling direction there are 1624 data points, and 1619 of them belong to the first tensile test (zero prestrain). The code will retain only every "Xth" point from the 1619 data points and remove the remaining data. Figure 5-5 and 5-6 show how the parameters in the power law function (the strain hardening index and the constant value K) are affected when

they are fitted after removing different numbers of data points. The frequency of points retained on this graph means that every "X" data point was retained for curve fitting.
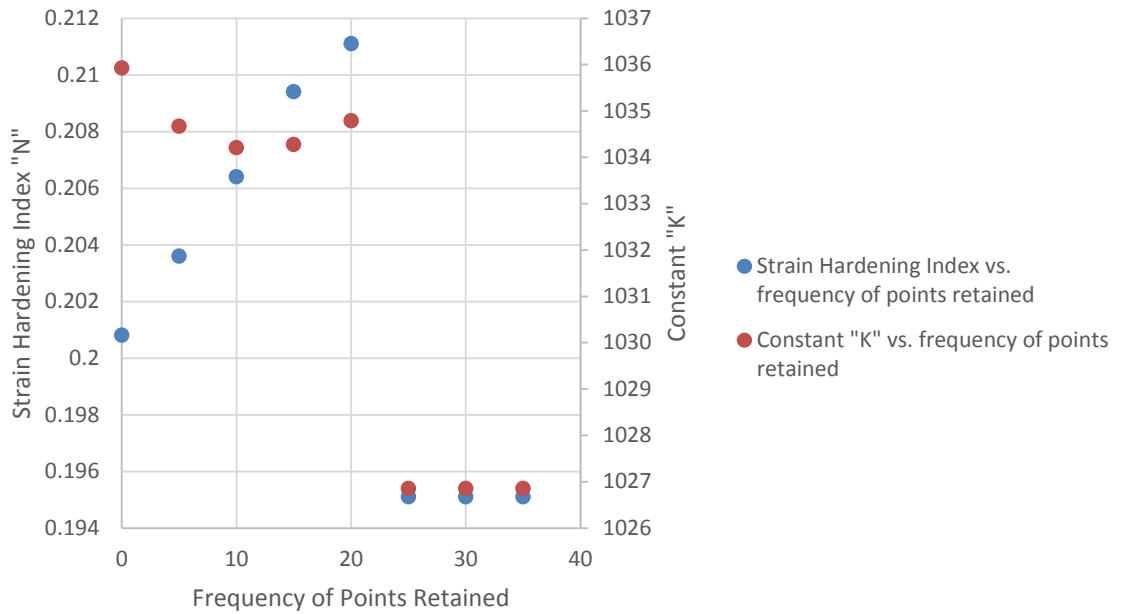
Figure 5-5. Frequency of points retained vs. power law parameters for the rolling direction
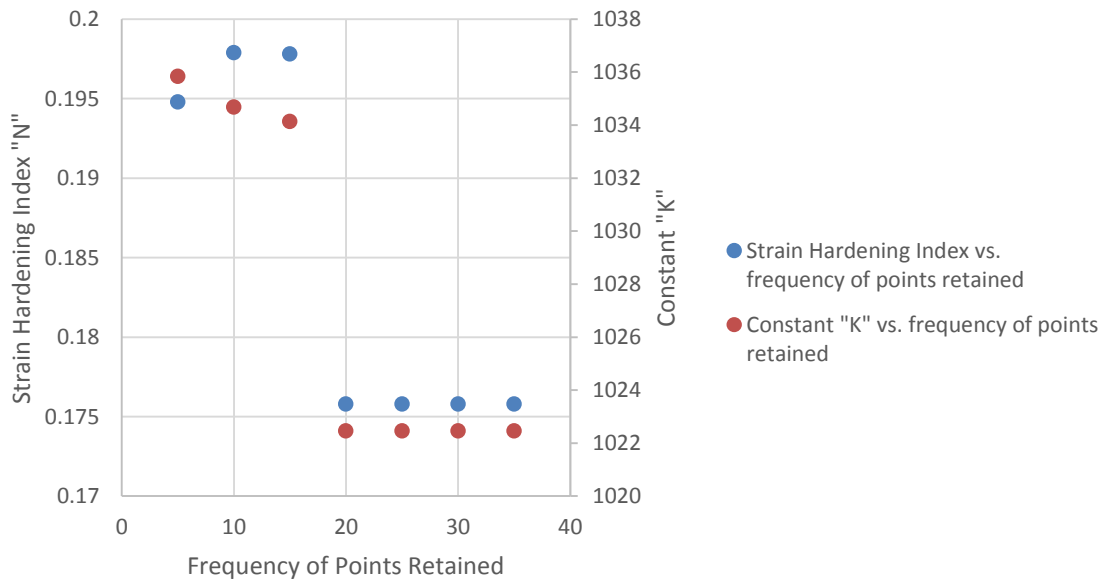
Figure 5-6. Frequency of points retained vs. power paw parameters for the transverse direction

As presented in these figures, the parameters in the power law function reach stable values when at least every 25th point is retained for the rolling direction, and when at least every 20th point is retained for the transverse direction.

"Xth" point retained for curve fitting	N	K
5	0.200	1035
10	0.203	1034
15	0.206	1034
20	0.209	1034
25	0.211	1034
30	0.195	1026
35	0.195	1026

Table 14. Frequency of points retained for the rolling direction

"Xth" point retained for curve fitting	N	K
5	0.194	1035
10	0.197	1034
15	0.197	1034
20	0.175	1022
25	0.175	1022
30	0.175	1022
35	0.175	1022

Table 15. Frequency of points retained for the transverse direction

Figure 5-7 and Figure 5-8 show the effective stress vs. effective strain curves when every 35th point was retained from the tensile data obtained after 0.0 effective prestrain.

Figure 5-7. Effective stress vs. effective strain in the rolling direction when retaining every 35th data point

Figure 5-7 and Figure 5-8 show the effective stress vs. effective strain curves when every 35th point was retained from the tensile data obtained after 0.0 effective prestrain.
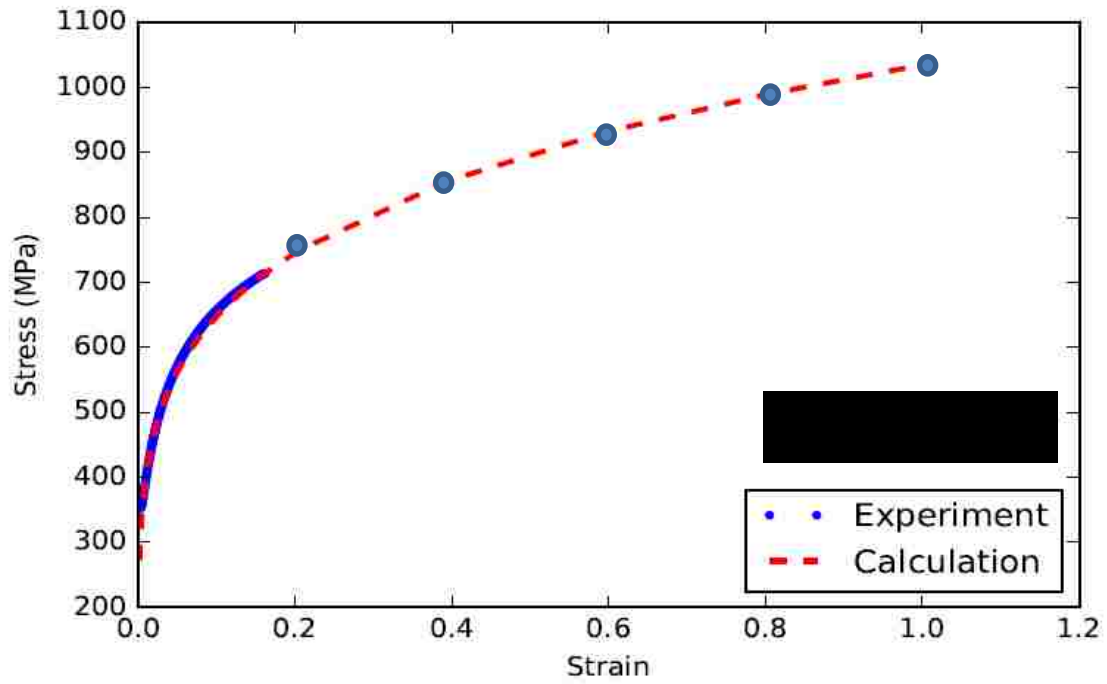
Figure 5-7. Effective stress vs. effective strain in the rolling direction when retaining every 35th data point
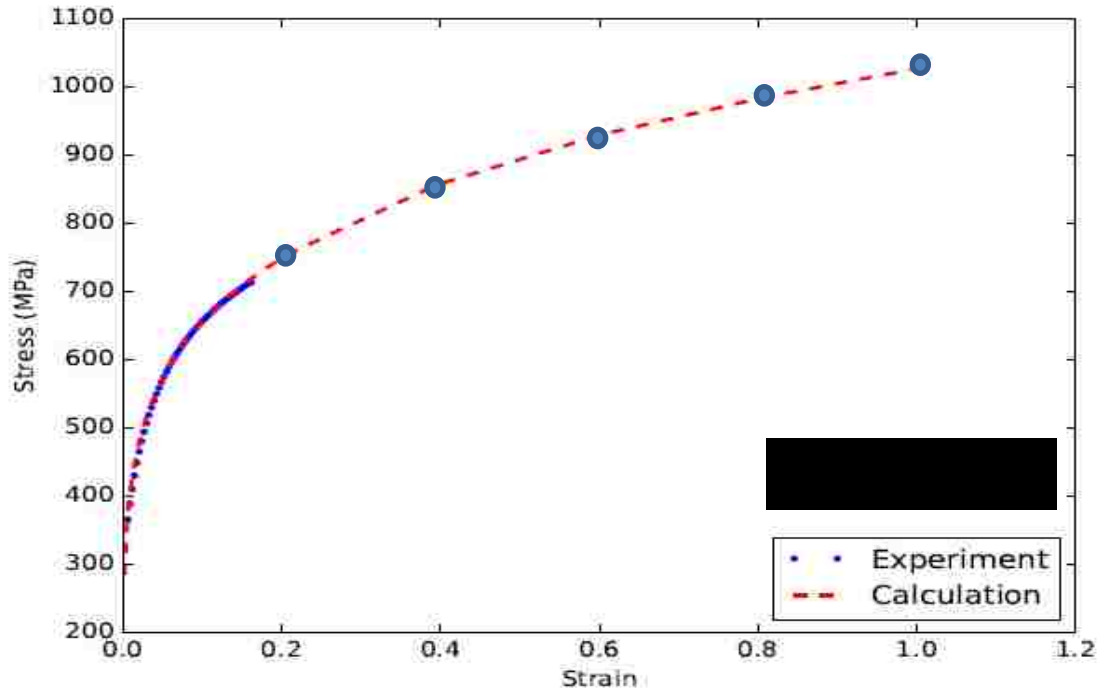
Figure 5-8. Effective stress vs. effective strain curve in the transverse direction when retaining every 35th data point

5.2 Bulge test results

All bulge test results were processed using the MATLAB code attached in the appendix. In order to produce a flow curve from the hydraulic bulge test data, the following equations were used to calculate the effective stress and effective strain:

$$\bar{\sigma} = \left[\frac{R_D}{t_d} + 1\right]\frac{P}{2} \tag{5}$$

$$\bar{\varepsilon} = -ln\frac{t_d}{t_o} \tag{6}$$

Table 16 shows the variables required and whether they were calculated or measured.

	Variable	Equation	How was data Obtained
Original thickness of sheet	t_o	N/A	Measured
Radius of the fillet	R_c	N/A	Measured
Diameter of the Cavity	d_c	N/A	Measured
Dome Height	h_d	N/A	DIC Software
Pressure	P	Force/Area	Eagle Press Software / Pressure Transducer
Radius of the Dome Height	R_D	$\dfrac{((d_c/2) + R_c)^2 + h_d{}^2 -}{2h_d}$	Calculated
Thickness at the apex of the dome	t_d	$t_o\left(\dfrac{R_c/R_D}{\sin^{-1}(\frac{R_c}{R_D})}\right)^2$	Calculated

Table 16. Bulge test parameters

The variables and equations in Table 16 were entered into the MATLAB code, which calculated the flow curve data. Section one of the MATLAB code loads the displacement file from the DIC software and the press data file from the hydraulic press. The test duration, and the position, displacement and load of the piston are extracted from the data. The actual piston load (kN) is then converted into a pressure (MPa), by using Eqn. (24).

Section two of the MATLAB code interpolates the displacement of the dome height, which is recorded by the DIC software in terms of a frame number and a corresponding displacement, so as to convert these data into time vs. displacement data. All other measured variables including sheet thickness, diameter of the cavity and radius of the fillet are entered here as well.

Section three calculates the flow stress, point by point, using the equations listed in Table 16. Bulge test parameters, and a graph is then created showing the final flow curve. The data is exported to an ASCII file.

In order to determine the burst pressure of DP600, three bulge tests were conducted until the specimen failed. These tests were used to determine the maximum piston load that leads to the failure of this DP600 sheet material. The maximum piston load was determined to be 258, 262 and 263 kN, in successive bulge tests conducted to failure. Figure 5-9 shows the experimental data recorded during one of these tests that were conducted in order to determine the maximum piston load. The press was programmed to record the position of the piston, the position of the outer ram, the clamping load which was set to 1000 kN, the piston load which was continuously monitored and lastly the process point (PP) of the test. As expected, DP600 showed evidence of necking, as seen by the decrease in the piston load between 4700-5000 ms. Necking occurs as a result of strain localizing in a small region of the material [70].
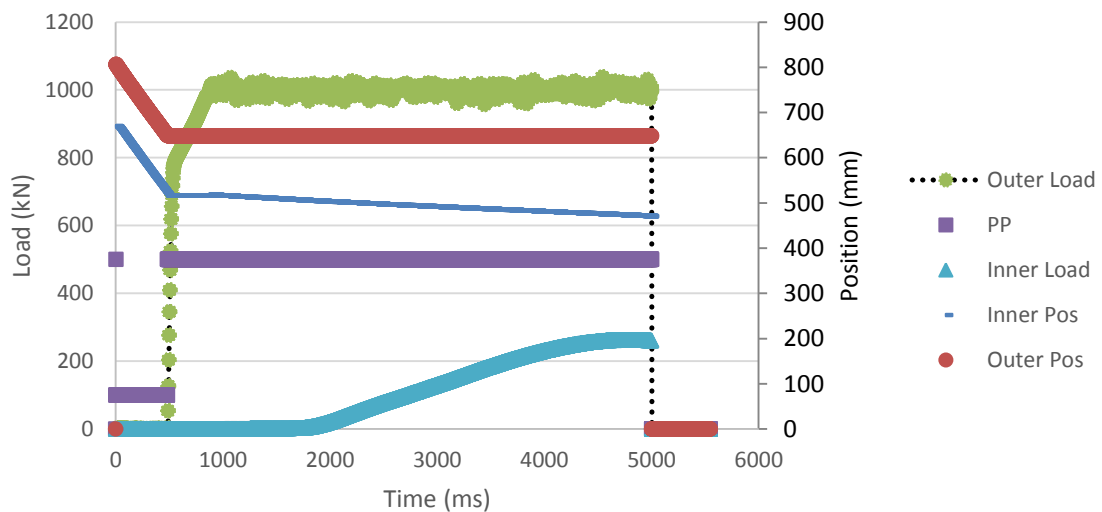
Figure 5-9. Bulge test trial run to determine maximum load

Once the burst pressure was known for this DP600 sheet material, a series of bulge tests was then conducted while recording digital images with stereo cameras. In order to ensure that the specimen did not burst and risk damaging the cameras and lenses, these tests were terminated when the piston load reached 260 kN, which corresponds to a

pressure of 23 MPa. Figure 5-10 shows the data when the piston load was stopped at 260 kN.
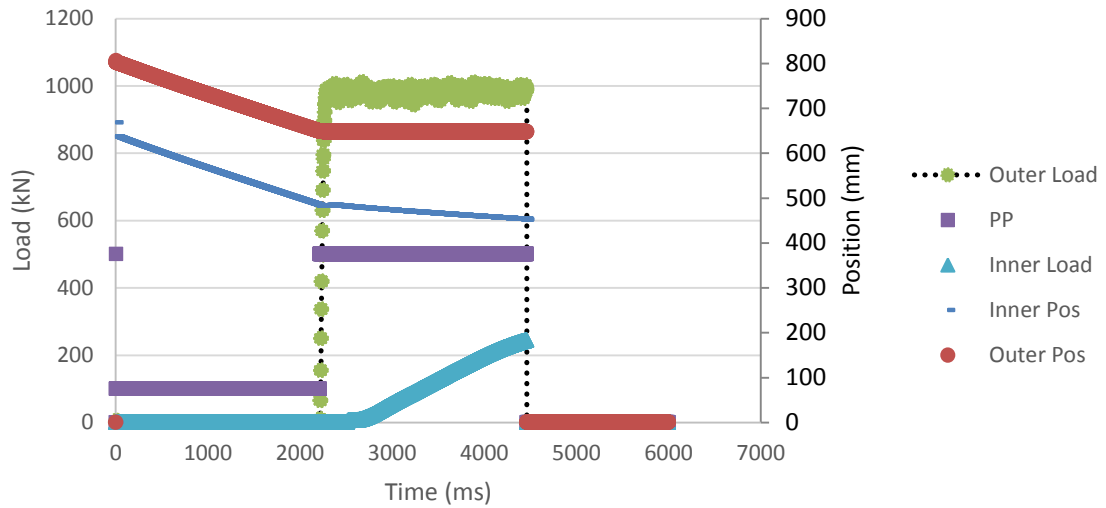
Figure 5-10. Bulge test final run

The final flow stress curve obtained from the bulge test is shown in Figure 5-11 with a fitted power law curve. The result is the average of three successful tests completed at a maximum inner piston load of 260 kN.

$$\bar{\sigma} = 1104.6\bar{\varepsilon}^{\,0.2029}$$
$$R^2 = 0.9936$$
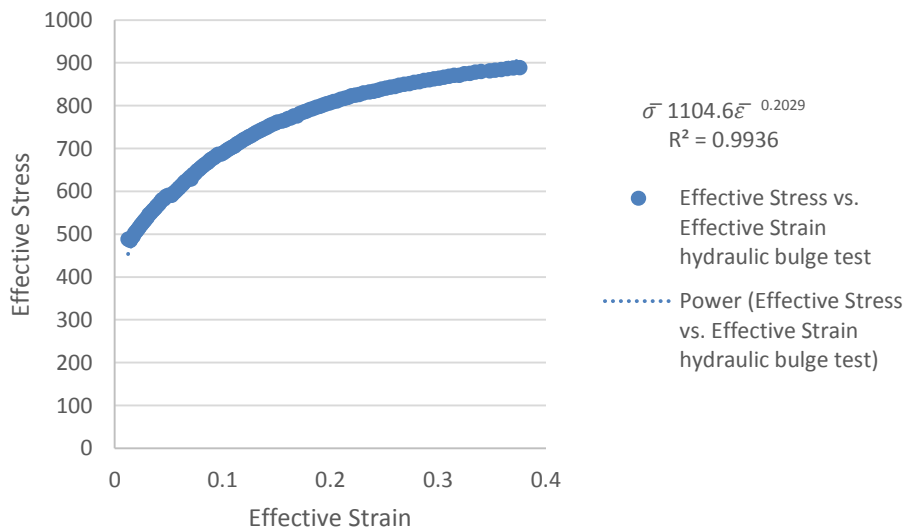
Figure 5-11. Flow stress curve of DP600 steel obtained from the bulge test

Fitting a power law curve to the data results in a strain hardening index n = 0.2029 and a constant K of 1104.6.

The final flow stress curves for the tensile test was determined to be $\bar{\sigma}=1026.851\bar{\varepsilon}^{\,0.1951}$ in the rolling direction and in the transverse direction $\bar{\sigma}=1022.456\bar{\varepsilon}^{\,0.1758}$. The hydraulic bulge test flow curve produced a power law curve fitting of $\bar{\sigma} = 1104.6\bar{\varepsilon}^{\,0.2029}$. The FEA models presented in Chapter 6 will use the original tensile test flow curve and a hydraulic bulge test flow curve as input to determine the work hardening behaviour of DP600 steel. A discussion on the extended tensile test after successive flat rolling and the hydraulic bulge test curves will be presented in chapter 7.

Chapter 6   Finite Element Analysis

FEA models of both the tensile test and the hydraulic bulge test were created in order to be able to numerically predict the outcome of both these experimental tests. Each simulation model must also be validated in order to ensure that the results obtained follow the fundamental energy laws and accurately predict the mechanical behaviour of DP600 sheet as determined experimentally. The results of both FEA models will be evaluated by comparing them with corresponding experimental data, and a validation metric will be calculated in order to provide a measure of the agreement between the experimental results and FEA model. Furthermore, a mesh sensitivity study will be conducted for both models in order to ensure that the mesh does not influence the results. A Dell precision T7610 with a E5-2687W v2 @ 3.4 GHz processor and 32 GB of ram was used for all simulations.

The material model used for both tests will be an isotropic power law hardening function, material model 18 in LS-DYNA. However, since two different experimental flow curves were obtained, the power law function will be fitted to each experimental curve, and both fitted curves will be used in the numerical simulations. The power law was fitted to the tensile curve (Figure 5-1), the extended tensile flow curve in the rolling direction (Figure 5-7) and to the flow curve obtained from the hydraulic bulge test (Figure 5-9). The power law parameters fitted to these three experimental flow curves are provided in Table 17, and both models will be analyzed and compared to one another using a quantitative metric.

Material property	Tensile test	Tensile test with successive flat rolling	Bulge test
N	0.199	0.195	0.2029
K (MPa)	1035.8	1026	1104.6
Density (tonne/mm^3)	8.050e-009	8.050e-009	8.050e-009
Elastic Modulus (MPa)	1.50e+05	1.50e+05	1.50e+05
Poisson's ratio	0.27	0.27	0.27

Table 17. Power law material properties

6.1   Finite element model of the tensile test

A FEA model of the standard tensile test was created using 1400 shell elements and 1595 nodes. Element formulation 2 (Belytschko-Tsay) was used since these elements use single point integration, are the most economical and are generally recommended unless features particular to the model are needed. The thickness was set to 1.5 mm, and 60 elements were used to cover the length of the 60 mm gauge area. The purple rectangle in the centre of Figure 6-1 shows the area of the gauge. The red rectangle on the left illustrates the area of the model that was fully constrained, so that no displacement or rotation is allowed to occur at the nodes in this area. The black rectangle on the far right of Figure 6-1 shows the nodes that were displaced in a single direction, considered the positive x-direction. The boundary-prescribed-motion option was used to displace the nodes using a load curve of XY input data as follows: 0,0 and 1,20 (s,mm). The input curve for the power law material model was used from the original as-received tensile test.
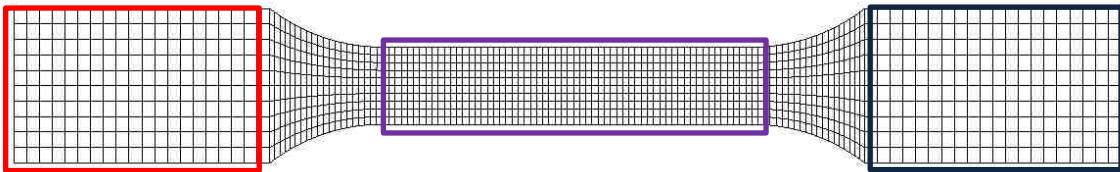
Figure 6-1. FEA model of tensile test

A time-scaled solution was used for this simulation. The end time of the simulation was set to 1.1 seconds so as to ensure that the last step of the simulation is accounted for (if an end time of 1.0 was used for a 1 second load curve, it is possible for LS-DYNA to skip the last step in the load curve). Using a time-scaled solution significantly decreases the computation time from hours (for 30.1 seconds end time) to minutes (for 1.1 seconds end time). An implicit time integration scheme was used with an absolute convergence tolerance of 1.0e-08 and a step of 0.01. However, results need to be compared to a more realistic termination time. In section 6.2 a comparison between the time-scaled

78

solution (end-time of 1.1.s) and a more realistic time solution, in this case an end time of 5.1 seconds and 20.1 seconds, will be analyzed.

6.2   Validation and verification of implicit tensile test model

In order to validate the FEA model of the tensile test, a comparison was made between the FEA model and the experimental results from the as-received tensile test. From the FEA model two nodes were chosen to create a 25 mm gauge, and the distance between these nodes was tracked throughout the test and exported to an Excel file. Using the distance between these two nodes, true strains were calculated. The forces throughout the test were also exported using *DATABASE_SPCFORC. The force was plotted as a function of true strain. A power law function was fitted to the predicted force vs. strain data and the equation obtained was $y=16,552x^{0.1591}$ with an R^2 value of 0.9903, as shown in Figure 6-2.
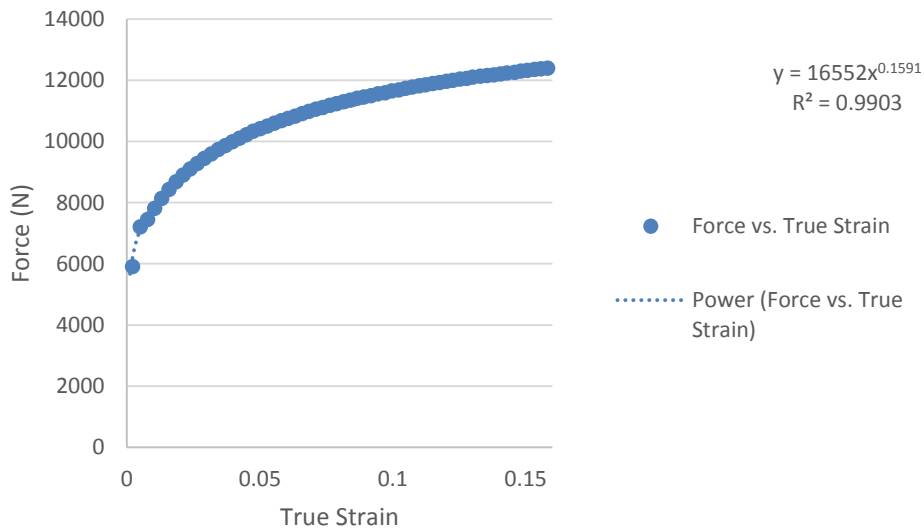
Figure 6-2. FEA LS-DYNA model - 1 second end time – predicted force vs. true strain in uniaxial tension

The same procedure was followed using the experimental results of the as-received tensile flow curve. The experimental setup incorporated a 25 mm gauge on the specimen, a load vs. true strain was plotted once again. A power law function was fitted

to the data and another equation was obtained y = 16,572x$^{0.1791}$ with an R^2 value of 0.9721, as illustrated in Figure 6-3.
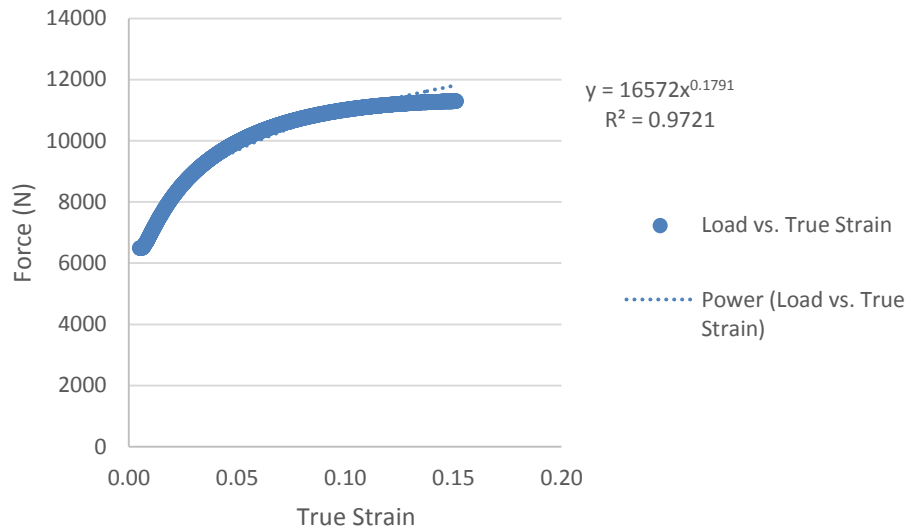
Figure 6-3. Experimental tensile test – force vs. true strain

As can be noted, the experimental results were only plotted from the onset of yielding up to the maximum load, which occurred at about 0.15 true strain. If the results were continued beyond uniform elongation (i.e. the strain at maximum load), necking would be observed. However, the results from the FEA model would show no necking due to the fact that shell elements are being used. Shell elements are plane stress elements, whereas necking is a 3D phenomenon, thus shell elements are not able to predict the onset of a local neck.

In order to quantify the difference between the predicted and experimental flow curves, the following validation metric was used [10]:

$$V = 1 - \frac{1}{L}\int_0^L tanh\left|\frac{y(x)-Y(x)}{Y(x)}\right| dx \qquad (37)$$

where Y(x) is the accepted experimental results, in this case load vs. true strain and y(x) is the theoretical results predicted by the LS-DYNA FEA model, once again load vs. true strain. The advantage of this particular metric is that it normalizes the difference between the numerical results and the experimental data. The absolute value of the relative error only accumulates, a positive and negative value do not add up. When the difference between the experimental data and the predicted results are zero, this metric has a value of 1.0, and when the summation of the relative error becomes relatively large, the validation metric approaches zero [10]. Computing this metric from 0-.15 leads to a validation score of 0.9630: this shows that the numerical simulation of the tensile test correlates very well with the actual material behaviour in uniaxial tension, and thereby validates the numerical simulations.

The results for the simulation with a specified 5.1-second end time are illustrated in Figure 6-4. Fitting the data to a power law results in $y = 16,506x^{0.1577}$ with an R^2 value equal to 0.988. Running the same validation metric and comparing it to the experimental results leads to a validation score of 0.9783, almost the exact same result as the time-scaled solution (1 second end time).
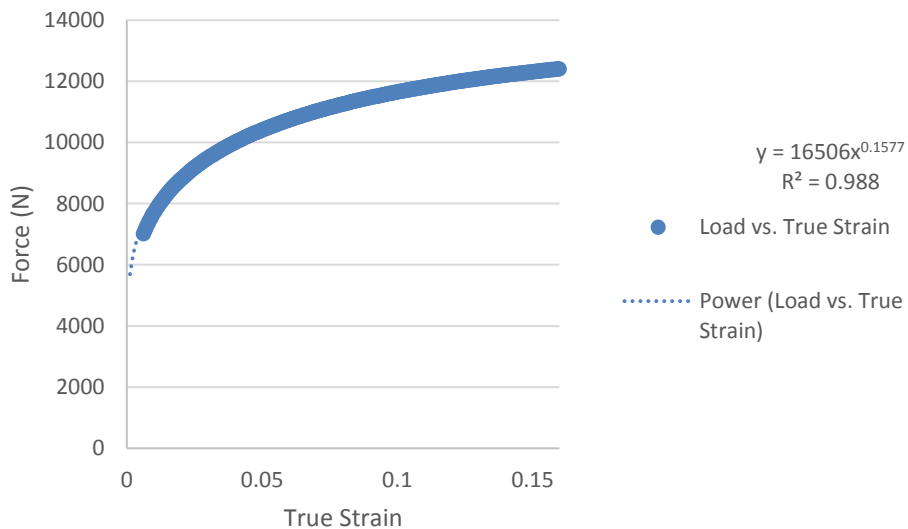
Figure 6-4. FEA LS-DYNA model tensile test - 5 second end time – predicted load vs. true strain in uniaxial tension

The results for the simulation with a 20.1-second end time are illustrated in Figure 6-5. Fitting the data to a power law results in $y = 16,530x^{0.1586}$ with an R^2 value equal to 0.9807. Running the same validation metric and comparing it to the experimental results leads to a validation score of 0.9680, almost the exact same result as the time-scaled solution (1 second end time).
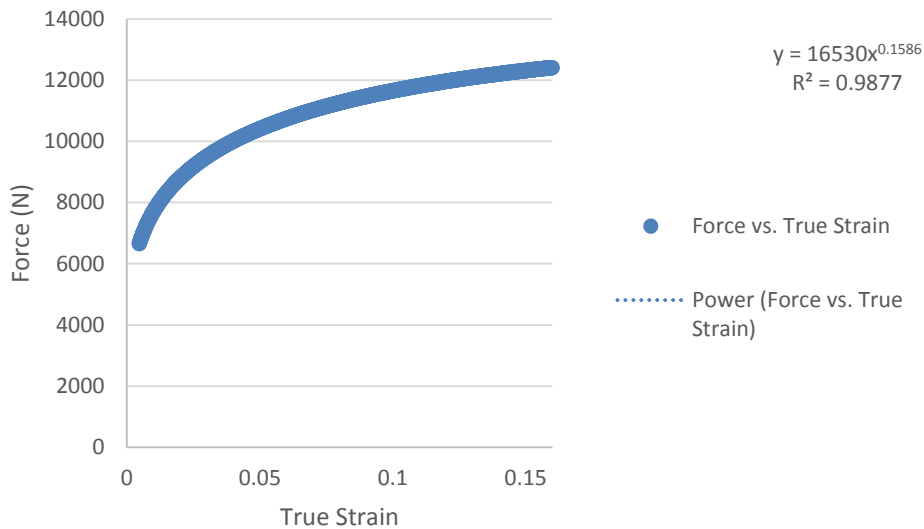
Figure 6-5. FEA LS-DYNA model tensile test - 20 second end time – predicted load vs. true strain in uniaxial tension

The energy verification in Figure 6-6 shows that the total kinetic energy of the specimen throughout the entire test is 0 at all times. This is to be expected since the specimen does not have any velocity or acceleration applied to it. The internal energy of the specimen is equal to the total energy of the specimen, which is also to be expected. The only energy in this test is the build-up of internal energy from the displacement of the nodes, which should equal the total energy of the test. The energy balance below verifies that the model indeed follows the fundamental laws of energy conservation. The energy balance below also shows that the test is still quasi-static in nature and that dynamic effects are not being introduced due to time scaling. Hourglass energy was also 0.
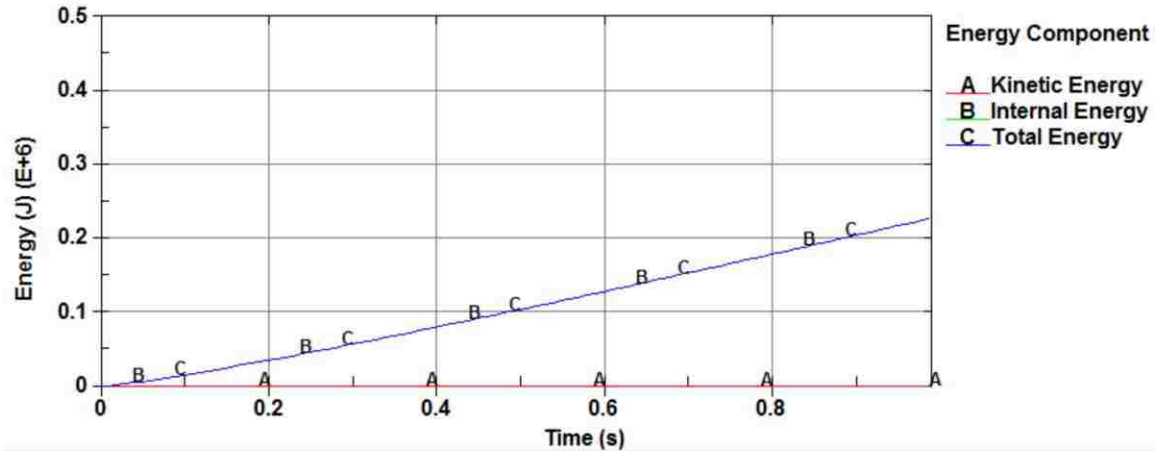
Figure 6-6. Energy Balance in the FE simulation of the tensile test

6.3   Mesh sensitivity study for the tensile test model

A mesh sensitivity study was conducted on the gauge area of the tensile test specimen. The gauge has a length of 60 mm and a width of 12.5 mm. Different models were constructed having a number of elements along the length of the gauge ranging from 20 to 60 elements, and in each case, the rest of the specimen was meshed accordingly in order to maintain an element aspect ratio near to 1.0. From the results in Figure 6-7 it can be seen that for 20 or more elements in the length of the gauge the simulation results converge to the same solution.

83
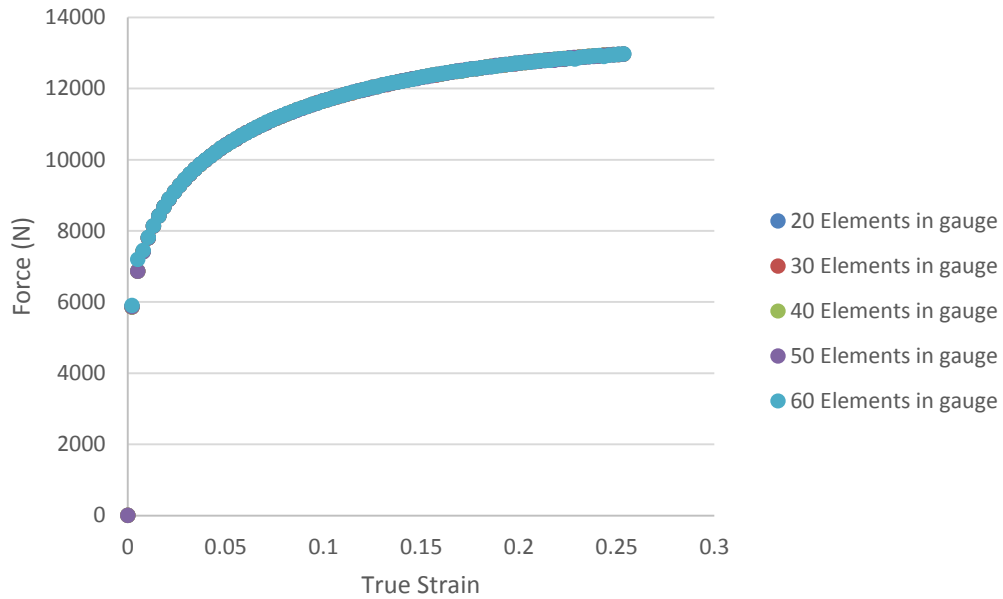
Figure 6-7. Mesh sensitivity study conducted on tensile test, 20 to 60 elements were used in the length of the gauge. Results were plotted as a function of force vs. true strain

6.4   Finite element model of the hydraulic bulge test

A quarter model of a bulge test was created using shell elements for the specimen as well as for the radius of the die fillet. 38,998 nodes and 16,048 elements were used to model both the sheet and the die. Element formulation 16, which is fully-integrated shell elements, was used for both the sheet and die, and the die was modelled using a rigid material model. A density of 7.806e-9 tonne/mm^3, an elastic modulus of 200 GPA, and a Poisson's ratio of 0.29 were used for the rigid material model. These material properties are required for rigid entities in LS-DYNA as they are used in the calculation of penalty-based stiffness contacts.

An automatic-surface-to-surface contact was used between the specimen blank and the 3-mm die fillet radius. An implicit time integration scheme was used with an absolute convergence tolerance of 1.0e-10 and a 0.01 step.

A *Load_Segment was used to apply a uniform pressure to one side of the sheet specimen with a prescribed load curve of 0,0 (s,MPa) as point 1 and 48.2,23 (s,MPa) as

point 2. An end-time of 48.2 s was selected since this was the duration of the loading phase of the experimental bulge test.

The finite element mesh of the sheet specimen is illustrated in Figure 6-8. The element size increases as the distance from the centre increases, while still maintaining an aspect ratio relatively close to 1.0, as shown in Figure 6-9.
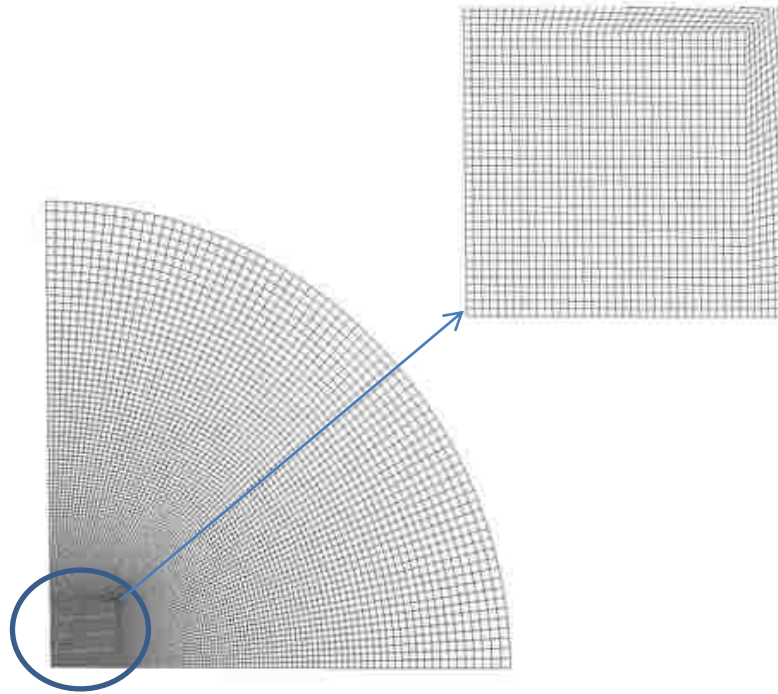
Figure 6-8. Finite element mesh for the bulge test model focusing on the central region of the blank
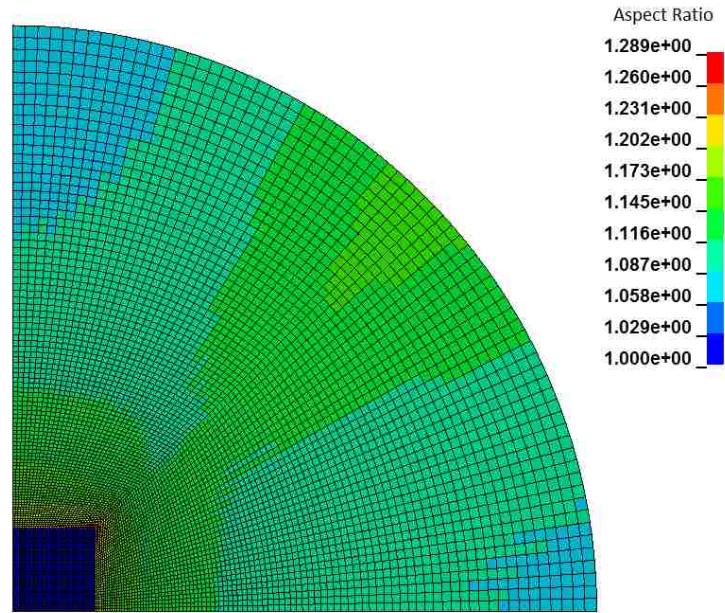
Figure 6-9. Aspect ratio of the elements in the model of the bulge test specimen
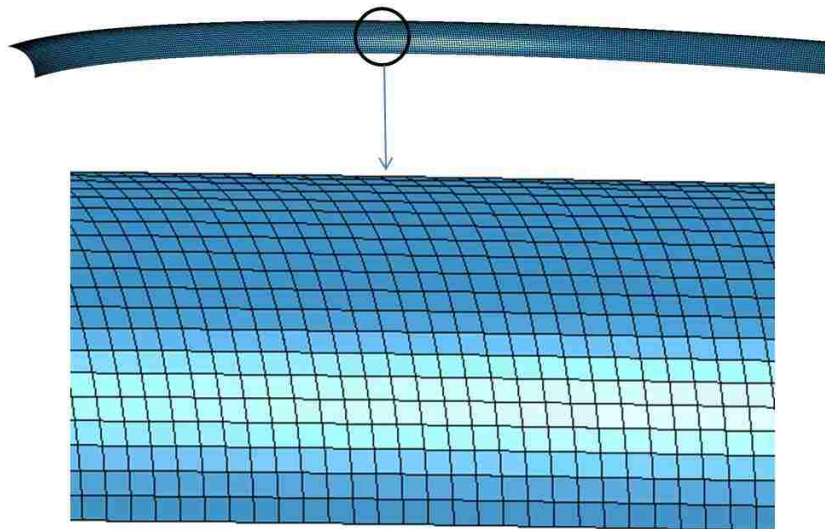
Figure 6-10. Bulge test 3 mm radius fillet

Four distinct boundary conditions were required in this quarter model. The first two boundary conditions were used to create orthogonal symmetry planes, and rectangle 1 and 2 in Figure 6-11 show the location of these symmetry planes. Table 18 shows the constraints that were applied to the nodal displacements and rotations along these two symmetry planes.

Constraint	Symmetry Plane One (Rectangle 1) Constrained (Yes/No)	Symmetry Plane One (Rectangle 2) Constrained (Yes/No)
X	Yes	No
Y	No	Yes
Z	No	No
RX	No	Yes
RY	Yes	No
RZ	Yes	Yes

Table 18. Symmetry planes for the hydraulic bulge test
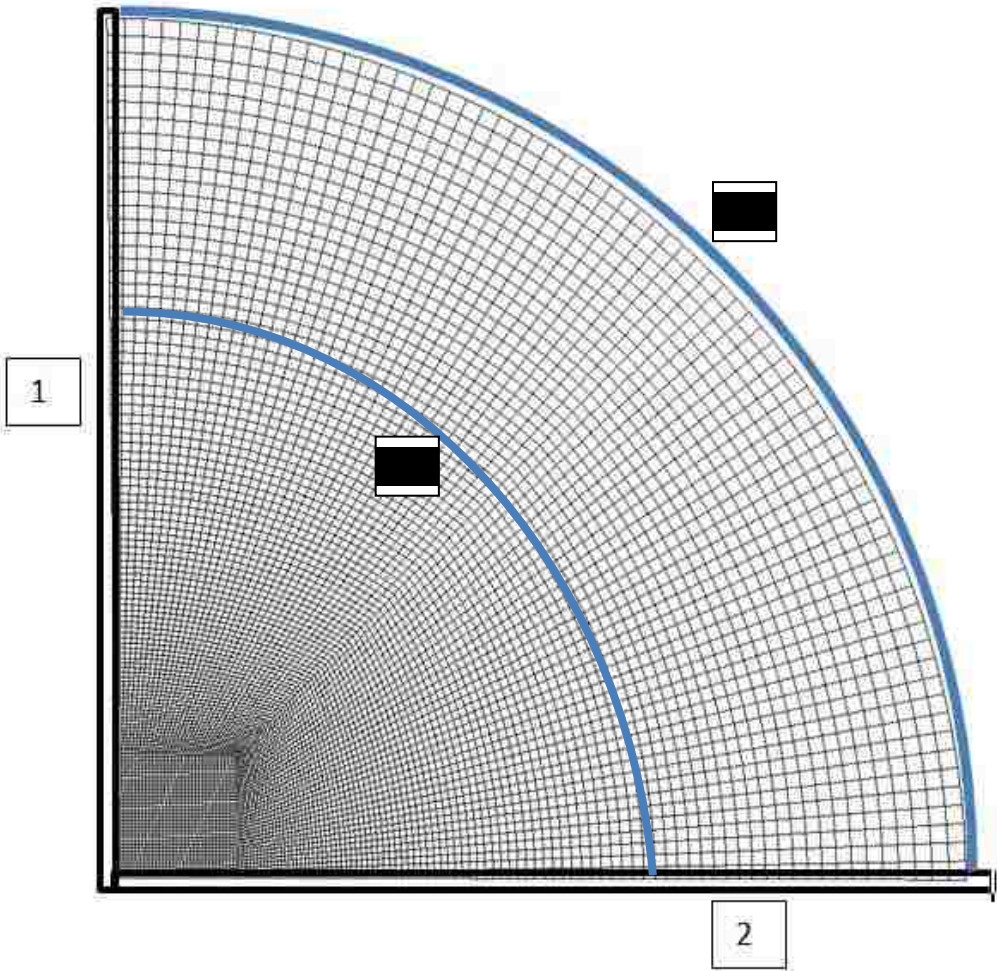
Figure 6-11. One quarter of the bulge test specimen showing the nodes at which boundary conditions were applied

The bulge test must be conducted without any material flowing into the forming zone, and therefore a full constraint is necessary to achieve this. The third boundary condition is a quarter of a circle that corresponds with the area between arc 3 and 4 shown in Figure 6-11. The nodal displacements and rotations are fully constrained in order to simulate the effect of the secure clamping of the blank between the clamping ring and the lower die. The final constraint is another full nodal and rotational displacement placed on the 3 mm radius fillet around the die cavity, this is to ensure that this boundary does not draw into the forming zone.

6.5   Validation and verification of implicit hydraulic bulge test simulation

A comparison was made between the pressure (MPa) and height at the apex of the dome (mm) for both the experimental and FEA model of the bulge test. Fourth order polynomial functions were fitted to the predicted and experimental pressure vs. bulge height data so that the two sets of data could be more easily compared. The equation that provided the best fit to the experimental data was y = -0.0044x^2 + 0.8547x - 1.6726 with R^2 = 0.9964 and the equation that best fit the predicted results was -0.0031x^2 + 0.7967x - 1.349 with R^2= 0.9997 and Figure 6-12 and Figure 6-123 show these data, respectively.
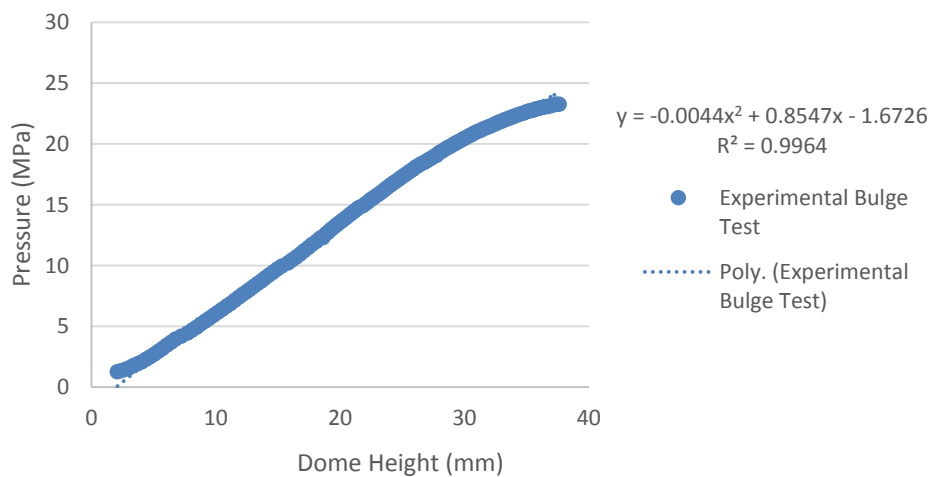
Figure 6-12. Experimental bulge test pressure vs. height at the apex of the dome
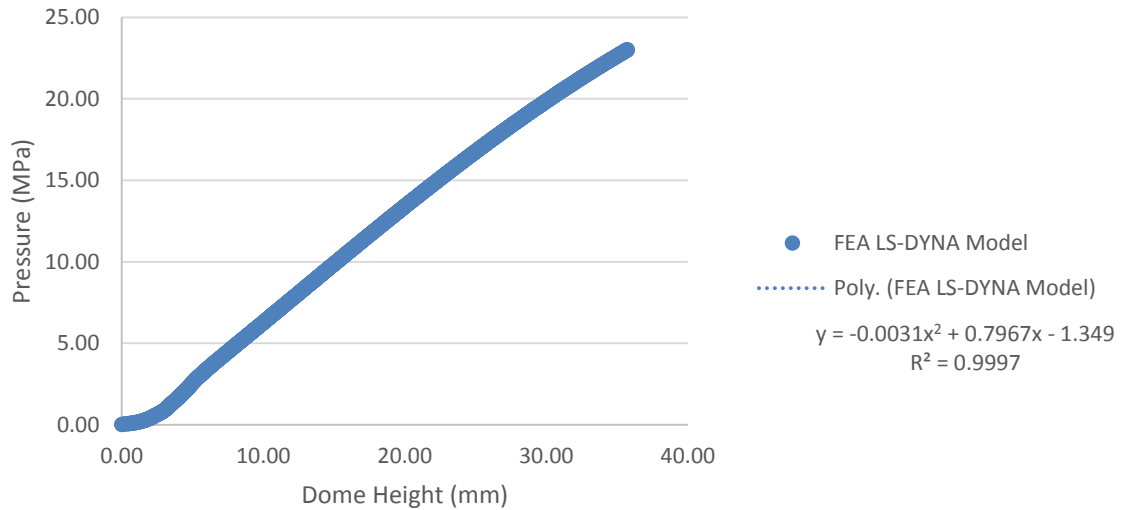
Figure 6-13. LS-DYNA Model – predicted bulge test pressure vs. height at the apex of the dome

The predicted pressure vs. bulge height curve was compared to the corresponding experimental curve using the same metric as in Equation (37), and the validation score was calculated to be 0.98. This indicates that the finite element model of the bulge test correlates well with the experimental data throughout the duration of the test.

Once again, the energy balance was evaluated in order to verify that the model follows the fundamental laws of energy conservation. Figure 6-14 shows that the total kinetic energy of the specimen throughout the entire test remained at 0. This is to be expected since the specimen does not have any velocity or acceleration applied to it. The internal energy of the specimen is equal to the total energy of the specimen, which is also to be expected. Hourglass energy was 0 throughout the test.
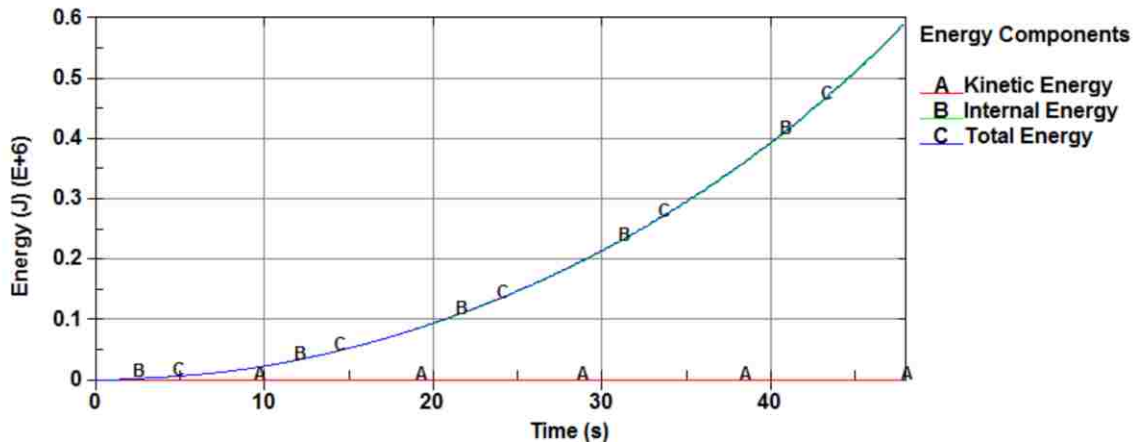
Figure 6-14. Energy Balance in the FE simulation of the Bulge Test

6.6   Mesh sensitivity study

A mesh sensitivity study was conducted for the 3-mm fillet radius that the bulge test specimen must wrap around as it bulges. Several different models were constructed, in which the number of elements around the 3-mm die radius was increased from a minimum of 4 elements up to a maximum of 18 elements. The results were plotted as a function of the radius of curvature (mm) at the pole of the bulging specimen vs. time (s) and are displayed in Figure 6-15. As can be seen from the results, the element size on the 3 mm radius did not have a significant effect on the results of the bulge test.
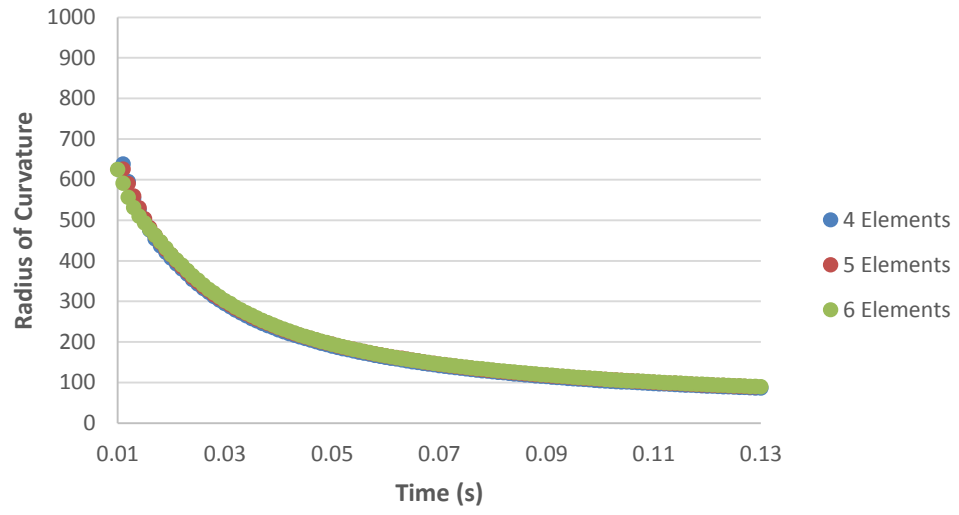
Figure 6-15. Mesh sensitivity study on 3 mm radius fillet of the die - radius of curvature vs. time

Chapter 7   Discussion

7.1   Comparison of Bulge Test Results

Unlike the tensile test, there is no standard for conducting hydraulic bulge tests. The bulge test tooling designed in this research is unique and there is no duplicate of this tool. Results obtained from this specific design need to be compared to other published and accepted data. However, different bulge test facilities may lead to slightly different results due to the different parameters in the die design, such as the radius of the fillet on the cavity of the tool. It is also expected that published bulge test data for DP600 will differ somewhat since every batch of DP600 steel will have slightly different material characteristics. Nevertheless, comparing the experimental flow curves of this DP600 steel to other similar data from the literature will ensure that the work hardening behaviour of DP600 steel obtained with this bulge test facility follows the same general trends.
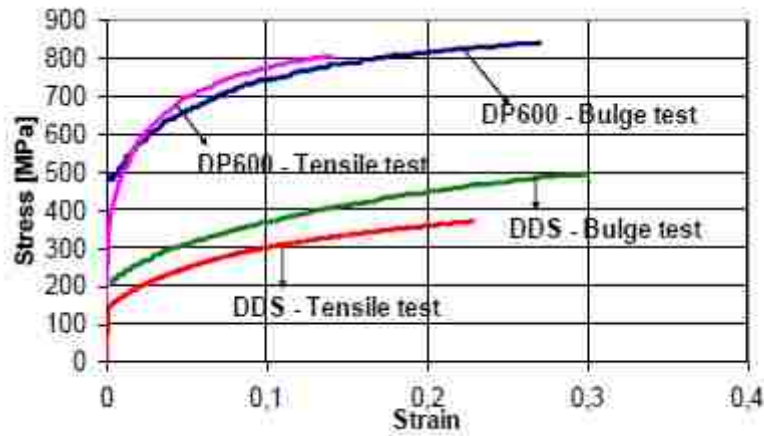
Figure 7-1. Comparison of flow stress curves from determination of sheet material properties using biaxial bulge tests [71]
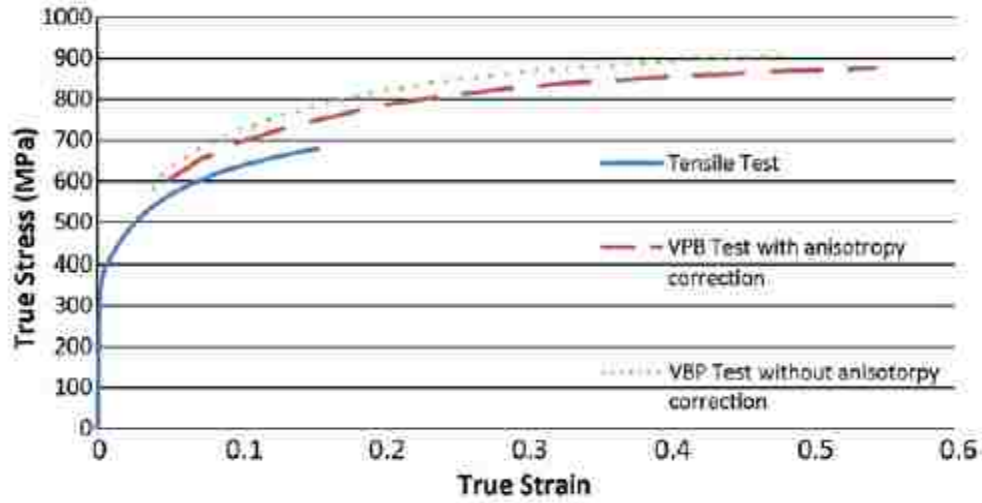
Figure 7-2. Comparison of flow stress curves from A. Nasser et al. [22]
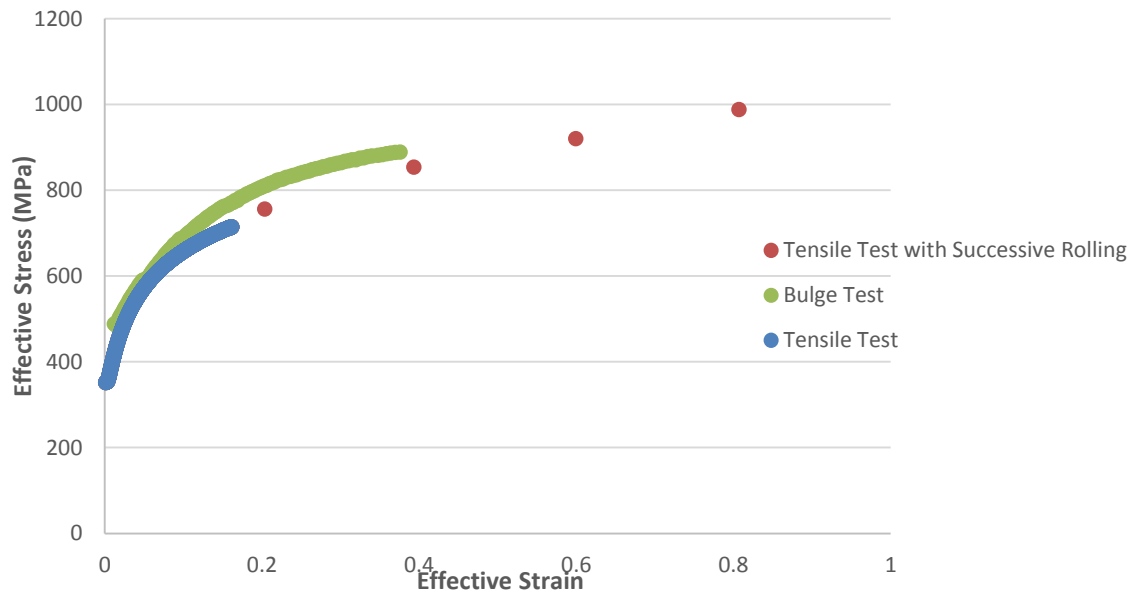
Figure 7-3. Comparison of flow stress curves obtained at the University of Windsor

The DP600 flow curve obtained using this bulge test facility is similar to the curve provided by A. Nasser et al. [22]. Moreover, the bulge test flow curve starts at approximately the same stress values as the tensile test flow curve. However, after

approximately 10 percent effective strain, the effective stress in the bulge test curve increases above that of the flow curve in uniaxial tension.
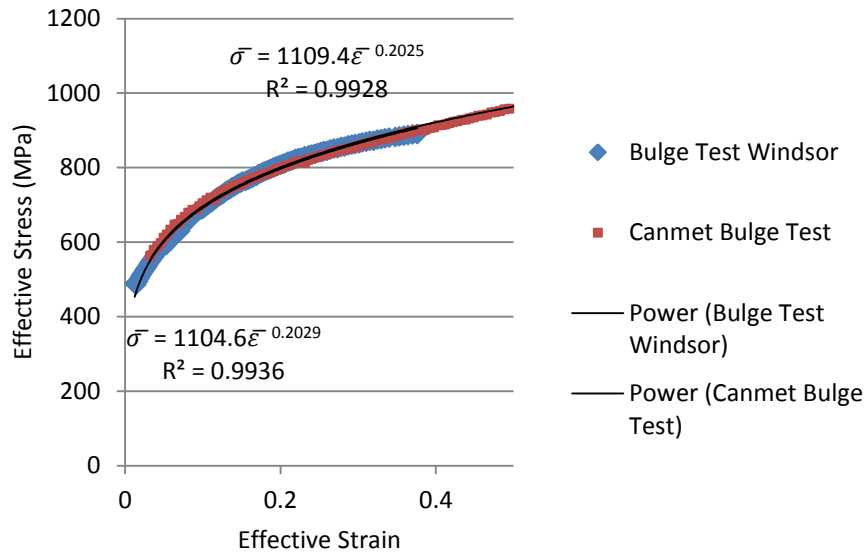
Figure 7-4. Comparison of Windsor and Canmet bulge test results

The same batch of DP600 was tested using the hydraulic bulge test at the Canmet Materials (NRC) research facility. Figure 7-4 shows the results match extremely well with the results obtained from the hydraulic bulge test apparatus designed in Windsor, further showing that the tooling, testing and data analysis methodology provide consistent data with other research facilities.

7.2   Tensile Test with successive cold rolling vs. Bulge Test Flow Curve

The power law fit of the extended tensile flow curve in the sheet rolling direction (obtained after successive flat rolling) is $\bar{\sigma}=1026.851\,\bar{\varepsilon}^{0.1951}$ and the power law fit of the bulge test flow curve is $\bar{\sigma}=1104.6\,\bar{\varepsilon}^{0.2029}$. The slight difference in the two power law curves highlight the differences between the uniaxial tension test data and the biaxial bulge test data. In order to quantitatively determine the discrepancy between the two curves, an error and validation metric was calculated using Equation (37). Since the tensile test power law fit is the industry-accepted description of sheet material behaviour, the bulge test power law function is therefore compared to the tensile data.

The error across the range from 0-40 % strain is only 0.03 and the validation metric is 0.96. There is some difference between the two power law curves but the comparison of the curves using these metrics show that the difference is relatively small. The stress state in the hydraulic bulge test is biaxial, thus leading to higher strain values without localized necking in comparison to the traditional uniaxial tensile test. In industrial metal forming processes, the state of stress is generally not uniaxial, thus making uniaxial tensile conditions unrepresentative of general sheet forming operations. Furthermore, Figure 7-5 highlights the extrapolation that is required to extend tensile test data up to the same percent strain as that attained with the bulge test. As can be seen, the bulge test data extends to far greater strain levels than what can be obtained in uniaxial tension. And if the bulge test was continued to even greater levels of strain (section 7.3 discusses this issue) there would be even more data that would need to be extrapolated.
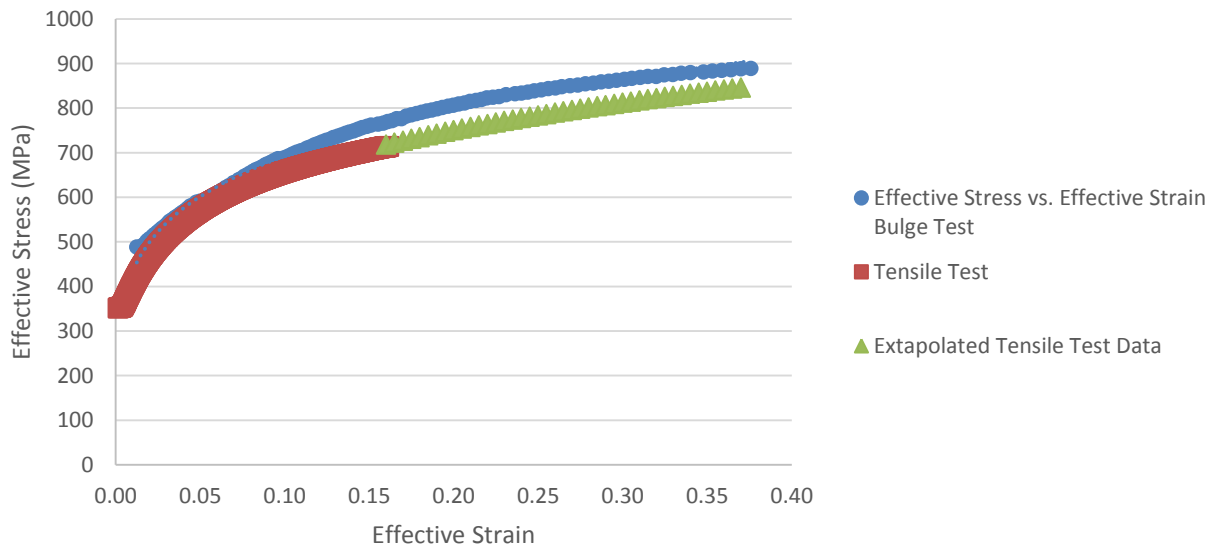
Figure 7-5. Extrapolated tensile data

Sarraf et al. [72] developed several Python codes that are capable of fitting constitutive equations to experimental data as shown in Figure 7-6. Various constitutive equations can lead to different results in terms of the flow stress curve, some deviating further

from others. The maximum difference can be seen between the Johnson-Cook model [72] and the modified Voce-Johnson-Cook model in this comparison.

In order to see the relationship between various fitted curves, both the extended tensile curve and the hydraulic bulge test flow curve were fitted using a power law function, as well as the Ludwik [72] and Voce [72] constitutive equations and were plotted on the same graph shown in Figure 7-7. The fitted curves match the respective experimental data well for both the extended tensile data and the hydraulic bulge test data, the exception being the Ludwik fit of the hydraulic bulge test data. The Ludwik fit matched well for the tensile test data but not for the hydraulic bulge test data, which demonstrates that appropriate constitutive equations must be used in order to obtain accurate simulation results. The data was plotted up until the effective strain of the hydraulic bulge test.
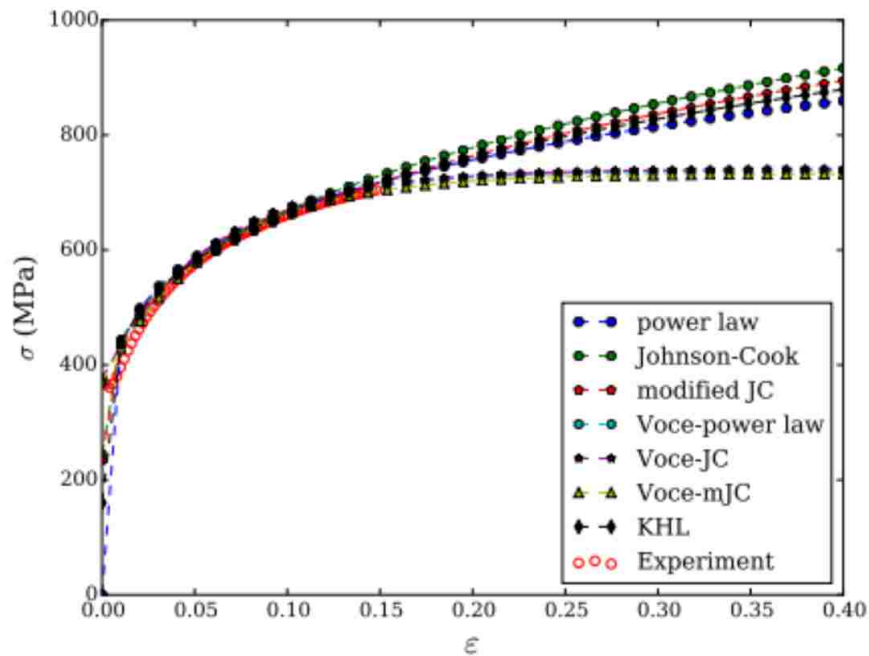
Figure 7-6. Fitting of uniaxial tension curve of DP600 with various constitutive equations – courtesy of Sarraf et al. [72]
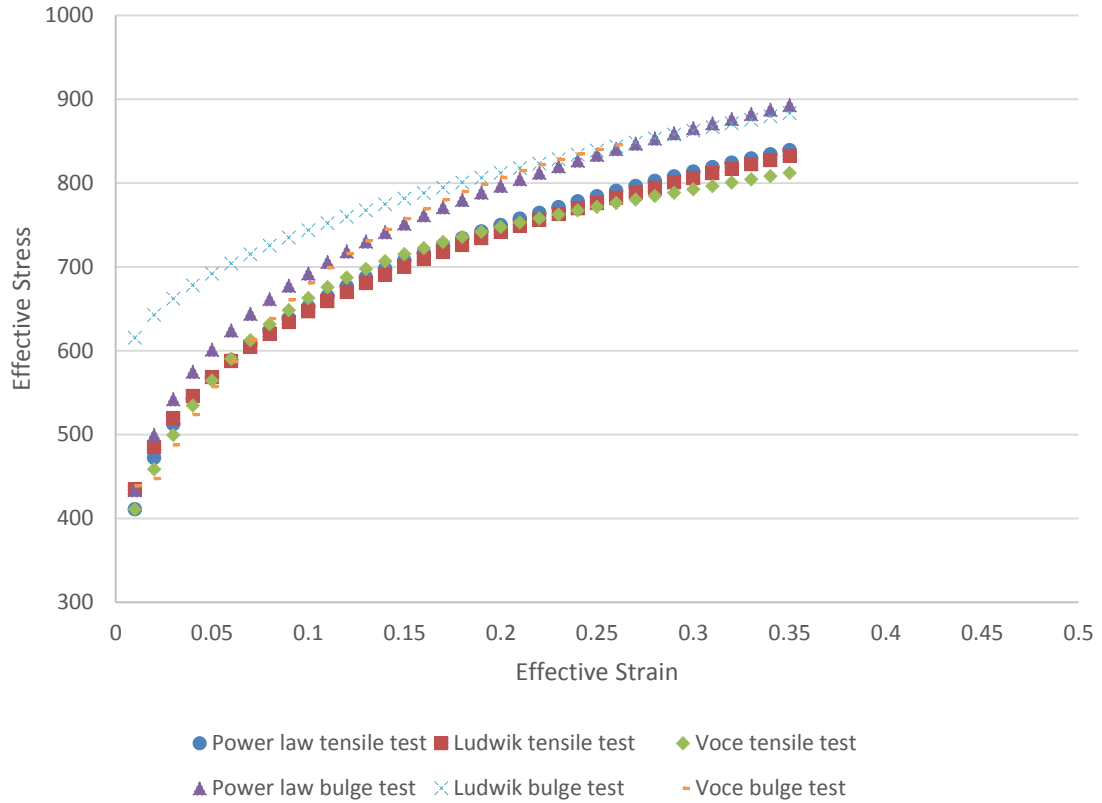
Figure 7-7. Fitting of the extended tensile flow curve and the hydraulic bulge test curve using power law, Ludwik, and Voce functions

The general equation of a power law function is:

$$\bar{\sigma}=C_1\bar{\varepsilon}^{c2} \tag{38}$$

The general expression of the Ludwik constitutive model is:

$$\bar{\sigma}=C_1+ C_2\bar{\varepsilon}^{c3} \tag{39}$$

The general equation for the Voce constitutive model is:

$$\bar{\sigma}= (C_2 - (C_2-C_1)) (1 + e^{(-C3\bar{\varepsilon})})+ C_4\bar{\varepsilon} \tag{40}$$

The error metric that was used to compare the extended tensile test and the bulge test and evaluate different hardening models is from [10]:

$$E = 1 - \frac{1}{L}\int_0^L \left|\frac{y(x)-Y(x)}{Y(x)}\right| dx \tag{41}$$

	Extended Tensile Test	Hydraulic Bulge Test	Comparison Metric [10]	Error
Power law Equation	$\bar{\sigma}=1026.9\bar{\varepsilon}^{\,0.1951}$	$\bar{\sigma}=1104.6\bar{\varepsilon}^{\,0.2029}$	0.94	0.06
Ludwik Equation	$\bar{\sigma}=191.2+853.8\bar{\varepsilon}^{\,0.2726}$	$\bar{\sigma}=532.8+537.24\bar{\varepsilon}^{\,0.4064}$	0.87	0.12
Voce Stage 4 hardening Equation	$\bar{\sigma}=(354.6-(354.6-683.9)(1-e^{(-17.4\bar{\varepsilon})})+368\bar{\varepsilon}$	$\bar{\sigma}=(353.86-(353.86-822.94)(1-e^{(-10.6\bar{\varepsilon})})+201.84\bar{\varepsilon}$	0.94	0.06

Table 19. Comparison Metrics

Figure 7-7 shows the results from the extended tensile curve and the hydraulic bulge test flow stress curves with various fitted functions up to the effective strain of the hydraulic bulge test flow stress curve. The comparison metric in Table 19 [10] shows that the hydraulic bulge test data correlate well with the extended tensile flow curve, except for the Ludwik function.

7.3 Future Recommendations

1. In order to obtain a better fit of the flow curve, experimental bulge tests should be conducted to a higher level of effective strain. As shown in the Figure 7-8 and Figure 7-9, when terminating the biaxial bulge test at a pressure somewhat lower than the burst pressure of the material, leads to a significant amount of data being missed. These figures also illustrate the large amount of strain data that can be achieved from a bulge test.

Figure 7-8. Pressure vs. dome height curve extrapolated from 212 bars to a burst pressure of 226 bars [22]
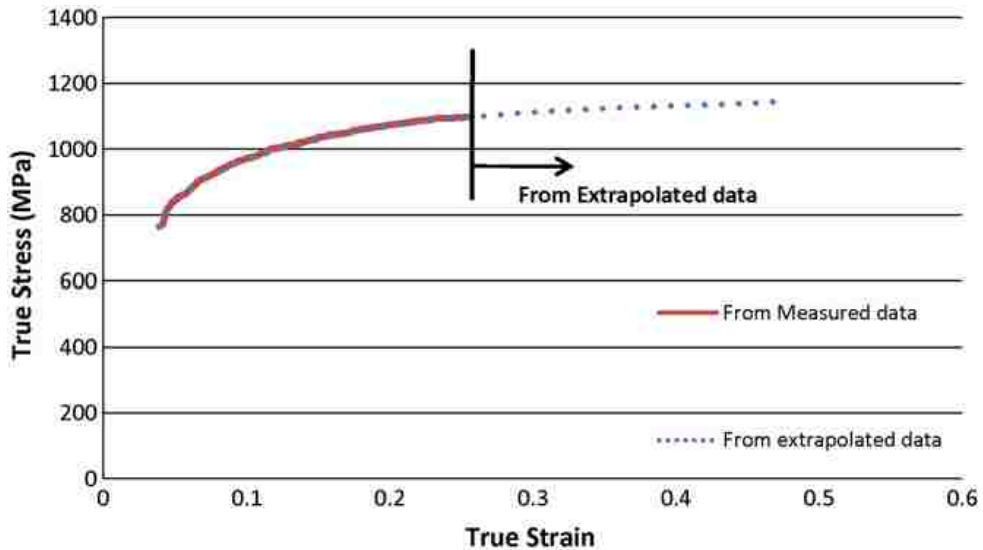
Figure 7-9. The flow curve of TRIP 780 obtained from both experimentally obtained data and extrapolated data [22]

2. A precise torque gun should be used when torqueing the bolts to clamp the bulge test specimen into place. This insures that a more uniform clamping force is distributed into the bolts. The clamping ring with no bolts is not adequate to provide a constant clamping force, thus should only be used for very formable, low strength sheet materials.

3. The clamping ring with no bolts should be resized in order to make the clamping area/diameter smaller, as the reduced contact area would lead to a greater

contact stress on the specimen. This could potentially save the operator a significant amount of time if the clamping ring with bolts does not have to be used.

4. The piston seal is extremely tight, and therefore requires a significant amount of force to move the piston prior. The friction force created by the seal against the cylinder wall, which likely increases with increasing pressure, may have led to an incorrect calibration of the pressure transducer, thus causing the calculated stress values to be increasingly overestimated. This friction force should be measured and quantified for future tests. And the pressure transducer should be calibrated with another pressure transducer rather than from the pressure that is calculated from the piston force.

5. Bulge tests should be carried out with a decreasing piston velocity in order to maintain a constant strain rate at the pole of the bulging sheet specimen. If a constant speed is used the strain rate increases as the test progresses. However, the press control system does not currently allow for a programmable reduction of the piston velocity throughout the forming process.

As can be seen in Figure 7-10 the strain deviates from linearity as the test progresses in time, this can be fixed with the recommendations made above.
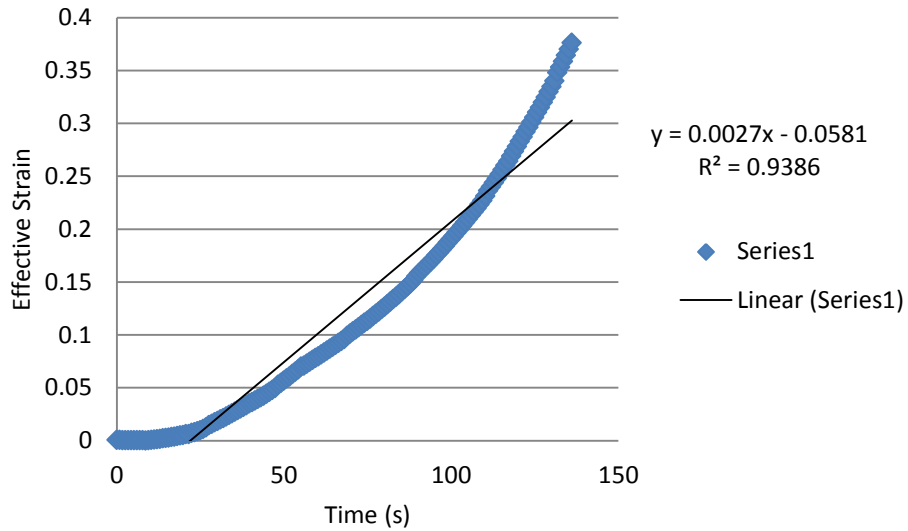
Figure 7-10. Effective strain vs. time - Illustrates approximate strain rate

7.4 Conclusions

Tensile tests after prestraining by successive flat rolling were conducted in order to obtain a flow curve that could reach 100% effective strain. Increments of 20% strain were selected with a minimum of 3 tensile tests at each prestrain increment. The final flow curves was determined to be $\bar{\sigma}=1026.851\bar{\varepsilon}^{0.1951}$ in the rolling direction and $\bar{\sigma}=1022.456\bar{\varepsilon}^{0.1758}$ in the transverse direction.

A hydraulic bulge test facility was developed with a 3 mm radius on the fillet of the die cavity with a 135 mm-diameter opening, a 120 mm-diameter piston that is capable of a maximum force of 1000 kN, leading to a pressure of up to 69.9 MPa. The final flow curve of DP600 steel obtained from the hydraulic bulge test was determined to be $\bar{\sigma}=1104.6\bar{\varepsilon}^{0.2029}$.

FEA models were created and were verified through the use of energy balances as well as validated using the validation metric proposed by Oberkampf et al. [10]. The predicted flow curve for the uniaxial tensile test showed a validation score of 0.97 and that for the hydraulic bulge test 0.98.

Flow curves obtained from the tensile test after successive flat rolling and from the hydraulic bulge test were compared using the same metrics [10]: this showed that the two flow curves are similar. Comparing the power law fit of the two flow curves yielded a comparison metric of 0.94; the same comparison using a Ludwik fit of the experimental data yielded a value of 0.87, and 0.94 when the Voce (stage 4 hardening) function was used to fit the data.

The hydraulic bulge test flow curve was compared to the tensile test data after successive flat rolling as both sets of data reach much higher levels of effective strain than a tensile test. The tensile test after flat rolling and the hydraulic bulge test yield similar flow curves which gives evidence that the hydraulic bulge test tooling, testing procedures and analysis methodology were successfully developed to generate reliable experimental data. Hydraulic bulge tests conducted on the same batch of DP600 steel sheet using the University of Windsor's testing facility and the Canmet Materials' facility, lead to practically identical flow curves.

In order to produce a flow curve using this hydraulic bulge test facility, the testing and analysis take approximately 20 minutes. The experimental testing and analysis required to produce a tensile flow curve with successive flat rolling took almost two weeks. The difference in time commitment between the two tests is very significant. In order to support industrial sheet metal forming applications, the hydraulic bulge test is a convenient and practical method to obtain a flow curve up to large deformation, whereas tensile tests after successive flat rolling require far too much of a time commitment.

BIBLIOGRAPHY

[1] C. Jones, "Biaxial testing of polymer composites," *Material World,* vol. 9, no. 11, pp. 19-21, 2001.

[2] "Sheet Metal Basics," [Online]. Available: http://thelibraryofmanufacturing.com/sheetmetal_basics.html. [Accessed 3 October 2015].

[3] Secretary, "Obama Administration Finalizes Historic 54.5 MPG Fuel Efficiency Standards," 28 August 2012. [Online]. Available: https://www.whitehouse.gov/the-press-office/2012/08/28/obama-administration-finalizes-historic-545-mpg-fuel-efficiency-standard.

[4] D. Schaeffler, "Introduction to advanced high-strength steels - Part I," *STAMPING JOURNAL,* no. 1, pp. 1-4, 2004.

[5] T. Altan and A. E. Tekkaya, Sheet Metal Forming: Processes and Applications, ASM International, 2012.

[6] C. Jones, "Biaxial testing of polymer composites," *Material World ,* vol. 9, no. 11, pp. 19-21, 2005.

[7] S. Semiatin, "Metalworking: sheet forming," *ASM Handbook,* vol. 14 B, 2006.

[8] J. Pang, Mechanics and Reliability, Springer, 2012.

[9] H. Rodrigues, Engineering Optimization 2014, Lisbon: CRC Press, 2014.

[10] W. L. Oberkampf and T. G. Trucano, "Verification and validation in computational fluid dynamics," *Progress in Aerospace Sciences,* vol. 38, no. 3, pp. 209-272, 2002.

[11] E. P. Degarmo, J. T. Black and R. A. Kohser, Materials and Processes in Manufacturing (9th ed.), Wiley, 2003.

[12] R. Mayagüez, "Work Hardening MechMet," 08 September 2012. [Online]. Available: http://academic.uprm.edu/pcaceres/Courses/MechMet/MET-6A.pdf. [Accessed 8 November 2015].

[13] R. Brannon, "Define your strain," 27 07 2000. [Online]. Available: http://www.mech.utah.edu/~brannon/public/strain.pdf. [Accessed 21 July 2016].

[14] Y. Fung, A first Course In Continuum Mechanics, Englewood Cliffs: Prentice-Hall, 1994.

[15] G. Gutscher, H.-C. Wu, G. Ngaile and T. Altan, "Determination of flow stress for sheet metal forming using the viscous pressure bulge (VPB) test," *Journal of Materials Processing Technology,* vol. 146, no. 1, pp. 1-7, 2004.

[16] A. Hedrick, "The Fabricator," 19 February 2001. [Online]. Available: http://www.thefabricator.com/article/stamping/controlling-flow-and-obtaining-stretch-in-deep-draw-operations.

[17] C. Koh, "Design of a Hydraulic Bulge Test Apparatus," *Department of Mechanical Engineering at Massachusetts Institute of Technology,* 2012.

[18] G. Gutscher, "Determination of flow stress for sheet metal forming using the viscous pressure bulge (VPB) test," *Journal of Materials Processing Technology,* vol. 146, no. 1, pp. 1-7, 2004.

[19] Q. Li, E. Y. Chen, D. R. Bice and D. C. Dunand, "Transformation Superplasticity of Cast Titanium and Ti-6Al-4V," *The Minerals, Metals & Materials Society and ASM International,* vol. 38a, no. 1, pp. 53-63, 2007.

[20] B. Tomov, E. Yankov and R. Radev, "Research highlights of sheet metal testing by hydraulic bulging," *Journal of Achievements in Materials and Manufacturing Engineering,* vol. 46, no. 1, pp. 65-70, 2011.

[21] B. Toga, E. Alacaa and K. Bugra, "Strain-controlled bulge test," *J. Material Resistance,* vol. 23, no. 12, pp. 3295-3302, 2008.

[22] A. Nasser, A. Yadav, P. Pathak and T. Altan, "Determination of the flow stress of five AHSS sheet materials (DP 600, DP 780, DP780-CR, DP 780-HY and TRIP 780) using the uniaxial tensile and the biaxial Viscous Pressure Bulge (VPB) tests," *Journal of Materials Processing Technology,* vol. 210, no. 3, pp. 429-436, 2010.

[23] F. Gologranc, "Beitrag zur Ermittlung von Fließkurven im kontinuierlichen hydraulischen Tiefungsversuch (Evaluation of the flow stress curve with the continuous hydraulic bulge test)," Institute for Metaling Forming Technology, University of Stuttgart, Stuttgart, Germany , 1975.

[24] M. Merklein and V. Godel, "Characterization of the flow behavior of deep drawing steel grades in dependency of the stress state and its impact on FEA," *International Journal of Material Forming 2,* vol. 2, no. 1, pp. 415-418, 2009.

[25] D. Rees, "Plastic flow in the elliptical bulge test," *International Journal of Mechanical Sciences,* vol. 37, no. 4, pp. 373-389, 1995.

[26] A. Diehl, D. Staud and U. Engel, "Investigation of the mechanical behaviour of thin metal sheets using the hydraulic bulge test," in *Proceedings of the 4th International Conference "Multi-Material Micro Manufacture"*, Cardiff, 2008.

[27] M. Atkinson, "Accurate determination of biaxial stress-strain relationships from hyraulic bulging test of sheet metals.," *International Journal of Mechanical Sciences ,* vol. 39, no. 7, pp. 761-769, 1997.

[28] E. Edge, "Mechanics of Materials Pressure Vessel Design and Calculators," Solutions by Design, 08 March 2012. [Online]. Available: http://www.engineersedge.com/material_science/hoop-stress.htm. [Accessed 8th October 2016].

[29] Efunda, "Spherical Pressure Vessel," Efunda, 21 March 2015. [Online]. Available: http://www.efunda.com/formulae/solid_mechanics/mat_mechanics/pressure_vessel.cfm. [Accessed 4 January 2016].

[30] W. Pankin, "Der hydraulische Tiefungsversuch und die Ermittlung von Fließkurven (The hydraulic bulge test and the determination of the flow stress curves)," Institute for Metal Forming Technology, University of Stuttgart, Stuttgart, Germany , 1959.

[31] R. Hill, "A theory of the plastic bulging of a metal diaphragm by lateral pressure," *Philosophical Magazine,* vol. 7, pp. 1133-1142, 1950.

[32] J. Chakrabarty and J. Alexander, "Hydrostatic bulging of circular diaphragms," *J. Strain Anal.,* vol. 5, no. 2, pp. 155-161, 1970.

[33] A. Kruglov, F. Enikeev and R. Lutfullin, "Superplastic forming of a spherical shell out a welded envelope," *Material Science Engineering,* vol. 323, no. 1-2, pp. 416-426, 2002.

[34] M. Koc, E. Billur and O. N. Cora, "An experimnetal study on the comparative assessment of hydraulic bulge test analysis methods," *Materials and Design,* vol. 31, no. 1, pp. 272-281, 2011.

[35] ASTM International, "Standard Test Method for Plastic Strain Ratio r for Sheet Metal," 2010. [Online]. Available: http://compass.astm.org/download/E517.21868.pdf. [Accessed 25 July 2015].

[36] H. Palaniswamy and T. Altan, "Process simulation and optimization in metal forming-selected examples and challenges," *Steel Research International,* no. 78, pp. 733-735, 2007.

[37] K. Miyauchi, "Stress Strain Relationship in Simple Shear of In-Plane Deformation for Various Steel Sheets," *Efficiency in Sheet Metal Forming,* vol. IDDRG (1984), no. 1, pp. 360-371, 1984.

[38] H. Berg, P. Hora and J. Reissner, "Simulation of Sheet Metal Forming Processes using Different Anisotropic constitutive Models," *Numiform 98,* pp. 775-780, 1998.

[39] P. Flores, P. d. Montleau, V. Mathonet, P. Moureaux and A. Habraken, "Identification of material parameters using a bi-axial machine," *Proc. ESAFORM'04,* vol. 7, no. 1, pp. 237-240, 2004.

[40] Y. An, H. Vegter, L. Elliott and J. Bottema, "A comparison of yield loci derived from different approaches for aluminium alloys," *Aluminium,* vol. 4, no. 80, pp. 674-679, 2004.

[41] B. Zillmann, T. Clausmeyer, S. Bargmann, T. Lampke, M. Wagner and T. Halle, "Validation of simple shear tests for parameter indetification considering the evolution of plastic anisotropy," *Technology Mech.,* vol. 32, no. 2-5, pp. 622-630, 2012.

[42] A. Brosius, Q. Yin, A. Guner and A. Tekkaya, "A new shear test for sheet material characterization," *Steel Res. Int.,* vol. 82, no. 4, pp. 323-328, 2011.

[43] Q. Yin, C. Soyarslan, A. Brosius and A. Tekkaya, "A cyclic twin bridge shear test for the indentification of kinematic hardening parameters," *International Journal of Mechanical Sciences,* vol. 59, no. 1, pp. 31-34, 2012.

[44] D. Shouler and J.M Allwood, "Design and use of a novel sample design for forambility testing in pure shear," *Journal of Material Processing Technology,* vol. 210, no. 10, pp. 1304-1313, 2010.

[45] J. Kang, D. Wilkinson, P. Wu, M. Bruhis, M. Jain, J. Embury and R. Mishra, "Constitutive behavior of AA5754 sheet materials at large strains," *Engineering Material Technology,* vol. 3, no. 130, p. 031001–031005, 2008.

[46] M. Merklein and M. Biasutti, "Forward and reverse simple shear test experiments for material modeling in forming simulations," in *Proceedings of the 10th International Conference on Technology of Plasticity*, Aachen, Germany, 2011.

[47] J. Peirs, P. Verleysen and J. Degrieck, "Novel technique for static and dynamic shear testing of Ti6Al4V sheet.," *Experimental Mechanics,* vol. 52, no. 7, pp. 729-741, 2011.

[48] Y. Hanabusa, H. Takizawa and T. Kuwabara, "Numerical verification of a biaxial tensile test method using a cruciform specimen," *Journal of Materials Processing Technology,* vol. 213, no. 6, pp. 961-970, 2013.

[49] A. Smits, D. V. Hemelrijck, T. Philippidis and A. Cardon, "Design of a cruciform specimen for biaxial testing of fibre reinforced composite laminates," *Composites Science and Technology,* vol. 66, no. 7-8, pp. 964-975, 2006.

[50] Z. Marciniak and K. Kuczyński, "Limit strains in the process of stretch-forming sheet metal," *International Journal of Mechanical Science,* vol. 609, no. 9, p. 620, 1967.

[51] D. Kelly, "Problems in creep testing under biaxial stress systems," *Journal of Strain Analysis for Engineering Design,* vol. 11, no. 1-6, p. 1:11, 1976.

[52] W. Müller and K. Pöhlandt, "New experiments for determining yield loci of sheet metal," *Material Processing Technology,* vol. 60, no. 1-4, pp. 648-651, 1996.

[53] E. Hoferlin, A. V. Bael, P. V. Houtte, G. Steyaert and C. D. Maré, "Biaxial tests on cruciform specimens for the validation of crystallographic yield loci," *Material Processing Technology,* Vols. 80-81, pp. 550-555, 1998.

[54] Y. Hanabusa, H. Takizawa and T. Kuwabara, "Numerical verification of a biaxial tensile test method using a cruciform specimen," *Journal of Materials Processing Technology,* vol. 213, no. 6, pp. 961-970, 2013.

[55] K. Pascoe and J Villiers, "Low cycle fatigue of steels under biaxial straining," *Journal of Strain Analysis,* vol. 2, no. 2, pp. 117-126, 1967.

[56] E. Shiratori and K. Ikegami, "Experimental study of the subsequent yield surface by using cross-shaped specimens," *Journal of the Mechanics and Physics of Solids,* vol. 16, no. 6, pp. 373-394, 1968.

[57] T. Kuwabara, S. Ikeda and T. Kuroda, "Measurement and analysis of differential work hardening in cold-rolled steel sheet under biaxial tension," *Journal of Materials Processing Technology,* Vols. 80-81, no. 1, pp. 517-523, 1998.

[58] T. Kuwabara, M. Kuroda, V. Tvergaard and K. Nomura, "Use of abrupt strain path change for determining subsequent yield surface: experimental study with metal sheets," *Acta Materalia,* vol. 48, no. 9, pp. 2071-2079, 2000.

[59] Y. Yu, M. Wan, X. D. Wu and X.-B. Zhou, "Design of a cruciform biaxial tensile specimen for limit strain analysis by FEM," *Material Process Technology,* vol. 123, no. 67, pp. 70-73, 2002.

[60] D. Green, K. Neale, S. MacEwen and R. Perrin, "Experimental investigation of the biaxial behaviour of an aluminum sheet," *International Journal of Plasticity* , vol. 20, no. 8-9, pp. 1677-1706, 2004.

[61] V. Al, "Varmint Al's Engineering Page," 19 07 2015. [Online]. Available: http://www.VarmintAl.com/aengr.htm. [Accessed 08 02 2016].

[62] Auto Steel, "DP600," 15 04 2014. [Online]. Available: www.autosteel.org/research/ahss-data-utilization/dp600.aspx. [Accessed 04 03 2016].

[63] ISO, "ISO 898-1:2013," ISO Standards, 2013.

[64] A. Hedrick, "Key design principles for successful deep drawing," STAMPING JOURNAL, 1999. [Online]. Available: http://www.thefabricator.com/article/stamping/key-design-principles-for-successful-deep-drawing. [Accessed 19 July 2015].

[65] ASME International, "ASTM E8/E8M-15a Standard Test Methods for Tension Testing of Metallic Materials," West Conshohocken, PA, 2015.

[66] ASME Committee, "Standard Test Method for Tensile Strain-Hardening Exponents (n-Values) of Metallic Sheet Materials," *ASTM* , no. E28.02, pp. 646-647, 2007.

[67] V. G. Magorien, "Effects of Air on Hydraulic Systems," *Hydraulics & Pneumatics,* pp. 48-51, 2013.

[68] "Metal Forming Processess Research," 8 May 2012. [Online]. Available: https://web2.uwindsor.ca/apc-ehf/index.html. [Accessed 10 October 2016].

[69] D. Schwarz, "Math Works," MathWorks, 27 Jan 2010. [Online]. Available: https://www.mathworks.com/matlabcentral/fileexchange/11837-fast-and-robust-curve-intersections/content/intersections.m. [Accessed 20 Feb 2015].

[70] S. P. Keeler, "Plastic instability and fracture in sheets stretched over rigid punches," *ASM Transactions Quarterly,* vol. 56, no. 11, pp. 25-48, 1963.

[71] T. Altan, H. Palaniswamy, M. M. Paolo Bortot, W. Heidl and A. Bechtold, "Determination of sheet material properties using biaxial bulge tests," Proceedings of the 2nd Int. Conference on Accuracy in Forming Technology, The Ohio State University, Columbus, OH, USA, 2006.

[72] I. S. Sarraf, A. Jenab, D. E. Green and K. P. Boyle, *Effect of rate-dependent constitutive equations on the tensile flow,* 2016.

APPENDICES

Appendix A – Matlab Code

```matlab
% Tensile Test Code created by Yang Song and Mario Vasilescu
%% ====================================== %
% Variable Naming Convensions
% sig - stress
% eps - strain
% _1 - major
% _2 - minor
% _3 - thickness
% _t - true (relative to engineering)
% _f - flow (plastic)
% _m - from mechanical gauge
% _v - from video extensometer
% _d - from DIC
% _sm - filtered
% _vm - von Mises
% _oa - overall
% _ro - rolling
%  ====================================== %

%       Available interpolation methods are:
%       'nearest'  - nearest neighbor interpolation
%       'next'     - next neighbor interpolation
%       'previous' - previous neighbor interpolation
%       'linear'   - linear interpolation
%       'spline'   - piecewise cubic spline interpolation (SPLINE)
%       'pchip'    - shape-preserving piecewise cubic interpolation
%       'cubic'    - same as 'pchip'
%       'v5cubic'  - the cubic interpolation from MATLAB 5, which does
not
%                    extrapolate and uses 'spline' if X is not equally
%                    spaced.
%%
format shortg
clear
clc
% Section 1
pois = 0.33; % Poisson's ratio
width = 12.5; % mm
thickness = 1.493; % mm
Ep1 = 100; % 1st point x for defining modulus line MPa
Ep2 = 300; % 2nd point x for defining modulus line MPa
mlsf = 1; % modulus line length scaling factor, default 1
cdata = 0; % additional data truncating in the end of arrays, default 0
Rp1 = 0.5; % R value portion 1
Rp2 = 0.75; % R value portion 2

eps_ro = 0; % rolling strain
name = 'RD1_2.txt'; % output name
```

```matlab
interpm_d = 'linear'; % interpolation method for DIC data on MTS time
frame
interpm_i = 'nearest'; % interpolation method for calculating interval
points
use_filter = 0; % switch for using filter on DIC minor strain, 1 for
yes, 0 for no
SPAN = 12; % SPAN for filter, should be lower than 10% of # of data
points
E_choice = 1; % swtich for choosing modulus line fitting method, 1 for
line defined by [Ep1 Ep2] and [p1 p2]

% Section 2
%% Loading data from MTS output
load data.txt
major = csvread('major.csv');
major2 = csvread('major2.csv');
minor = csvread('minor.csv');
c = data(1:end-cdata,1); % crosshead displacement
F = data(1:end-cdata,2)/1000; % load
t = data(1:end-cdata,3)*1000; % test time (MTS machine)
mech = data(1:end-cdata,12)*100; % strain from mechanical extensometer
v12 = (data(1:end-cdata,5)*100+mech(1)); % video strains v12-v67
v15 = (data(1:end-cdata,6)*100+mech(1));
v23 = (data(1:end-cdata,7)*100+mech(1));
v24 = (data(1:end-cdata,8)*100+mech(1));
v34 = (data(1:end-cdata,9)*100+mech(1));
v45 = (data(1:end-cdata,10)*100+mech(1));
v67 = (data(1:end-cdata,11)*100-mech(1)*pois);
vt = data(1:end-cdata,13)*1000; % video time as a function of MTS time

% Section 3
%% Syncing DIC data and convert eng stress and strain to true
frame = vt/1000*17; % frame #
d15 = 100*interp1(major(:,1),major(:,4),frame,interpm_d)+mech(1); % DIC
major strain eng
d24 = 100*interp1(major2(:,1),major2(:,4),frame,interpm_d)+mech(1); %
DIC major2 strain eng
d67 = 100*interp1(minor(:,1),minor(:,4),frame,interpm_d)-mech(1)*pois;
% DIC minor strain eng
sig_t_m = F*1000/(width*thickness).*(1+(mech/100)); % true stress from
strain measured by mechanical gauge
sig_t_v = F*1000/(width*thickness).*(1+(v15/100)); % true stress from
strain measured by video extensometer
sig_t_d = F*1000/(width*thickness).*(1+(d15/100)); % true stress from
strain measured by DIC
eps_1_t_m = log(1+(mech/100)); % true major stain mech
eps_1_t_v = log(1+(v15/100)); % true major stain Vid
eps_1_t_d = log(1+(d15/100)); % true major stain DIC
eps_2_t_v = log(1+(v67/100)); % true minor stain Vid
eps_2_t_d = log(1+(d67/100)); % true minor stain DIC

%% Determination of E modulus and yield stress
p1 = interp1(sig_t_m,eps_1_t_m,Ep1,interpm_i); % 1st point y for
defining modulus line
p2 = interp1(sig_t_m,eps_1_t_m,Ep2,interpm_i); % 2st point y for
defining modulus line
```

```matlab
% [p1 p1y] = intersections(eps_1_t_m,sig_t_m,[-5,5],[Ep1,Ep1]);
% [p2 p1y] = intersections(eps_1_t_m,sig_t_m,[-5,5],[Ep2,Ep2]);
E = (Ep2-Ep1)/(p2-p1) % Young's modulus MPa
linex = linspace(0,0.01*mlsf); % modulus line x array for major strain
liney = linex*E-0.002*E; % modulus line y array for major stess

p3 = ((p2-p1)*(-5*mlsf)+p1); %extrapolated x value to extend the line
downward
Ep3 = ((Ep2-Ep1)*(-5*mlsf)+Ep1); %extrapolated y value to extend the
line downward
p4 = ((p2-p1)*(15*mlsf)+p1); %extrapolated x value to extend the line
upward
Ep4 = ((Ep2-Ep1)*(15*mlsf)+Ep1); %extrapolated y value to extend the
line upward
if E_choice == 1
    linex = linspace(p3,p4)+0.002;
    liney = linspace(Ep3,Ep4);
end
linex2 = -linspace(0,0.0033*mlsf); % modulus line x array for minor
strain
liney2 = -linex2*E/pois-0.002*E*pois; % modulus line y array for minor
stress
[ystrain,yield] = intersections(linex,liney,eps_1_t_m,sig_t_m) % strain
and stress at yield

%% Truncating data for plastic range
index = 1:1:length(sig_t_m)';
trunc1 = ceil(interp1(sig_t_m,index,yield,interpm_i))
[Fmax,trunc2] = max(F)
sig_t_m_f = sig_t_m(trunc1:trunc2); % true stress mech truncated
sig_t_v_f = sig_t_v(trunc1:trunc2); % true stress Vid truncated
sig_t_d_f = sig_t_d(trunc1:trunc2); % true stress DIC truncated
eps_1_t_m_f = eps_1_t_m(trunc1:trunc2)-sig_t_m_f/E; % true major stain
mech plastic
eps_1_t_v_f = eps_1_t_v(trunc1:trunc2)-sig_t_v_f/E; % true major stain
Vid plastic
eps_1_t_d_f = eps_1_t_d(trunc1:trunc2)-sig_t_d_f/E; % true major stain
DIC plastic

%% R Value Calculations
if use_filter == 1
    eps_2_t_v_sm = smooth(eps_2_t_v,SPAN,'rloess');
    eps_2_t_d_sm = smooth(eps_2_t_d,SPAN,'rloess');
    RMSE(1) = sqrt(mean((eps_2_t_v(trunc1:trunc2) -
eps_2_t_v_sm(trunc1:trunc2)).^2))./sqrt(mean((eps_2_t_v(trunc1:trunc2))
.^2))*100;
    RMSE(2) = sqrt(mean((eps_2_t_d(trunc1:trunc2) -
eps_2_t_d_sm(trunc1:trunc2)).^2))./sqrt(mean((eps_2_t_d(trunc1:trunc2))
.^2))*100;
    fprintf('Filter activated, RMS error for filtered/unfiltered data
are shown below:\n')
    fprintf('Video   DIC\n')
    fprintf('%2.3f%%  %2.3f%%\n\n', RMSE)
    eps_2_t_v_f = eps_2_t_v_sm(trunc1:trunc2)+sig_t_v_f/E*pois; % true
minor stain vid plastic
```

```matlab
        eps_2_t_d_f = eps_2_t_d_sm(trunc1:trunc2)+sig_t_d_f/E*pois; % true
minor stain DIC plstic filtered
elseif use_filter == 0
        eps_2_t_v_f = eps_2_t_v(trunc1:trunc2)+sig_t_v_f/E*pois; % true
minor stain vid plastic
        eps_2_t_d_f = eps_2_t_d(trunc1:trunc2)+sig_t_d_f/E*pois; % true
minor stain DIC plstic filtered
else
        fprintf('Error. The switch "use_filter" must be equal to 0 or
1.\n');
        return;
end
eps_3_t_v_f = 0-eps_2_t_v_f-eps_1_t_m_f; % true thickness stain vid
eps_3_t_d_f = 0-eps_2_t_d_f-eps_1_t_m_f; % true thickness stain DIC
R_v = eps_2_t_v_f./eps_3_t_v_f;
R_d = eps_2_t_d_f./eps_3_t_d_f;


% Section 4
%% Effective Strain
eps_vm =
sqrt((2/3)*((eps_1_t_m_f).^2+(eps_2_t_d_f).^2+(eps_3_t_d_f).^2));
eps_oa = eps_vm+eps_ro;

%% Output data
output = [eps_oa,sig_t_m_f];
save(name,'output','-ascii')

%% Ploting figures

figure(1)
hold on
grid on
plot(c,eps_1_t_m)
xlabel('Displacement)')
ylabel('True strain')
title('Crosshead v.s. Time','fontweight','bold')

figure(2)
hold on
grid on
plot(t,F)
xlabel('Time (ms)')
ylabel('Load (kN)')
title('Load v.s. Time','fontweight','bold')

figure(3)
hold on
grid on
plot(t,mech)
plot(t,v15,'LineStyle','--')
plot(t,d15,'LineStyle','-.')
plot(t,v67)
plot(t,d67,':')
xlabel('Time (ms)')
```

```matlab
ylabel('Eng Strain (%)')
legend('Mechanical Extensometer','Video
Extensometer','DIC','v67','d67')
title('Strain v.s. Time - Different Extensometer in
Comparison','fontweight','bold')

figure(4)
hold on
grid on
plot(mech,F)
plot(v15,F,'LineStyle','--')
plot(d15,F,'LineStyle','-.')
xlabel('Eng Strain (%)')
ylabel('Load (kN)')
legend('Mechanical Extensometer','Video Extensometer','DIC')
title('Load v.s. Strain - Different Extensometer in
Comparison','fontweight','bold')

figure(5)
hold on
grid on
plot(v12,F)
plot(v15,F)
plot(v23,F)
plot(v24,F)
plot(v34,F)
plot(v45,F)
plot(v67,F)
plot(mech,F,'LineStyle','-','LineWidth',1)
plot(d15,F,'LineStyle','--')
plot(d24,F,'LineStyle','-.')
plot(d67,F,'LineStyle',':')
xlabel('Eng Strain (%)')
ylabel('Load (kN)')
legend('V12','V15','V23','V24','V34','V45','V67','mech','D15','D24','D6
7')
title('Load v.s. Strain - All in Comparison','fontweight','bold')

figure(6)
hold on
grid on
plot(eps_1_t_m,sig_t_m)
plot(eps_1_t_v,sig_t_v,'LineStyle','--')
plot(eps_1_t_d,sig_t_d,'LineStyle','-.')
plot(eps_2_t_v,sig_t_v)
plot(eps_2_t_d,sig_t_d,':')
xlabel('True Strain')
ylabel('True Stress (MPa)')
legend('Major Strain Mech','Major Strain Vid','Major Strain DIC','Minor
Strain Vid','Minor Strain DIC')
title('True Stress v.s. True Strain - 3 in
Comparison','fontweight','bold')

figure(7)
hold on
grid on
```

```matlab
plot(eps_1_t_m(1:length(sig_t_v)),sig_t_m(1:length(sig_t_v)),'LineWidth
',2)
plot(eps_1_t_v(1:length(sig_t_v)),sig_t_v(1:length(sig_t_v)),'--')
plot(eps_1_t_d(1:length(sig_t_v)),sig_t_d(1:length(sig_t_v)),'-.')
plot(linex-0.002,liney)
plot(linex,liney)
plot(eps_2_t_v(1:length(sig_t_v)),sig_t_v(1:length(sig_t_v)))
plot(eps_2_t_d(1:length(sig_t_v)),sig_t_d(1:length(sig_t_v)),':')
plot(linex2,liney2)
if use_filter == 1

plot(eps_2_t_v_sm(trunc1:trunc2),sig_t_v(trunc1:trunc2),'LineWidth',1)

plot(eps_2_t_d_sm(trunc1:trunc2),sig_t_d(trunc1:trunc2),'LineWidth',1)
end
xlabel('True Strain')
ylabel('True Stress (MPa)')
legend('Major Strain Mech','Major Strain Vid','Major Strain DIC','E
Modulus Line','E Modulus Line Offset','Minor Strain Vid','Minor Strain
DIC','E/\nu Modulus Line Offset')
if use_filter == 1
    legend('Major Strain Mech','Major Strain Vid','Major Strain DIC','E
Modulus Line','E Modulus Line Offset','Minor Strain Vid','Minor Strain
DIC','E/\nu Modulus Line Offset','Minor Strain DIC Filtered
Truncated','Minor Strain Vid Filtered Truncated')
end
title('True Stress v.s. True Strain - E modulus & Yield
point','fontweight','bold')

figure(8)
hold on
grid on
plot(eps_1_t_m_f,sig_t_m_f)
plot(eps_vm,sig_t_m_f,'--')
plot(eps_oa,sig_t_m_f,'-.')
xlabel('True Plastic Strain')
ylabel('True Stress (MPa)')
legend('True Stress vs Major Strain','True Stress vs Effctive
Strain','True Stress vs Overall Effctive Strain')
title('Flow Curve','fontweight','bold')


% Hydraulic bulge test flow curve code
% Mario Vasilescu
% Variables
% Section 1
dis = csvread('Displacement2.csv');
pressinfo = csvread('Test8PressDataMatLab2.csv');
name = 'dataflowcurves.txt'

%Section 2
t = pressinfo(:,11); % test time (MTS machine)
innerpos=pressinfo(:,3)% Inner Position
Innerload = (pressinfo(:,5))*1000 / 60 / 60 / 3.141614; % load
Hd= dis(:,2);
```

```matlab
newtime=linspace(0,48.359095,567); % Interpoolation of Displacement
(frames to time (s))
Hdf=interp1(newtime,Hd,t);
Rc= 3;
Dc= 135
Rad=135/2;
To= 1.5;


% Section 3
Rd= (((Dc/2)+Rc).^2 + Hdf.^2 - 2.*Rc.*Hdf) ./(Hdf.*2);
Td= (To.*(((Rad./Rd)./ (asin(Rad./Rd))).^2)) ;
EffStress= ( Rd./Td + 1 ) .* (Innerload./2)
EffStrain= -1*log((Td./To));


%plot(EffStrain,smooth(EffStress))
testtime=linspace(0,48.359095,1613)
plot(EffStrain,EffStress)


output = [EffStrain,EffStress];
save(name,'output','-ascii')
```

Appendix B – Technical drawings for hydraulic bulge test and pressure transducer

4X Ø 14
Ø 20
25

8 X Ø 28

Ø 190
Ø 100
Ø 152.4
Ø 120
Ø 410

400
30°

395

12 X Ø 12

Top view

Ø 12
Ø 8

240   265

Front view

This drawing is our property. It can't be reproduced or communicated without our written agreement.		University of Windsor			
		DRAWING TITLE			
DRAWN BY	DATE	**Main Block**			
Mario Vasilescu	11/01/2018				
CHECKED BY	DATE	SIZE	DRAWING NUMBER		REV
Mario Vasilescu	11/01/2018	A	1		1
DESIGNED BY	DATE	SCALE 1:9			SHEET 1/1
Mario Vasilescu	11/01/2018				

Main Block Technical Drawing

116

Clamping Ring Technical Drawing
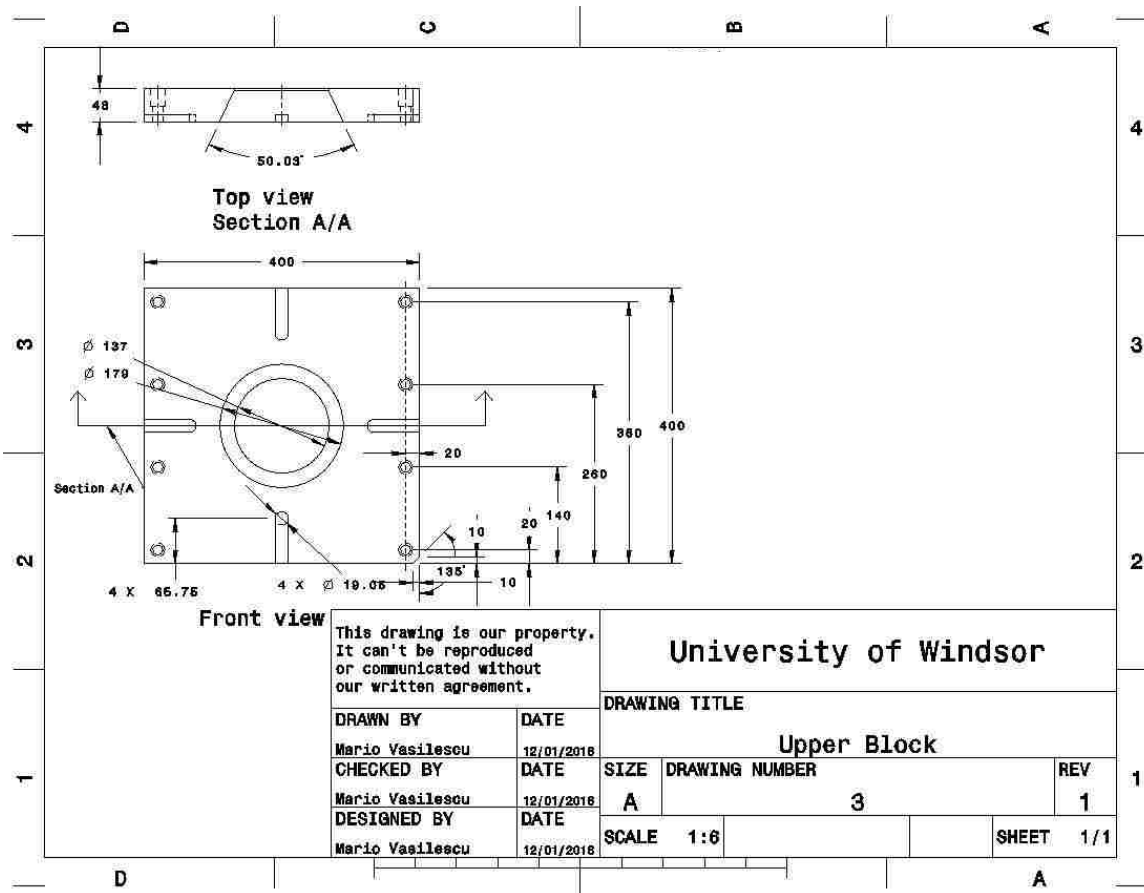
Upper block Technical Drawing
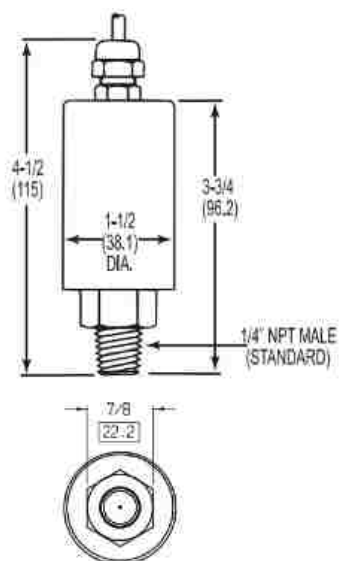
Barksdale 423 series Pressure Transducer Technical Drawing

Item	Quantity
Main block	1
Upper block	1
Clamping ring (12 M12 Bolts configuration)	1
Clamping ring	1
Custom piston head 120 mm	1
Team Tube-Metric honed tubing	1
Selemaster DSM Piston Seal	1
Pipe fitting 1/2'' NPT nipple	1
Pipe fitting 1/2'' NPT elbow	1
Barksdale 423 series pressure transducer	1
One way 10,000 PSI exit valve	1
M12 Bolts	12

Bill of Materials

Appendix C – Step by step procedure to operate hydraulic bulge test

1. Insert key to start up press and switch from "off" to either manual or auto mode.

2. Restart and/or turn off master stop and emergency stop buttons

3. Reset all faults, first by pressing the master control reset and then the emergency stop reset

4. Press the pump start button, this will allow the actuators to load. The operator must wait until actuators are fully loaded to operate the press

5. If manual mode is selected:

    a. Press the manual setup button

    b. Close and open speed is defined as percentage of the press maximum close and open speed. The "lock enabled" button locks the inner and outer together, allowing the punch and press slide to travel together. This can be turned off to allow independent motions.

6. If automatic mode is selected a profile needs to be chosen. Press "Active Recipe" in the bottom left corner, then press "Load" and choose the bulge test recipe.

7. Press "Active Recipe" again in order to confirm that the bulge test profile was chosen

8. Select "Process Setup" and manually move inner and outer to starting position. The key will need to be moved to the manual mode selection.

9. Move the key back to automatic mode and press "cycle press enable" and "cycle press" to begin the cycle

Appendix D - Tabular Data (Effective Stress, Effective Strain)

Hydraulic Bulge Test

445.9217	0.002831	595.2718	0.054499	739.76	0.133613
431.6153	0.003217	599.8103	0.056523	742.9646	0.135985
430.727	0.003688	605.2465	0.058662	746.2984	0.138313
429.1683	0.00426	610.2288	0.060536	749.2148	0.140907
427.508	0.004715	615.9921	0.062904	752.4514	0.14346
432.7255	0.005186	621.9719	0.065088	755.7825	0.14589
439.1197	0.006157	626.1767	0.067278	758.8	0.14866
446.5046	0.006203	632.4234	0.069761	761.9136	0.151143
455.6371	0.007214	628.4119	0.070945	763.7137	0.155244
465.2446	0.00793	638.8736	0.072691	766.445	0.158304
477.3136	0.008758	641.7014	0.074499	769.9154	0.160978
484.8494	0.009748	647.3121	0.076209	771.5416	0.163663
490.2318	0.010977	650.3513	0.077984	776.0182	0.166351
488.2705	0.01242	654.3622	0.079564	776.2699	0.169128
485.0213	0.014434	658.1386	0.081494	781.7313	0.17197
491.3187	0.015641	661.8396	0.083148	784.6299	0.175073
495.077	0.017142	665.1659	0.08511	787.4415	0.17802
501.7367	0.018568	668.4518	0.086901	790.6902	0.181019
506.4859	0.019895	672.8896	0.088641	793.0962	0.184041
510.72	0.021323	675.6255	0.090405	795.8246	0.187187
515.9206	0.022829	679.1889	0.092351	798.4848	0.190292
521.036	0.024363	682.6477	0.094143	801.3301	0.193299
525.3	0.025825	686.2305	0.096029	804.1786	0.19669
530.1402	0.027279	687.163	0.098949	806.2705	0.199791
533.4955	0.028655	689.8959	0.101037	809.2846	0.203089
539.403	0.030301	693.7058	0.103058	811.3903	0.206371
545.6569	0.031908	697.4258	0.104985	815.012	0.209611
549.0775	0.033372	700.53	0.107079	817.1577	0.213169
554.2898	0.03503	703.7225	0.10919	819.5031	0.216435
557.4902	0.036418	705.9686	0.111234	822.6676	0.219786
561.7489	0.037936	710.1238	0.113236	824.5239	0.223299
566.0579	0.039328	713.2766	0.11531	825.6521	0.226867
569.6046	0.040986	717.1507	0.117592	829.7664	0.231025
574.6959	0.042482	720.4061	0.119694	832.0955	0.236372
579.8986	0.044085	723.6516	0.121926	833.8474	0.240095
582.67	0.045911	727.0764	0.12441	835.7647	0.244007
588.6565	0.047693	729.6931	0.126568	838.4482	0.24777
590.7555	0.049766	733.6863	0.128822	840.9509	0.251798
590.6927	0.052767	736.9671	0.131277	843.3526	0.25608

844.8044	0.260228	862.6556	0.296347	877.9782	0.334741
847.871	0.26406	864.3399	0.301119	879.4562	0.34005
850.18	0.268859	866.7174	0.305529	880.994	0.347869
851.2796	0.273457	868.8683	0.310395	882.9928	0.3532
854.2928	0.277985	870.6738	0.314948	884.6631	0.358691
855.9638	0.282781	871.0984	0.319816	886.3039	0.364209
858.6672	0.287225	874.5413	0.324549	888.0188	0.370066
860.4838	0.291866	875.4471	0.329724	888.6697	0.37598

Tensile Test Rolling Direction

0.001402	351.4054	0.085577	638.1501
0.005578	365.781	0.089175	643.1841
0.008376	388.3179	0.092785	648.0346
0.011225	410.2268	0.096435	652.7629
0.014126	430.2601	0.100112	657.3147
0.017056	448.6092	0.103812	661.6303
0.020045	465.3249	0.107542	665.8361
0.023064	480.4522	0.111296	670.0737
0.026121	494.3582	0.115078	674.1047
0.029197	507.1347	0.118884	678.0086
0.032296	519.1022	0.12273	681.8218
0.035429	529.9652	0.126606	685.4589
0.038583	540.2402	0.130515	689.1238
0.041736	549.7697	0.134452	692.7286
0.044927	558.747	0.138421	696.1794
0.04814	567.1979	0.142409	699.5534
0.051378	575.2885	0.146434	702.8969
0.054679	582.8684	0.150484	706.2307
0.057995	590.1441	0.154584	709.3948
0.061317	597.0629	0.158742	712.4474
0.064684	603.6872	0.160789	713.3657
0.068077	610.0661	0.203543	756.1626
0.071496	616.0638	0.393536	853.4196
0.074963	621.8634	0.599365	919.9831
0.078464	627.4505	0.807238	987.7113
0.08201	632.9253	1.003936	1033.318

Tensile Test Transverse Direction

0.001736	369.8657	0.008819	406.2316
0.005974	383.76	0.011749	427.9214

0.014691	448.041	0.797669	979.7765
0.017677	466.3625	0.987033	1025.403
0.020704	483.1258		
0.02377	498.4644		
0.026867	512.4053		
0.029992	525.3135		
0.033138	537.1332		
0.036311	548.1417		
0.039498	558.3703		
0.042688	567.8793		
0.045921	576.7885		
0.04918	585.2348		
0.052462	593.2493		
0.055783	600.8308		
0.059141	608.0715		
0.062525	614.9749		
0.065947	621.5257		
0.069385	627.8033		
0.072861	633.7833		
0.076358	639.5587		
0.079898	645.0886		
0.083461	650.4057		
0.087051	655.5009		
0.090671	660.4506		
0.094321	665.2375		
0.097997	669.8811		
0.101712	674.3593		
0.105457	678.6904		
0.109219	682.9156		
0.113019	687.0005		
0.116838	690.9557		
0.120693	694.8543		
0.124572	698.6806		
0.128487	702.3329		
0.132443	705.9177		
0.136427	709.4467		
0.140442	712.9076		
0.144479	716.1526		
0.148547	719.372		
0.152653	722.5988		
0.200939	773.5923		
0.389335	862.7231		
0.598023	932.762		

VITA AUCTORIS

NAME: Mario Vasilescu

PLACE OF BIRTH: Windsor, ON

YEAR OF BIRTH: 1992

EDUCATION: Vincent Massey Secondary High School, Windsor, ON, 2010

                              University of Windsor, B.Sc., Windsor, ON, 2014

                              University of Windsor, M.Sc., Windsor, ON, 2016